

A NOVEL FORMALISM FOR THE STUDY OF THE ELECTRONIC AND OPTICAL PROPERTIES OF HIGH SYMMETRY HETEROSTRUCTURES

THÈSE N° 3879 (2007)

PRÉSENTÉE LE 17 AOÛT 2007

À LA FACULTÉ DES SCIENCES DE BASE
LABORATOIRE DE PHYSIQUE DES NANOSTRUCTURES
PROGRAMME DOCTORAL EN PHYSIQUE

ÉCOLE POLYTECHNIQUE FÉDÉRALE DE LAUSANNE

POUR L'OBTENTION DU GRADE DE DOCTEUR ÈS SCIENCES

PAR

Sascha DALESSI

ingénieur physicien diplômé EPF
de nationalité suisse et originaire de Cavigno (TI)

acceptée sur proposition du jury:

Prof. A. Bay, président du jury
Dr M.-A. Dupertuis, directeur de thèse
Prof. G. Fishman, rapporteur
Prof. O. J. F. Martin, rapporteur
Prof. L. R. Ram-Mohan, rapporteur



ÉCOLE POLYTECHNIQUE
FÉDÉRALE DE LAUSANNE

Suisse
2007

To my family

Abstract

The theories used up to now to model theoretically and numerically nanostructures, and more specifically semiconductor heterostructures, do not allow to include efficiently at the envelope function level, in a $k \cdot p$ approach, the effects imposed by a possible symmetry of the problem. The most elaborated techniques available only allow to take into account the existence of a single symmetry plane, or deal with global symmetry, but not with envelope functions.

The most important part of this thesis deals with the development of a novel formalism, very general, which allows to study the electronic and optical properties of high symmetry nanostructures. This new *Maximal Symmetrization and Reduction (MSR) formalism* allows to maximally symmetrize the eigenstates and significantly reduce the size of the spatial domain of solution. The formalism was explicitly developed with the aim to study a C_{3v} quantum wire, with three symmetry planes at 120° , and allowed to analytically justify some numerical result obtained without an adapted theoretical formalism. In addition, some other physical results related to the effects of symmetry were highlighted and understood. To cite a simple example, it is possible to demonstrate a perfect isotropy polarization with respect to two directions in the cross-section of a wire. In addition, for some transitions new analytical expressions were found for the polarization anisotropy between a direction in the plane and a direction along the wire. The new formalism allows also to understand, in much more details, a number of effects in a qualitative and quantitative way, e.g. symmetry breaking effects.

For the example of the C_{3v} wire, the conduction and valence bands are treated separately in the $k \cdot p$ approximation, with respectively one (spinless) band and four bands (describing the valence band mixing).

For the scalar wavefunction problem of the conduction band, we propose a new systematic Spatial Domain Reduction (SDR) method. For every different symmetry of the problem (irreducible representation), the independent sub-domains can be identified and a reduced Hamiltonian on the minimal domain can be obtained (numerical optimization).

For a spinorial problem, the spatial and spinorial (Bloch functions) parts, have to be considered separately (both for operators and the eigenstates) although treated simultaneously. Whatever the number of bands considered, completely symmetrized bases can be chosen according to the symmetry properties of the heterostructure. This approach allows to classify with respect to the symmetry not only any spinorial states, but every one of their spinorial components (envelope functions) separately. The physical under-

standing as well as subsequent analytical treatment are considerably simplified. Finally we propose to apply the spatial domain reduction technique to the spinorial components, which ensure to solve the spinorial problem on a minimal domain with numerical optimization.

The proposed approach is valid in a much larger framework than $k \cdot p$ theory, and is applicable to arbitrary systems of coupled partial differential equations, e.g. strain equations in heterostructures or the Maxwell equations describing an impurity state in a photonic band-gap.

Keywords:

Heterostructure, semiconductor band structure, quantum dot, quantum wire, quantum well, nanostructure, photonic band-gap, solid state theory, symmetry, group theory, electronic properties, multiband $k \cdot p$ theory, optical properties, finite elements method.

Version abrégée

Les théories utilisées jusqu'à ce jour pour modéliser théoriquement et numériquement les nanostructures, en particulier les hétérostructures semiconductrices, ne permettaient pas d'inclure efficacement au niveau des fonctions enveloppe, dans un approche $k \cdot p$, les effets imposés par une éventuelle symétrie de la structure quantique. Les techniques les plus élaborées permettaient uniquement de prendre compte de l'existence d'un seul plan de symétrie, ou de traiter les effets de symétrie globaux, mais pas au niveau des fonctions enveloppe.

La partie principale de cette thèse a ainsi consisté à établir un nouveau formalisme, très général, permettant d'étudier les propriétés électroniques et optiques de nanostructures avec un degré de symétrie élevé. Le nouveau formalisme, appelé MSR, de l'anglais "*Maximal Symmetrization and Reduction*", permet d'obtenir une symétrisation maximale des fonctions enveloppe des états propres et une réduction significative du domaine spatial.

Le formalisme a été explicitement développé pour étudier un fil quantique avec symétrie C_{3v} , possédant trois plans de symétrie à 120° . Ceci a permis d'une part de justifier analytiquement les considérations numériques établies précédemment sans l'utilisation d'un formalisme théorique adapté, d'autre part de mettre en évidence et de comprendre d'autres propriétés physiques découlant des contraintes imposées par la symétrie. Pour ne donner qu'un exemple, il est possible de démontrer une parfaite isotropie de polarisation par rapport à deux directions dans le plan du fil. Par ailleurs, pour certaines transitions de nouvelles expressions analytiques ont pu être obtenues pour l'anisotropie de polarisation (entre une direction dans le plan et l'autre selon le fil). Nous montrerons que ce nouveau formalisme permet de comprendre plus en détails, de manière qualitative et quantitative, plusieurs autres effets, comme par exemple les brisures de symétrie.

Dans l'exemple considéré, les bandes de conduction et de valence sont traitées de manière séparée dans l'approximation $k \cdot p$ avec un modèle à une bande (sans spin) et, respectivement, quatre bandes (décrivant le mélange de bande de valence).

Pour le problème scalaire de la bande de conduction, nous proposons une nouvelle méthode systématique pour réduire le domaine spatial (Spatial Domain Reduction : SDR). Pour chaque symétrie du problème (représentation irréductible), les sous-domaines indépendants sont identifiés et l'Hamiltonien réduit sur le domaine minimal est obtenu (optimisation numérique).

Pour un problème de type spinoriel, les parties spatiale et spinorielle (fonctions de Bloch) des opérateurs et des états propres doivent être considérées séparément bien que traitées simultanément. Indépendamment du nombre de

bande considéré, des bases complètement symétrisées peuvent être choisies selon les propriétés de symétrie de l'hétérostructure. Cette approche permet de classer en fonction de la symétrie non seulement les états mais aussi chaque composante spinorielle (fonction enveloppe) des différents états, simplifiant ainsi considérablement la compréhension et les développements analytiques subséquents. La technique de réduction du domaine spatial est finalement aussi appliquée aux composantes spinorielles, optimisant ainsi aussi le côté numérique.

L'approche que l'on propose dans cette thèse a cependant un champ d'application beaucoup plus large que la théorie $k \cdot p$: elle est applicable à un système arbitraire d'équations différentielles couplées, comme par exemple les problèmes de contrainte pour les hétérostructure ou les équations de Maxwell qui décrivent un état d'impureté dans une bande interdite photonique ("photonic band-gap").

Mots-clés :

Hétérostructure, semiconducteur, structure de bande, boîte quantique, fil quantique, puit quantique, nanostructure, band gap photonique, théorie de la matière de l'état solide, symétrie, théorie des groupes, propriétés électroniques, théorie $k \cdot p$ multibande, propriétés optiques, méthode des éléments finis.

Riassunto

I metodi teorici e numerici fino ad oggi utilizzati per modellizzare le nanostrutture, ed in particolare le eterostrutture a semiconduttore, non permettono di includere efficacemente al livello delle funzioni involuppo, in un approccio $k \cdot p$, gli effetti dovuti ad eventuali simmetrie della struttura quantistica. Le tecniche più elaborate finora disponibili consentivano solo la descrizione di un unico piano di simmetria o di trattare gli effetti di simmetria a livello globale, non a livello delle funzioni involuppo.

Gran parte di questa tesi è stata quindi volta a sviluppare un nuovo formalismo, molto generale, per studiare le proprietà elettroniche e ottiche di nanostrutture con un grado elevato di simmetria. Il nuovo formalismo MSR, dall'inglese "*Maximal Symmetrization and Reduction*", qui proposto, permette di ottenere una simmetrizzazione massimale degli autostati, oltre ad una riduzione del dominio spaziale.

Tale formalismo è stato specificamente sviluppato per studiare un "quantum wire" (filo quantico) a simmetria C_{3v} , che possiede tre piani di simmetria a 120° , permettendo non solo la giustificazione analitica delle considerazioni numeriche ottenute in precedenza senza l'utilizzo di un formalismo teorico adeguato, ma anche la comprensione di altre proprietà fisiche imposte dalla simmetria del problema. Per citare un solo esempio, è stato possibile dimostrare l'esistenza di una perfetta isotropia di polarizzazione rispetto a due direzioni nel piano del filo. In aggiunta, si sono ottenute nuove espressioni analitiche per l'anisotropia di polarizzazione (per una direzione lungo il filo e l'altra nel piano ad essa perpendicolare). Questo nuovo formalismo permette inoltre una comprensione sia qualitativa che quantitativa di differenti altri effetti, come ad esempio la rottura di simmetria.

Nell'esempio considerato, le bande di conduzione e valenza sono trattate separatamente nell'approssimazione $k \cdot p$ con un modello rispettivamente a una banda (senza spin) e a quattro bande (che permette di descrivere il "valence band mixing").

Per il problema scalare della banda di conduzione è stato sviluppato un nuovo metodo sistematico per ridurre il dominio spaziale ("Spatial Domain Reduction" : SDR) consistente, per ogni simmetria del problema (rappresentazione irriducibile), nell'identificazione dei sottodomini indipendenti e nell'ottenimento dell'Hamiltoniano ridotto sul dominio minimale (ottimizzazione numerica).

Per un problema di tipo spinoriale, le parti spaziale e spinoriale (funzioni di Bloch) degli operatori e autostati devono essere separate ma trattate simultaneamente. A tal proposito, indipendentemente dal numero di bande considerato, si possono scegliere in accordo con le proprietà di simmetria del-

l'eterostruttura, delle basi completamente simmetrizzate. Ciò permette di classificare, in funzione della simmetria, non unicamente gli autostati ma pure ogni singola componente spinoriale (funzioni involuppo) dei differenti stati, semplificando così considerevolmente la comprensione e gli sviluppi analitici ulteriori. La tecnica di riduzione del dominio spaziale può infine essere applicata alle componenti spinoriali, ottimizzando la risoluzione numerica. Tuttavia, l'approccio proposto ha un campo d'applicazione molto più vasto che la teoria $k \cdot p$ ed è applicabile ad un sistema arbitrario di equazioni differenziali accoppiate, come ad esempio i problemi di costrizione per le eterostrutture o le equazioni di Maxwell che descrivono uno stato d'impurità in un bandgap fotonico.

Parole chiave :

Eterostruttura, semiconduttore, struttura a bande, quantum dot, quantum wire, quantum well, nanostruttura, band gap fotonico, teoria della materia nello stato solido, simmetria, teoria dei gruppi, proprietà elettroniche, teoria $k \cdot p$ multibanda, proprietà ottiche, metodo degli elementi finiti.

Remerciements

Je tiens tout d'abord à remercier chaleureusement Marc-André Dupertuis, mon directeur de thèse, pour sa sympathie, son enthousiasme, sa compétence et la disponibilité qu'il a montré pendant les innombrables heures de discussion à la cafet' ou dans son bureau. Pendant ces quatre années de thèse, Marc-André a été un directeur de thèse exceptionnel qui m'a toujours guidé avec passion et considéré plus comme son collaborateur que comme son étudiant.

Ensuite, je remercie les autres membres du labo, actuels et anciens, en particulier Nicolas qui a partagé mon bureau, et qui a dû me supporter pendant ces trois dernières années. Merci aussi à Fabienne, qui a en particulier passé beaucoup de temps à répondre avec patience à mes nombreuses questions en début de thèse. Merci au Professeur Eli Kapon qui m'a donné la possibilité de faire une thèse dans son laboratoire.

Merci à Marc-André, Nicolas, Valentina et Guillaume pour leur conseils linguistiques ainsi qu'à Rico pour ses conseils informatiques, ceux-ci ont été très importants pendant la rédaction de ma thèse.

Je remercie aussi les Professeurs L. R. Ram-Mohan, G. Fishman, O. J. F. Martin et A. Bay pour tout leur travail, ainsi que d'avoir accepté de faire partie de mon jury de thèse.

Je tiens à remercier mes parents, Renzo et Erica, ainsi que mon frère Alan, pour tout le soutien qu'ils m'ont donné pendant ces dernières années.

Enfin, je remercie tous mes amis de Lausanne, du Tessin et d'ailleurs pour les bons moments que j'ai passé en leur compagnie.

List of abbreviations

MSR:	Maximal Symmetrization and Reduction
SDR:	Spatial Domain Reduction
HSR:	High Symmetry Heterostructures
OBB:	Optimal Bloch function Basis
OQA:	Optimal Quantization Axis
ZC:	Zone-Center
WET:	Wigner-Eckart Theorem
ITO:	Irreducible set of Tensorial Operators
FEM:	Finite Elements Methods
irrep:	irreducible representation
QW:	Quantum Well
QWR:	Quantum Wire
VQWR:	Vertical Quantum Wire
QD:	Quantum Dot

Contents

Abstract	ii
Version abrégée	iv
Riassunto	vi
Remerciements	viii
List of abbreviations	ix
1 Introduction	1
1.1 Objectives of the thesis work	1
1.2 State of knowledge and limit of previous methods	2
1.3 The new formalism: basic ideas	4
1.4 Outline	6
2 Group theory background	9
2.1 Group theory: definitions and basic concepts	9
2.1.1 Group	9
2.1.2 Linear representation of a group: definition	10
2.1.3 Representation of a group: basic concepts	10
2.1.4 Table of characters	12
2.2 Application to the Schrödinger equation	13
2.2.1 Transformation laws	13
2.2.2 Symmetry of the functions	14
2.3 From single group to double group	16
2.3.1 The point group	16
2.3.2 The rotational $SO(3)$ group	16
2.3.3 The $SU(2)$ group	17
2.3.4 Link between $SU(2)$ and $SO(3)$	18
2.3.5 The inversion	18
2.3.6 The double group	18

2.3.7	Transformation law for the “spinorial” Bloch function basis	19
2.3.8	Transformation law for spinorial functions	20
2.4	Wigner-Eckart theorem and selection rules	21
2.4.1	Conjugated representations	22
2.4.2	Direct product of representations	22
2.4.3	Irreducible set of Tensorial Operators (ITO)	23
2.4.4	The Wigner-Eckart Theorem (WET)	23
2.5	Group theory tables	24
2.5.1	Character table	24
2.5.2	Multiplication table	25
2.5.3	Matrix representations	25
2.5.4	Direct products of representations	25
2.6	Effects of symmetry: illustration of group theory	26
2.6.1	C_s group	26
2.6.2	C_{2v} group	28
2.6.3	C_{3v} group	28
2.6.4	Illustration of the WET	32
2.7	References	33
3	Band structure and heterostructures	35
3.1	Bulk semiconductors	35
3.1.1	The crystalline structure	35
3.1.2	Translational symmetry and Bloch theorem	36
3.1.3	Energy bands in a crystal	37
3.1.4	The $Al_xGa_{1-x}As$ semiconductors	39
3.1.5	Point groups and related definitions	40
3.1.6	The $k \cdot p$ approximation	40
3.2	Discussion about the inversion	47
3.3	Low dimensional semiconductor heterostructures	48
3.3.1	2D Quantum Wells (QWs)	50
3.3.2	1D Quantum Wires (QWRs)	50
3.3.3	0D Quantum Dots (QDs)	51
3.3.4	Complex connected structures	52
3.4	Electronic properties of semiconductor heterostructures	53
3.4.1	The envelope function approximation: historical approach	54
3.4.2	The conduction band Hamiltonian	54
3.4.3	The valence band Hamiltonian	55
3.4.4	The exact envelope function formalism	55
3.4.5	Interface terms	59

3.5	References	60
4	Optical properties of semiconductor heterostructures	61
4.1	Absorption spectra	61
4.2	Excitons	63
4.3	References	64
5	Numerical methods	65
5.1	The Finite Elements Method (FEM): general theory	66
5.1.1	Introduction to the physical problem	66
5.1.2	Weak formulation	67
5.1.3	Galerkin approximation	67
5.2	FEM: computation of matrix elements	68
5.2.1	Meshing and basis function	68
5.2.2	The master (isoparametric) element	69
5.2.3	Gauss-Legendre integration	70
5.3	Numerical computation and resolution of the linear problem	70
5.3.1	Structured matrices	71
5.3.2	Resolution of a linear problem: ARPACK library	71
5.4	References	72
6	From low to high symmetries: a new formalism	73
6.1	The effects of low symmetry: scalar functions	74
6.2	The effects of low symmetry: envelope functions of spinorial problems	75
6.3	From low to high symmetry	80
6.4	Optimal Bloch function basis	84
6.5	High symmetry: a new formalism	85
7	Spatial Domain Reduction (SDR) technique for the scalar functions	87
7.1	Decomposition in disjoint sub-domains	88
7.2	Minimal independent sub-domains	89
7.3	The structure of the full Hamiltonian	93
7.4	The reduced Hamiltonians	94
7.5	Conclusion	96
8	The MSR formalism for spinorial problems	99
8.1	The Luttinger Hamiltonian: transformation rules	99
8.2	The fully symmetrized basis and the separation of spinorial and spatial parts	100

8.3	Reduction of a spinorial sets of functions	105
8.4	Selection rules and matrix elements with the MSR formalism .	108
8.5	Discussion	110
9	Application to C_{3v} vertical quantum wires: analytical and numerical results	113
9.1	C_{3v} VQWR and pyramidal QDs	113
9.1.1	Motivation for the study	114
9.1.2	Fabrication of pyramidal QDs	114
9.1.3	Model of VQWR	115
9.2	Analytical and numerical results	117
9.2.1	The Luttinger Hamiltonian and additional time-reversal symmetry	118
9.2.2	Band structure and electronic states	119
9.2.3	Optical properties	123
9.2.4	Additional symmetries and symmetry breaking	129
9.2.5	Additional study	142
10	Application of MSR formalism to some other group	147
10.1	C_{6v} group	147
10.2	D_{3h} group and study of approximated symmetries	149
10.3	The C_n groups: subgroups of the rotations group	150
10.4	Return to the C_s group	151
11	Conclusion and outlook	153
11.1	Conclusion	153
11.2	Outlook	154
	Bibliography	154
	Publications and conferences	161
	Curriculum vitæ	163

Chapter 1

Introduction

1.1 Objectives of the thesis work

At the origin, the aim of this thesis work was the study of the electronic and optical properties of quantum wires (QWRs) and we started with a C_{3v} Vertical QWR (VQWR) self-formed on each side of pyramidal quantum dots (QDs). An important aspect is that it serves as main channel for QD carrier capture [1] and is quite influential on the electronic properties of this QD [2]. Quickly we realized that a beautiful feature of the VQWR was its high symmetry: three symmetry planes intersecting on the same vertical axis, leading to a “triangular” symmetry (C_{3v} group [3]). Indeed very little work was done on the specific properties of such “high symmetry” quantum wires and we were able to find in the literature only four theoretical articles dealing with triangular QWRs [4–7]. A closer look revealed that equilateral triangular QWRs, i.e. C_{3v} QWRs, were addressed only in the work of Lassen [8], very shortly, without any detailed considerations and numerical calculations.

The motivation of the study on this type of quantum structure is manifold. From the scientific point of view, a good understanding of the VQWR is very important to model a pyramidal QD (the VQWR is the main channel for the electron capture) and from the didactical point of view we had an original problem to start the study of electronic and optical properties of quantum wires. We soon realized that for a “high symmetry structure” it is not possible to reach a sufficient physical understanding without developing new tools, which finally became the major aspect of this thesis.

Therefore, the central and more important part of the thesis is the development of a new Maximal Symmetrization and Reduction (MSR) formalism to study the electronic and optical properties of High Symmetry Heterostruc-

tures (HSH). It is important to note that in the following, we first present the general formalism, and only then we use this novel tool to study the electronic and optical properties of the C_{3v} VQWR.

1.2 State of knowledge and limit of previous methods

The study of low dimensional solid state nanostructures is a very interesting and promising domain. Indeed, a good knowledge of the electronic and optical properties of nanostructures like metallic [9] or semiconductor [10] nanostructures, or photonic crystals [11], is now essential for many applications in advanced lasers, photonics and telecommunications. New truly quantum applications like quantum cryptography may also make extensive use of semiconductor quantum heterostructures like quantum wells, quantum wires and quantum dots [12]. The quality of semiconductor quantum wires and dots have been extensively improved during the last 15 years, and one is now able to produce high quality structures with higher and higher symmetries (e.g. C_{6v} quantum dots [13,14]). In such a case a group-theoretical approach is usually the most powerful tool for describing the effects issuing from symmetry on the electronic states, as well as their optical properties. However the problem is rather complicated since in heterostructures one must take into account both the underlying microscopic crystalline structure and the mesoscopic heterostructure confinement potential.

The theoretical study of low symmetry effects in semiconductor heterostructures (like quantum wires with C_s symmetry, e.g. T- and V-shaped quantum wires [15,16]) is already well developed [17] and has led to fundamental conclusions regarding their electronic and optical properties. First, electronic and excitonic states can be labelled with respect to their characteristic transformation properties under symmetry operations. Second, rigorous and important selection rules were readily obtained on the basis of such a classification, useful even in a low symmetry case [17,18]. The effects of lateral confinement to the polarization anisotropy were largely studied [5,19–22]. However, it should be pointed out that up to now only very little work has been devoted to higher symmetries, for example C_{3v} structures [2,23], or even C_{6v} [24]. A particularity of HSH is to allow the existence of degenerate states, related to 2D irreducible representations (irreps) [3,25], and much more complex eigenstate behavior under symmetry operations. In [26], the author studied a C_{4v} quantum wire and put in evidence the existence of an

additional symmetry operation (leading to extra degeneracy in the spectra) as a consequence of the separability of the potential in a model with infinite barriers.

The electronic structure of semiconductor heterostructures are often studied in the frame of the $k \cdot p$ envelope function approaches [27], with at least four bands for the valence band. In such a frame the behavior of the different envelope functions (components of the spinorial eigenstates) under symmetry operations illustrates our point: they are *mutually coupled*, which complicates significantly their shapes. Up to now there has been very few attempts to use an Optimal Bloch function Basis (OBB). In [17] for example the authors tried to rely on the choice of an “Optimal Quantization Axis (OQA) direction” (a Bloch function basis which diagonalizes the component of angular momentum in the chosen optimal direction). In fact we shall show in the following that such a method is optimally adapted only in very low symmetry cases like C_s structures! Moreover for a QWR with a higher symmetry group, the previously defined OQA direction may be an improved choice only.

The use of group theory considerably simplifies the analytical treatment of electronic and optical properties of low symmetry semiconductor heterostructures like T- and V-shaped QWRs (C_s symmetry group). Every conduction band state is even or odd with respect to the symmetry plane and allows to introduce irreducible representation classifications according to the symmetry. For the valence band states, double group irreps are involved to classify the spinorial eigenstates [17]. Finally, rigorous selection rules for the operators are obtained (e.g. forbidden transitions for the dipolar matrix elements) and excitons as well can be labelled with respect to the symmetry [18].

Numerical computation of the eigenstates are optimized by the previous analytical considerations: only one half of the spatial domain has to be used and we solve a smaller different problem for every irrep of the group.

Since C_s is a subgroup of C_{3v} , it would still be possible to use the previous technique to obtain the electronic structure of the VQWRs but one should note that:

- it is necessary to solve on the half plane whereas the minimal domain could be smaller (numerical optimization!)
- one only obtains even/odd solutions with respect to a single symmetry plane without classification with respect to all the C_{3v} symmetries

- it is not possible to find a true OQA direction which would allow to obtain really nice symmetry properties for the components of a spinorial problem

These problems are linked with the appearance of degenerate irreps for the electronic states, where symmetry properties can not be found simultaneously with respect to every symmetry plane. In addition, we shall show that only an improved formalism can allow more insight, and finally gives new analytical expressions for some operators matrix elements.

In the literature, to the best of our knowledge there is no theory able to include effects of discrete symmetry for the study of the envelope function properties of HSH. In [28] the author proposes an interesting formalism to calculate the band structure in the axial approximation, but for the valence band this corresponds to partially neglect the crystal structure and approximate the confinement potential by a cylinder: in their case the new continuous symmetry group of the Hamiltonian is C_∞ and not the point group of the underlying bulk semiconductors.

Finally, we hope to convince the reader that, to obtain a rigorous analytical description taking into account the microscopic crystal symmetry as well as the macroscopic symmetry group of the heterostructure simultaneously with optimized numerical solution for real HSH problems, we need to introduce the new formalism developed below, which allows to obtain *Maximal Symmetrization and Reduction* for the envelope functions: the MSR formalism.

1.3 The new formalism: basic ideas

For scalar problems, like the single band $k \cdot p$ spinless conduction band Hamiltonian, we propose a systematic *Spatial Domain Reduction (SDR) technique*. The spatial domain is first decomposed in disjoint sub-domains, then one can obtain for every irrep a different reduced Hamiltonian on the corresponding reduced domain (only independent parameters are involved). The reduced Hamiltonian reflects the coupling between different sub-domains and possible non-trivial boundary conditions can be directly obtained.

With SDR there are many advantages: in particular by identifying the independent parameters one can solve minimal optimized problems on the minimal domain separately for every irrep of the group, and the different coupling in the Hamiltonians are clearly highlighted.

For the spinorial functions (e.g. four bands $k \cdot p$ Luttinger Hamiltonian for the

valence band with mixing), the basic ideas of the new formalism are threefold. First we explicitly separate the orbital (spatial 3D or Fourier space) part and the spinorial part of the operators and spinorial states (where the spinorial part is related to the Bloch function basis and not to the spin $j = \frac{1}{2}$ of the electrons!). In particular, every spinorial component can be treated as a scalar spinless function. Second, we choose, according to the symmetry, the optimal fully symmetrized basis for both orbital space and spinorial space, the Optimal Bloch function Basis (OBB), minimizing the coupling between different spinorial components. With respect to this basis, every envelope function can be decomposed in the simplest way with respect to the symmetry. Third for every irrep we identify the independent parameters (the orbital reduced domain) and apply the SDR to each scalar function to obtain a reduced Hamiltonian.

The advantages of the new MSR formalism are manifold and have been found to be greater than originally anticipated. Indeed, besides the possibility of performing SDR, we have found that there were many advantages gained from the analytical point of view: first, the Hamiltonian operator usually takes a simpler form in the adapted fully symmetrized basis. Second, the spinorial components of eigenstates (as well as the components of any operator in the spinorial basis) can be treated in the same way and easily decomposed into parts, to which simple group irreps can be associated (and for which “sub-selection rules” can be applied at an intermediate calculational level, further simplifying and enlightening the various couplings). In this way simple analytical expressions were obtained for the operator matrix elements, which allowed to find, for example, new analytical ratios in the polarization anisotropy that were previously unnoticed in the numerics. Other weak symmetry breaking mechanisms were understood more deeply with this technique at the analytical level. From the numerical point of view, with the systematic SDR we found that we were able to solve the eigenvalues problem independently for every irreps on a reduced solution domain, without the need of caring for non-trivial boundary conditions, which however can also be found systematically with the help of SDR.

We explicitly developed the MSR formalism with the aim of studying a C_{3v} VQWR (numerical resolution with a linear triangular finite elements code), but nevertheless the new formalism is very general and can be adapted to study other symmetry groups, heterostructure dimensionalities and even all other nanostructures spinorial-like or vectorial-like problems, with resolution in the real or Fourier space.

1.4 Outline

In the next four chapters, we recall the most important theoretical and numerical background concerning the heterostructures modelling. First in **Ch. 2** we give a short introduction on the most important and basic group theory concepts, essential to understand the following. In **Ch. 3** bulk semiconductors, low dimensionality heterostructures and band structure calculations are introduced. Finally, the optical properties of semiconductor heterostructures, with the corresponding theoretical tools, are discussed in **Ch. 4** and, in **Ch. 5**, the numerical methods are presented.

The aim of these chapters is to give a general overview and all the basic tools necessary to understand the new MSR formalism.

For the readers mastering these basic concepts, Chs. 2-5 simply represent a summary of most of the usual definitions and basic results needed later. In the following chapters every non-standard or essential concept will be introduced in details.

In **Ch. 6**, the limits of the previous methods for the high symmetry heterostructures are discussed in details and the basic concepts of the new Maximal Symmetrization and Reduction formalism are presented.

In **Ch. 7** the first part of the MSR formalism is presented: a systematic Spatial Domain Reduction technique for the scalar functions.

In **Ch. 8** the Maximal Symmetrization and Reduction formalism for High Symmetry Heterostructures is developed. In Sec. 8.2 we first show how to choose the optimal basis. In Sec. 8.3 the Spatial Domain Reduction technique is applied to spinorial functions and in Sec. 8.4 the possible consequences on matrix elements of operators and selection rules due to the new formalism are evidenced.

In **Ch. 9** the reader will find the most important analytical and numerical results of the study of a real C_{3v} VQWR, all obtained with the help of the new formalism. In particular, the conduction and valence band structure, as well as the eigenstates, are presented. The effects of symmetry and classification of the eigenstates are highlighted.

The optical properties of the quantum structure are also of interest to us and the dipolar interband transition spectra are computed at the center of zone $k = 0$. Selection rules are analytically studied and some “missing transitions” in the absorption spectra are identified. They are further understood by introducing an approximate Zone Center (ZC) symmetry for the valence

band problem. The origin of these “missing transitions” can be explained in a theoretical way by the introduction of a well symmetrized Hamiltonian, with a restored D_{3h} ZC symmetry group.

The qualitative and quantitative effects due to small symmetry breaking are also studied. In particular, in the last part, a π -rotated structure and the breaking of symmetry to C_s are discussed. Finally, theoretical and numerical results are compared with experiment with a reasonably good agreement.

In **Ch. 10**, we intend to give the reader some intuitions about other symmetry groups, and how the new formalism can be used. First the higher hexagonal symmetry group C_{6v} and the approximate ZC group D_{3h} are considered, allowing to understand the effects of additional symmetry operations. The pure rotation sub-groups C_n , corresponding to the important case where a magnetic field is applied to a structure with higher symmetry, are shortly studied (in this case every irrep is non-degenerate). Finally, as conclusion, we apply the MSR formalism to the C_s group, showing how to make the link with the old formalism.

In **Ch. 11**, a short conclusion summarizes the most important steps and results of the proposed MSR formalism. Further applications to more complicated problems (excitons or polarons for example) are also discussed.

Chapter 2

Group theory background

In this chapter we present an introduction to the group theory. The main definitions and theorems essential to understand any group theory-based model are presented and illustrated in the particular case of quantum mechanics applications. Only standard concepts and notations are introduced in this section (some interesting references are given in section 2.7).

In Sec. 2.5, we give an introduction on the group theory table for point group given in the table book of Altmann [3], a powerful and indispensable tool for people who want to apply group theory to study a physical problem.

In Sec. 2.6, explicit illustrations of the theoretical concepts defined this chapter, and related to the symmetry properties, are presented.

2.1 Group theory: definitions and basic concepts

In this section the basic concepts related to the general group theory applied to the solid state physics are introduced. First, the concepts of group and matrix representation of a group are mathematically defined, then some important definitions, properties and theorems related to the representations are presented.

2.1.1 Group

A **group** (\mathcal{G}, \cdot) is a set $\mathcal{G} = \{g_i\}_{i=1}^{|\mathcal{G}|}$ of elements, where $|\mathcal{G}|$ is the cardinality of the group, with a law \cdot that has three properties:

- $\forall g_1, g_2 \in \mathcal{G} \quad g_1 \cdot g_2 = g_3 \in \mathcal{G}$. Then, the product of two elements belong to the group and, for every group, one has a multiplication table.

- The law has the associative property: $(g_1 \cdot g_2) \cdot g_3 = g_1 \cdot (g_2 \cdot g_3)$
- The identity E belong to the group: $E \in \mathcal{G}$.

An equivalent expression of the third properties is that for every element, the inverse belong to the group: $\forall g \in \mathcal{G}, g^{-1} \in \mathcal{G}$. In the following one simply note $g_1 g_2$ for $g_1 \cdot g_2$.

2.1.2 Linear representation of a group: definition

The next important concept to introduce is the (linear) representations of a group and some preliminary definitions are necessary.

First one defines a **group homomorphism**: (\mathcal{G}, \cdot) and (\mathcal{H}, \times) are two groups, then $\Phi : \mathcal{G} \rightarrow \mathcal{H}$ is a group homomorphism if

$$\forall g_i, g_j \in \mathcal{G}, \Phi(g_i \cdot g_j) = \Phi(g_i) \times \Phi(g_j). \quad (2.1)$$

Then one says that the two group are **homomorphic**.

For a given group (\mathcal{G}, \cdot) , for every group homomorphism one obtains a homomorphic mapping onto a new group by considering the images with respect to Φ : $\mathcal{G} = \{g_i\} \Rightarrow \mathcal{H} = \{\Phi(g_i)\}$. In a more general way, one could associate two or more different elements to $g \in \mathcal{G}$: this means that the cardinality of \mathcal{H} can be higher with respect to the cardinality of \mathcal{G} . This will appear clearly in the following when one introduces the concept of double group of a group.

Finally, in the particular case if there exists a homomorphic mapping of a group (\mathcal{G}, \cdot) onto a group of non-singular $d \times d$ matrices $D(g)$, one has a d -dimensional **(linear) representation** (or matrix representation) of the group, where the multiplication rule corresponds to the matrix multiplication.

This is an crucial point for application of group theory to quantum mechanics: every element of a group can be represented by matrices and form a homomorphic group.

2.1.3 Representation of a group: basic concepts

The concept of representation is essential to apply group theory in physics. In this paragraph we introduce some important definitions and properties of the matrix representation. In the last paragraph, we give a rigorous definition of matrix representation. In a more practical way, one refers to a set of matrices $D(g)$, representing the elements g of a symmetry group \mathcal{G} and satisfying the multiplication table of the group, as a d -dimensional matrix

representation.

To give an example of matrix representation, one considers a 3D basis defined by the vectors $\hat{e}_x, \hat{e}_y, \hat{e}_z$. By application of every element $g \in \mathcal{G}$ to the basis (corresponding to a passive operation) one obtain a new basis \hat{e}'_i . The two basis can be related by introducing a rotation matrix $\mathfrak{R} = \mathfrak{R}(g) \forall g \in \mathcal{G}$ in such a way that

$$\hat{e}'_i = \sum_j \mathfrak{R}_{ji}(g) \hat{e}_j \quad (2.2)$$

The set of 3D matrix $\{\mathfrak{R}(g)\}$ satisfy the multiplication table of the group, then forms a 3D representation of the group.

If every matrix $D(g)$ is unitary, $\{D\}$ form a **unitary representation** and when one associates a different matrix $D(g)$ to every g the representation are called **faithful**. For a faithful representation, the homomorphic mapping is a one-to-one mapping (isomorphism) and if one knows a matrix one immediately identifies the corresponding element of the group.

For every non-singular matrix S (i.e. non-zero determinant \Leftrightarrow the inverse exists), the set of matrices

$$\{D'(g) = S^{-1}D(g)S\} \quad (2.3)$$

form an **equivalent representation** and one notes $D' \approx D$. If one comes back to the example of 3D representation presented above, if the \hat{e}_i basis transforms like $D(g)$, a new basis $\hat{e}_i \doteq \sum_j S_{ji} \hat{e}_j$ transforms with an equivalent representation $\{D'(g)\}$ as given in (2.3). For every matrix representation, one defines the **characters of the representation** as the traces of the matrices and note

$$\chi(g) = \text{tr}D(g) \quad (2.4)$$

Two equivalent representations have the same characters, then each representation is characterized in a unique way by the set of numbers $\{\chi(g)\}$ and corresponds to an infinite set of equivalent matrix representations. Indeed the concept of matrix representation is strictly related to a specific choice of the corresponding basis.

If a specific choice of basis vectors can be found in such a way that every matrix $D(g)$ has a block-diagonal form

$$D(g) = \left(\begin{array}{c|c} D^{(1)}(g) & 0 \\ \hline 0 & D^{(2)}(g) \end{array} \right) \quad (2.5)$$

one has a **reducible representation** and the block-diagonal form is called the reduced form of the representation. One formally notes

$$D \approx D^{(1)} \oplus D^{(2)} \quad (2.6)$$

and this means that the basis vectors of the first block cannot be coupled to those of the second block by operations of the group. To give an example, the rotation of an arbitrary basis $\{\hat{e}_x, \hat{e}_y, \hat{e}_z\}$ are represented by 3D matrices, but in the particular case of symmetry operation acting only in a plane, a particular set of basis vectors with \hat{e}_x perpendicular to the plane and \hat{e}_y, \hat{e}_z in the plane can be chosen (see Fig. 2.1). With respect to this basis, the rotation matrices can be written in a 1×2 block-diagonal form

$$\mathfrak{R}_{3D} = \left(\begin{array}{c|c} 1 & 0 \\ \hline 0 & \mathfrak{R}_{2D} \end{array} \right) \quad (2.7)$$

where \hat{e}_x is uncoupled and invariant with respect to every operation.

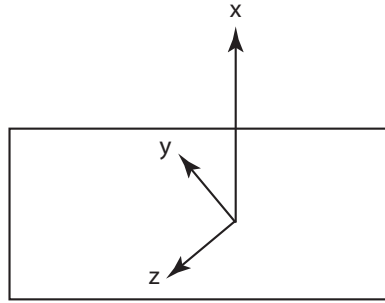


Figure 2.1: Schematic of optimal basis for 2D rotations

Finally, an **irreducible representation (irrep)** is a representation not reducible: the corresponding basis vectors are mutually coupled by the symmetry operation with respect to every choice of basis.

For a given group, it exists an infinity of representations (from two representations a new representation can always be constructed as in (2.5)), but only a small number of irreducible representation. In the next paragraph, we introduce the concept of **table of characters** characterizing every group \mathcal{G} by a list of the different irreps of the group with the corresponding characters.

2.1.4 Table of characters

Every group has only a small number of irreps, noted Γ in the following, and every irrep is characterized by the characters $\chi^\Gamma(g), \forall g \in \mathcal{G}$. In this

paragraph we want to show how to construct in a simple way the character table for a group.

First, one introduces the definition of **class of a group**: the elements $g \in \mathcal{G}$ can be regrouped in disjointed subsets called (conjugacy) classes of the group. Each class contains every mutually conjugate elements of \mathcal{G} where $g_1, g_2 \in \mathcal{G}$ are **conjugated elements** if exists an element $\tilde{g} \in \mathcal{G}$ in such a way that $g_2 = \tilde{g}^{-1}g_1\tilde{g}$.

Every element of a class have the same character, then for a group, the number of irreps correspond to the number of class. The dimensions d_i of the irreps Γ_i are related to the cardinality of the group $h = |\mathcal{G}|$: $\sum_i d_i^2 = h$. To give an example, for a group with six elements regrouped in three classes, one has the dimensions $d_1 = 1, d_2 = 1, d_3 = 2$.

A standard procedure to obtain characters for the irreps is presented in Bassani (Ch 1) [29], but in a more practical way, in the point-group table of Altmann [3] every information about classes and irrep can be found for every group (more information about the Altmann tables are given in 2.5). In Sec. 2.6, some groups (C_s , C_{2v} and C_{3v}) are presented to illustrate the concept of table of characters.

2.2 Application to the Schrödinger equation

In this section, one first applies group theory to a scalar Schrödinger equation to obtain transformation laws of Hamiltonian and wave functions, then one introduces the concept of symmetry group of an Hamiltonian and finally the effects of symmetry and relation with irreps on the functions are presented.

2.2.1 Transformation laws

In a passive point of view, symmetry operations are computed on the basis vectors $\{\hat{e}_i\}$ and the new basis

$$\hat{e}'_i = \sum_j \mathfrak{R}_{ji} \hat{e}_j \quad (2.8)$$

is obtained by introducing a matrix \mathfrak{R} . Considering a vector \vec{r} , the components $\mathbf{r} = (x_1, x_2, x_3)$ with respect to $\{\hat{e}_i\}$ and $\mathbf{r}' = (x'_1, x'_2, x'_3)$ with respect to $\{\hat{e}'_i\}$ are related by

$$\sum_i x_i \hat{e}_i = \sum_i x'_i \hat{e}'_i \quad \Rightarrow \quad \mathbf{r}' = \mathfrak{R}^{-1} \mathbf{r} \quad (2.9)$$

Then a scalar function $\psi(\mathbf{r})$ is described by a new mathematical function ψ' with respect to the new basis. At a fixed point \vec{r} , the functions have the same value and this allows to express the new function as

$$\psi'(\mathbf{r}') = \psi(\mathbf{r}) \quad \Rightarrow \quad \psi'(\mathbf{r}') = \psi(\mathfrak{R}\mathbf{r}') \quad (2.10)$$

To formalize, for every passive operation g an operator $\vartheta_{g^{-1}}$ can be introduced in such a way that

$$\psi'(\mathbf{r}) = \vartheta_{g^{-1}}\psi(\mathbf{r}) = \psi(\mathfrak{R}\mathbf{r}) \quad (2.11)$$

In the following, the prime label on \mathbf{r}' is omitted. Finally, with this notation, one obtains the following transformation law for a scalar Hamiltonian $H(\mathbf{r})$.

$$H'(\mathbf{r}) = \vartheta_{g^{-1}}H(\mathbf{r})\vartheta_{g^{-1}}^{-1} = H(\mathfrak{R}\mathbf{r}) \quad (2.12)$$

This transformation rule of Hamiltonians is easy understood considering that the energy (matrix element of the Hamiltonian) is a scalar and is independent of the choice of the basis: with the formal Dirac notation $|\psi'\rangle = \vartheta|\psi\rangle$, where the index referring to the symmetry operation g is understood

$$E' = \langle\psi'|H'|\psi'\rangle = \langle\psi|\underbrace{\vartheta^{-1}}_{\mathbb{I}}(\vartheta H \vartheta^{-1})\underbrace{\vartheta}_{\mathbb{I}}|\psi\rangle = \langle\psi|H|\psi\rangle = E \quad (2.13)$$

Finally, one defines the **symmetry group** of an Hamiltonian, as the group $\mathcal{G} = \{g\}$ of the elements g keeping the Hamiltonian invariant

$$H'(\mathbf{r}) = H(\mathbf{r}) \quad (2.14)$$

or in a more rigorous way, the elements commuting with the Hamiltonian $[H, \vartheta_g] = 0$. For a general Hamiltonian $H = -\frac{\hbar^2}{2m}\Delta + V(\mathbf{r})$, the kinetic part is invariant with respect to every symmetry operations and the shape of the potential is only invariant with respect to every symmetry operation of the group.

2.2.2 Symmetry of the functions

Considering a scalar Hamiltonian H with symmetry group \mathcal{G} , energy E and wave functions $|\psi\rangle$ are solution of an eigenvalue problem

$$H|\psi\rangle = E|\psi\rangle \quad (2.15)$$

With respect to an arbitrary symmetry operation $g \in \mathcal{G}$, one obtains from

$$H|\psi'\rangle = H\vartheta|\psi\rangle \stackrel{[H,\vartheta]=0}{=} \vartheta H|\psi\rangle \stackrel{(2.15)}{=} E|\psi'\rangle \quad (2.16)$$

that the new function have the same energy E ! This means that $\psi'(\mathbf{r})$ belong to the same eigen-space as $\psi(\mathbf{r})$ and, for a d -degenerate eigenstate, one has d linear independent functions $\psi_i(\mathbf{r})$ with the same energy E forming a d -D basis $\{\psi_i(\mathbf{r})\}$. The new functions $\psi'_i(\mathbf{r})$, $i = 1, \dots, d$ can then be decomposed with respect to this basis by introducing matrices $D(g)$ as

$$\psi'_i(\mathbf{r}) = \sum_j D_{ij}^*(g)\psi_j(\mathbf{r}) = \sum_j D_{ji}(g^{-1})\psi_j(\mathbf{r}) \quad (2.17)$$

The set of matrices $\{D(g)\}$ satisfy the multiplication of the group then from a d -D representation of the group and, in particular, the d -D are irreducible (except in the particular case of an accidental degeneracy, where the representation can be reduced).

One obtains one of the main results of application of group theory to the quantum mechanics: the energy levels and eigenstates of an Hamiltonian with symmetry group \mathcal{G} can be labelled with respect to the symmetry as

$$\begin{cases} E & = E^\Gamma \\ \psi(\mathbf{r}) & = \psi_i^\Gamma(\mathbf{r}) \end{cases} \quad (2.18)$$

where Γ represent the irreducible representation and $i = 1, \dots, d$ is the partner function index, labelling the different functions of the basis.

One notes that there are exactly the same transformations rules for the functions (2.18) as for the \hat{e}_i basis vector presented above, and the matrices $D(g)$ depend of the choice of the basis.

A particular case is for the non-degenerate states related to a 1D irrep: $\psi'(\mathbf{r})$ and $\psi(\mathbf{r})$ are simply linear dependent and the matrices correspond to the character of the corresponding representation $D(g) = \chi^\Gamma(g)$. From Eq. (2.10) and (2.17) one obtains the simple symmetry properties

$$\psi(\mathfrak{R}\mathbf{r}) = \chi^* \psi(\mathbf{r}) \quad (2.19)$$

with respect to every operation $g \in \mathcal{G}$. For the degenerate irreps, under a symmetry operation the different basis functions are mixed

$$\psi_i(\mathfrak{R}\mathbf{r}) = \sum_j D_{ij}^* \psi_j(\mathbf{r}) \quad (2.20)$$

One always can find a function basis in which one (or more) matrix is diagonal and obtain corresponding symmetry properties for every partner function

$$\psi_i(\mathfrak{R}\mathbf{r}) = D_{ii}^* \psi_i(\mathbf{r}) \quad (2.21)$$

but not with respect to every symmetry operation (the representation is irreducible, then one can not diagonalize every symmetry operation at the same time).

2.3 From single group to double group

In this section, we first quickly recall the definition of point group, then give an introduction to the 3D rotation group $SO(3)$ and spin group $SU(2)$ before introducing the concept of double group of a point group related to the spin dependent problems. In conclusion, some important remark on the inversion are presented.

2.3.1 The point group

In 3.1 a short introduction of the symmetry of crystal structure for the bulk semiconductors is given. Here, one only recall that a point group is the group composed of rotations and roto-inversions (improper rotations i.e. mirrors) keeping invariant a given point.

In a constructive approach, matrix representations of improper operations like $\sigma_{\hat{s}}$, a mirror symmetry defined by its normal \hat{s} , can be obtained by factor out the inversion i in such a way that $\sigma_{\hat{s}} = iC_2(\hat{s})$, where $C_2(\hat{s}) = R(\pi, \hat{s})$ is a π -rotation around the axis \hat{s} . For a 3D rotation, one obviously has the spatial inversion $\mathfrak{R}(i) = -I_3$ corresponding to $x_i \rightarrow -x_i$.

A pure rotational group is then a sub-group of the 3D rotational group $SO(3)$ and a more general point group, a sub-group of $O(3) = SO(3) \otimes C_i$, where $C_i = \{E, i\}$ is the group of the inversion. One recalls that a **sub-group** \mathcal{H} of a group \mathcal{G} , is a sub-set of \mathcal{G} with the same (multiplication) law.

In the next section, one presents the $SO(3)$ group. Three Euler Angles parametrize every 3D rotation and allow to obtain an analytical expression for the rotation matrices, then for every point group, one immediately obtains the 3D representation giving the transformation rules for the basis vectors $\{\hat{e}_i\}$ by taking the corresponding subset of matrices.

2.3.2 The rotational $SO(3)$ group

One defines the $O(n)$ group as the group of the $n \times n$ orthogonal matrices ($M^T M = \mathbb{I}$), where M^T is the transposition of the matrix M . $SO(n)$ is the group of the special ($|M| = 1$) $n \times n$ orthogonal matrices and the $SO(3)$ group is isomorphic to the subgroup of the proper rotations.

Every proper rotation can be parameterized by three Euler angles (α, β, γ) as presented in Messiah (appendix C) [30]. By introducing the generators of the rotation J_i one obtains an analytical expression for the matrices [30].

$$\begin{aligned} \mathfrak{R}(\alpha \beta \gamma) &= e^{-i\alpha J_z} e^{-i\beta J_y} e^{-i\gamma J_z} \\ &= \begin{pmatrix} \cos(\alpha) \cos(\beta) \cos(\gamma) - \sin(\alpha) \sin(\gamma) & -\cos(\gamma) \sin(\alpha) - \cos(\alpha) \cos(\beta) \sin(\gamma) & \cos(\alpha) \sin(\beta) \\ \cos(\beta) \cos(\gamma) \sin(\alpha) + \cos(\alpha) \sin(\gamma) & \cos(\alpha) \cos(\gamma) - \cos(\beta) \sin(\alpha) \sin(\gamma) & \sin(\alpha) \sin(\beta) \\ -\cos(\gamma) \sin(\beta) & \sin(\beta) \sin(\gamma) & \cos(\beta) \end{pmatrix} \end{aligned} \quad (2.22)$$

More information about the exponential form of the \mathfrak{R} matrices can be found in [25, 31] ($SO(3)$ is a Lie group and the generator of the rotation J_i are elements of the corresponding Lie algebra $\mathfrak{so}(3)$: using an exponential mapping one obtains the group elements from the algebra elements).

The 3D representation for the inversion is $\mathfrak{R}(i) = -\mathbb{I}_3$ and by factor out the inversion, every element of $O(3)$ can be construct with the help of Eq. (2.22).

2.3.3 The $SU(2)$ group

$SU(2)$ is the group of the special unitary ($M^+M = \mathbb{I}_2$) 2×2 matrices and correspond to the rotation matrices for a spinor $j = \frac{1}{2}$.

In the same way as Eq. (2.22) one obtains an explicit form for the rotation matrices

$$W^{1/2}(\alpha \beta \gamma) = e^{-i\alpha J_z^{1/2}} e^{-i\beta J_y^{1/2}} e^{-i\gamma J_z^{1/2}} = \begin{pmatrix} e^{-\frac{1}{2}i(\alpha+\gamma)} \cos(\frac{\beta}{2}) & -e^{-\frac{1}{2}i(\alpha-\gamma)} \sin(\frac{\beta}{2}) \\ e^{\frac{1}{2}i(\alpha-\gamma)} \sin(\frac{\beta}{2}) & e^{\frac{1}{2}i(\alpha+\gamma)} \cos(\frac{\beta}{2}) \end{pmatrix} \quad (2.23)$$

where the generators of the rotation are now related to the Pauli matrices

$$J_x^{1/2} = \frac{1}{2} \sigma_x = \begin{pmatrix} 0 & \frac{1}{2} \\ \frac{1}{2} & 0 \end{pmatrix} \quad ; \quad J_y^{1/2} = \frac{1}{2} \sigma_y = \begin{pmatrix} 0 & -\frac{i}{2} \\ \frac{i}{2} & 0 \end{pmatrix} \quad ; \quad J_z^{1/2} = \frac{1}{2} \sigma_z = \begin{pmatrix} \frac{1}{2} & 0 \\ 0 & -\frac{1}{2} \end{pmatrix} \quad (2.24)$$

One calls this matrices Wigner operator for $j = \frac{1}{2}$. There are two important remarks concerning the $SO(3)$ and $SU(2)$ group:

- Both 3D \mathfrak{R} and spin W matrices depend of the three Euler angles. In other words, the 3D matrices depend on the spin matrices: $\mathfrak{R} = \mathfrak{R}(W^{1/2})$.
- The rotation of 2π gives the identity for $SO(3)$ ($\mathfrak{R}(2\pi) = \mathbb{I}_3$) but $W^{1/2}(2\pi) = -\mathbb{I}_2$ and a rotation of 4π have to be computed to obtain the identity.

In the next paragraphs, one justifies the expression $\mathfrak{R} = \mathfrak{R}(W^{1/2})$, introduce the representation for the inversion and define the concept of double group for the spin-dependent problems.

2.3.4 Link between $SU(2)$ and $SO(3)$

The dependence between \mathfrak{R} and $W^{1/2}$ matrices can be easily understood by considering that the group $SU(2)$ and $SO(3)$ are homomorphic. More precisely, a two-to-one homomorphic mapping of the group $SU(2)$ onto the group $SO(3)$ exist. This means that $\forall W \in SU(2)$, one has $\mathfrak{R}(W) = \mathfrak{R}(-W)$ and the mapping can be chose so that

$$[\mathfrak{R}(W)]_{ij} = \frac{1}{2} \text{tr} (\sigma_i W \sigma_j W^{-1}) \quad (2.25)$$

where σ_i are the Pauli matrices. In other words, to every rotation R , one associates a 3D rotation matrix \mathfrak{R} and two matrices $\{W^{1/2}, -W^{1/2}\}$ for spin $j = 1/2$ rotation matrices.

Considering a point group \mathcal{G} , subgroup of pure rotation $SO(3)$, one can construct with Eq. (2.22) a 3D representation of the group: if $g_1 g_2 = g_3$ then $\mathfrak{R}(g_1) \mathfrak{R}(g_2) = \mathfrak{R}(g_3)$. In the same way, with Eq. (2.23) one constructs a set of matrices $\{W(g)\}$, but $W(g_1)W(g_2) = W(g_3)$ or $W(g_1)W(g_2) = -W(g_3)$ and this set of matrices do not form a representation of the group. In a rigorous way, one calls a set of matrices with transformation rule $W(g_1)W(g_2) = \omega(g_1, g_2)W(g_3)$, where $\omega(g_1, g_2)$ is a phase term, a **projective representation** of the group.

2.3.5 The inversion

The symmetry operations of a point group are rotations and roto-inversion, the next step is to introduce a matrix representation $W^{1/2}(i)$ for the inversion. First, one remarks that inversion commute with every rotation of $SO(3)$, then, according to the second Schur's lemma (see Cornwell [25]), is a multiple of the identity. Finally, it can be shown [29] that to the inversion i one can associate $W(i) = \mathbb{I}_2$.

2.3.6 The double group

To restore the group property for the $\{W\}$ matrices, one usually considers a new group, the **double group** $\tilde{\mathcal{G}}$ of \mathcal{G} defined by

$$\tilde{\mathcal{G}} = \{g, \tilde{g} = -g\} \forall g \in \mathcal{G} \quad (2.26)$$

This group has twice element and group properties is restored: $W(g_1)W(g_2) = W(g_3)$ or $W(g_1)W(g_2) = W(\tilde{g}_3)$

To conclude this paragraph, first one notes that $\tilde{\mathcal{G}}$ is not the same group as \mathcal{G} and this new group contain some additional irreps. Finally:

- scalar function transform with the single group irreps
- spinorial states transform with the additional irreps of the double group

From the more practical point of view, instead of deal with g and \tilde{g} one usually associates $W(g)$ or $W(\tilde{g})$ (arbitrary choice!) to the symmetry operation g taking in the mind that some -1 appear in the multiplication table. In the following, one takes the same conventions as Altmann [3] (more details are given in Sec. 2.5) with, in particular, $W(i) = +\mathbb{I}_2$ for the inversion.

2.3.7 Transformation law for the “spinorial” Bloch function basis

In paragraph 2.3.4 one showed that exist a two-to-one homomorphic mapping of the group $SU(2)$ onto the group $SO(3)$ then an explicit dependence $\mathfrak{R}(W^{1/2})$ exist between 3D and spin matrices.

In 3.1.6 we will introduce the $k \cdot p$ formalism to study energy band of semiconductors and here we only recall that for a model describing the conduction band involving spin of carriers, one will obtain 2×2 operator with respect to a so-called Bloch function basis $|\frac{1}{2}, \pm\frac{1}{2}\rangle = |s\rangle \otimes |\pm\rangle$ where $|s\rangle$ is a scalar function and $|\pm\rangle$ is the spin $j = \frac{1}{2}$ of the electrons.

$|\frac{1}{2}, m\rangle$ behaves in the same way as a state of a spin variable transforming with the Wigner representation $W^{1/2}$ as

$$|j, m\rangle' = \sum_n W_{nm}^j |j, n\rangle \quad (2.27)$$

but *is essential to note that $|\frac{1}{2}, m\rangle$ are not spin variables but transform like spin variables!*

In a spin-dependent problem with spin-orbit coupling, one can not separate the orbital and spinorial $|\pm\rangle$ part, but, and this is one of the main basic idea of this PhD thesis, one can explicitly separate orbital and Bloch function part. The Bloch function part is usual called spinorial part but is not related to the spin $j = \frac{1}{2}$ of the electron and \mathfrak{R} and $W^{1/2}$ can be consider completely independent.

In the same way, to study valence band, $|\frac{3}{2}, m\rangle$ Bloch function basis are

involved transforming like a $j = \frac{3}{2}$ 4D spinor. In Messiah [30], analytical expression for Wigner operator for the valence band are presented and obtain

$$W^{3/2}(\alpha \beta \gamma) = \begin{pmatrix} e^{\frac{1}{2}i(-3\alpha-3\gamma)} \cos^3\left(\frac{\beta}{2}\right) & -\sqrt{3}e^{\frac{1}{2}i(-3\alpha-\gamma)} \cos^2\left(\frac{\beta}{2}\right) \sin\left(\frac{\beta}{2}\right) \\ \sqrt{3}e^{\frac{1}{2}i(-\alpha-3\gamma)} \cos^2\left(\frac{\beta}{2}\right) \sin\left(\frac{\beta}{2}\right) & e^{\frac{1}{2}i(-\alpha-\gamma)} \left(\cos^3\left(\frac{\beta}{2}\right) - 2\cos\left(\frac{\beta}{2}\right) \sin^2\left(\frac{\beta}{2}\right)\right) \\ \sqrt{3}e^{\frac{1}{2}i(\alpha-3\gamma)} \cos\left(\frac{\beta}{2}\right) \sin^2\left(\frac{\beta}{2}\right) & e^{\frac{1}{2}i(\alpha-\gamma)} \left(2\cos^2\left(\frac{\beta}{2}\right) \sin\left(\frac{\beta}{2}\right) - \sin^3\left(\frac{\beta}{2}\right)\right) \\ e^{\frac{1}{2}i(3\alpha-3\gamma)} \sin^3\left(\frac{\beta}{2}\right) & \sqrt{3}e^{\frac{1}{2}i(3\alpha-\gamma)} \cos\left(\frac{\beta}{2}\right) \sin^2\left(\frac{\beta}{2}\right) \\ \sqrt{3}e^{\frac{1}{2}i(\gamma-3\alpha)} \cos\left(\frac{\beta}{2}\right) \sin^2\left(\frac{\beta}{2}\right) & -e^{\frac{1}{2}i(3\gamma-3\alpha)} \sin^3\left(\frac{\beta}{2}\right) \\ e^{\frac{1}{2}i(\gamma-\alpha)} \left(\sin^3\left(\frac{\beta}{2}\right) - 2\cos^2\left(\frac{\beta}{2}\right) \sin\left(\frac{\beta}{2}\right)\right) & \sqrt{3}e^{\frac{1}{2}i(3\gamma-\alpha)} \cos\left(\frac{\beta}{2}\right) \sin^2\left(\frac{\beta}{2}\right) \\ e^{\frac{1}{2}i(\alpha+\gamma)} \left(\cos^3\left(\frac{\beta}{2}\right) - 2\cos\left(\frac{\beta}{2}\right) \sin^2\left(\frac{\beta}{2}\right)\right) & -\sqrt{3}e^{\frac{1}{2}i(\alpha+3\gamma)} \cos^2\left(\frac{\beta}{2}\right) \sin\left(\frac{\beta}{2}\right) \\ \sqrt{3}e^{\frac{1}{2}i(3\alpha+\gamma)} \cos^2\left(\frac{\beta}{2}\right) \sin\left(\frac{\beta}{2}\right) & e^{\frac{1}{2}i(3\alpha+3\gamma)} \cos^3\left(\frac{\beta}{2}\right) \end{pmatrix} \quad (2.28)$$

2.3.8 Transformation law for spinorial functions

With respect to a spinorial Bloch function basis $\{|j, m\rangle\}$, where $m = j, \dots, -j$, eigenstates are represented by $(2j + 1)$ -D spinorial functions as

$$\underline{\psi}(\mathbf{r}) = (\psi_j(\mathbf{r}), \dots, \psi_{-j}(\mathbf{r}))^T = \sum_m \psi_m(\mathbf{r}) |j, m\rangle \quad (2.29)$$

where every (envelope) function $\psi_m(\mathbf{r})$ is a scalar function. For a conduction band problem including spin, $j = \frac{1}{2}$ and spinors have two components, for a valence band problem, $j = \frac{3}{2}$ and one deals with 4D spinors.

In the same as for scalar functions (2.11), one formally introduce an operator $\vartheta^{(j)}$ acting in the Bloch function basis space and the new spinorial state with respect to a new basis obtained by (2.27) is given by

$$\underline{\psi}'(\mathbf{r}) = W^{-1} \underline{\psi}(\mathbf{r}) \quad (2.30)$$

where $W = W^j$ (the index j is omitted in the following).

Finally, for a spinorial state $\underline{\psi}$ one has two basis:

- The 3D basis $\{\hat{e}_i\}$, new basis is obtained with a 3D matrix \mathfrak{R}_{g_1} according to Eq. (2.8) and the new function by (2.10) by introducing an operator $\vartheta_{g_1^{-1}}^{(3D)}$
- The $(2j + 1)$ -D spinorial basis $\{|j, m\rangle\}$, new basis is obtained with a $(2j + 1)$ matrix W_{g_2} according to Eq. (2.27) and the new function by (2.30) by introducing an operator $\vartheta_{g_2^{-1}}^{(j)}$

The two operators $\vartheta_{g_1^{-1}}^{(3D)}$ and $\vartheta_{g_2^{-1}}^{(j)}$ act in different spaces (3D space and Bloch function (“spinorial”) space, then one can construct a total operator by tensorial product as

$$\vartheta_{g_1^{-1}, g_2^{-1}} = \vartheta_{g_1^{-1}}^{(3D)} \otimes \vartheta_{g_2^{-1}}^{(j)} \quad (2.31)$$

In particular, one simply notes $\vartheta_{g^{-1},g^{-1}} = \vartheta_{g^{-1}}$. A fully transformation of a spinorial function is given by a change of both basis and the new function is given by

$$\underline{\psi}'(\mathbf{r}) = \vartheta_{g^{-1}}\underline{\psi}(\mathbf{r}) = \vartheta_{g^{-1}}^{(3D)} \otimes \vartheta_{g^{-1}}^{(j)}\underline{\psi}(\mathbf{r}) = \vartheta_{g^{-1}}^{(j)}\underline{\psi}(\mathfrak{R}\mathbf{r}) = W^{-1}\underline{\psi}(\mathfrak{R}\mathbf{r}) \quad (2.32)$$

The general expression (2.20) giving the symmetry properties of a scalar function can be immediately generalized to the spinorial problem and reads

$$\underline{\psi}'_i(\mathbf{r}) = W^{-1}\underline{\psi}_i(\mathfrak{R}\mathbf{r}) = \sum_j D_{ij}^* \underline{\psi}_j(\mathbf{r}) \quad (2.33)$$

In the same way as in Eq. (2.12), one obtains the transformation law for the Hamiltonian

$$\begin{aligned} H'(\mathbf{r}) &= \vartheta_{g^{-1}}H(\mathbf{r})\vartheta_{g^{-1}}^{-1} = \vartheta_{g^{-1}}^{(3D)} \otimes \vartheta_{g^{-1}}^{(j)}H(\mathbf{r})\vartheta_{g^{-1}}^{-1(j)} \otimes \vartheta_{g^{-1}}^{-1(3D)} = \vartheta_{g^{-1}}^{(j)}H(\mathfrak{R}\mathbf{r})\vartheta_{g^{-1}}^{-1(j)} \\ &\Rightarrow H'(\mathbf{r}) = W^{-1}H(\mathfrak{R}\mathbf{r})W \end{aligned} \quad (2.34)$$

To conclude this introduction to the transformation laws of spinorial states and Hamiltonians, one recalls that the different components of the $(2j+1) \times (2j+1)$ Hamiltonian act only on the scalar (envelope) functions $\psi_m(\mathbf{r})$ and not on the basis vectors $|j, m\rangle$ (considered as “spin variables”): this is an essential point because 3D space and Bloch function space are completely independent (the total Hilbert space $\mathcal{H}^{\otimes(2j+1)}$ is constructed by tensorial product from the scalar Hilbert space $\mathcal{H} \otimes \mathbb{C}^{2j+1}$) and allow to decompose every operator in the form (2.31).

Finally, we note that Eqs. (2.11) and (2.32) give the transformation law for scalar and spinorial functions respect to any new basis. Symmetry properties (2.20) and (2.33) are valid only for symmetry operations $g \in \mathcal{G}$

2.4 Wigner-Eckart theorem and selection rules

In this section, one introduces one of the most important theorems of group theory: the Wigner-Eckart Theorem (WET) allowing to obtain rigorous analytical selection rules for matrix elements of operators only linked with symmetry properties of operators and states. To gives an example, to study optical properties of heterostructures, one computes the dipolar matrix elements between a conduction and a valence band state and WET gives the forbidden transition.

First, one recalls some useful definition (conjugated representation, product of representations and irreducible set of tensorial operators) allowing to understand the WET theorem. In section 2.6.4, an illustration of WET is presented starting from the simple C_s group (even/odd functions).

2.4.1 Conjugated representations

One consider the matrix representation $\{D^\Gamma(g)\}$ for a given irrep Γ of a group \mathcal{G} .

The set $\{(D^\Gamma)^*(g)\}$ form a matrix representation of the **conjugate representation** Γ^* of Γ : $\{D^{\Gamma^*}(g)\}$.

Three cases are possible:

- (a) Γ is a real representation: $D^\Gamma(g) = D^{\Gamma^*}(g)$
- (b) Γ is a pseudoreal representation: the representations are complex but equivalent $D^\Gamma(g) \approx D^{\Gamma^*}(g)$. One calls Γ a **self-conjugated irrep**
- (c) Γ^* is not equivalent to Γ . One says that Γ and Γ^* are **mutually conjugated irrep**

The concept of conjugated irrep is very important in quantum mechanics.

First, in the Dirac notation a ket $|\psi\rangle$ represent a vector of an Hilbert space \mathcal{H} with transformation rule $|\psi'_i\rangle = \sum_j D_{ij}^* |\psi_j\rangle$. A bra $\langle\psi|$ is a co-vector (an element of the dual space of the linear applications) with transformation rule $\langle\psi'_i| = \sum_j D_{ij} \langle\psi_j|$, then transforming like the conjugated irrep.

Second, Hamiltonians are invariant with respect to an additional symmetry: the time reversal symmetry, represented by an anti-unitary operator T . If an eigenstate $|\psi\rangle$ transform like the Γ irrep, the function $T|\psi\rangle$ transform with Γ^* . Computing the conduction or valence band structure for a QWR, the symmetry with respect to the time reversal can give some additional degeneracy at the center of zone $\mathbf{k} = \mathbf{0}$ (Kramers degeneracy). As presented in Bassani [29], for the spinless eigenstates one has additional degeneracy for the cases (b) and (c), and for the spin-dependent eigenstates for cases (a) and (c).

2.4.2 Direct product of representations

The concept of product of representations is essential to understand WET. The simple way to introduce this concept, is to consider two set of partner functions: $\{\varphi_i\}$, $i = 1, \dots, d_{\Gamma_1}$ and $\{\phi_j\}$, $j = 1, \dots, d_{\Gamma_2}$ transforming with Γ_1 and, respectively, Γ_2 irreps. To obtain the transformation rule of the function product $\varphi_i\phi_j$ one considers a new basis, of dimension $d = d_{\Gamma_1}d_{\Gamma_2}$, given by every product of functions:

$$\{\psi_1 \doteq \varphi_1\phi_1, \psi_2 \doteq \varphi_1\phi_2, \dots, \psi_d \doteq \varphi_{d_{\Gamma_1}}\phi_{d_{\Gamma_2}}\} \quad (2.35)$$

This set of functions, transform with a new d -dimension representation noted $\Gamma_1 \otimes \Gamma_2$ and called the **direct product representation**. A matrix representation can be explicitly constructed with the direct product of matrices $D^{\Gamma_1 \otimes \Gamma_2} = D^{\Gamma_1} \times D^{\Gamma_2}$ as

$$A \times B = \begin{pmatrix} A_{11}B & A_{12}B & \dots \\ A_{21}B & A_{22}B & \dots \\ \vdots & \vdots & \ddots \end{pmatrix} \quad (2.36)$$

Two cases are conceivable:

- The direct product representation is irreducible $\Gamma_1 \otimes \Gamma_2 \approx \Gamma_3$
- The direct product representation is reducible. A new basis of function can be found block-diagonalizing the representation and one formally notes $\Gamma_1 \otimes \Gamma_2 \approx \oplus_i \Gamma_i$, where i label the different irreps Γ_i appearing in the reduction.

2.4.3 Irreducible set of Tensorial Operators (ITO)

One has introduced the transformation law for a function transforming with the irrep Γ : $\psi_i^\Gamma(\mathbf{r}) = \sum_j D_{ji}^\Gamma(g^{-1})\psi_j^\Gamma(\mathbf{r})$. In the same way a set of operators $\{A_i^\Gamma\}$ with transformation rule

$$A_i^\Gamma = \sum_j D_{ji}^\Gamma(g^{-1})A_j^\Gamma \quad (2.37)$$

is called a **set of Irreducible Tensorial Operators (ITO)** transforming with Γ .

The simplest example of ITO is the Hamiltonian: H is invariant with respect to every symmetry operation of the group, then H is an ITO transforming with the identity irrep (1D irrep with every characters equal to 1, noted A_1 in the Altmann notations [3], and existing for every group).

2.4.4 The Wigner-Eckart Theorem (WET)

Now one disposes of every definition to formulate and understand the Wigner-Eckart Theorem (WET). The aim of the theorem is to analytically obtain the selection rules for the matrix elements of an operator $\langle \psi_1 | A | \psi_2 \rangle$.

Label states and operator with respect to the irreps of the corresponding symmetry group \mathcal{G} , allow to formulate the WET:

$$\langle \psi_1^{\Gamma_1} | A^{\Gamma_3} | \psi_2^{\Gamma_2} \rangle = 0 \quad \Leftrightarrow \Gamma_1 \text{ don't appear in the reduction of } \Gamma_3 \otimes \Gamma_2 \quad (2.38)$$

The simplest way to understand the WET, is to consider the operator identity ($A = \mathbb{I}$): the matrix elements simply correspond to the scalar product $\langle \psi_1^{\Gamma_1} | \psi_2^{\Gamma_2} \rangle = 0$ if $\Gamma_1 \neq \Gamma_2$ (no overlap between function with different symmetry).

An alternative expression of the WET is: $\langle \psi_1^{\Gamma_1} | A^{\Gamma_3} | \psi_2^{\Gamma_2} \rangle = 0$ if the identity irrep A_1 do not appear in the reduction of $\Gamma_1^* \otimes \Gamma_3 \otimes \Gamma_2$. The matrix elements of the operator A^{Γ_3} , $\langle \psi_1^{\Gamma_1} | A^{\Gamma_3} | \psi_2^{\Gamma_2} \rangle$, are scalar (simply a number) and a scalar is always invariant with respect to every basis then belong inevitably to the identity irrep A_1 .

2.5 Group theory tables

The Point-group theory table of Altmann [3] is a powerful and almost essential tool for people who want to practically apply group theory to a physical problem: for every point-group, every important information is presented in the corresponding tables.

In this subsection, one wants to give a short introduction to how to use and find informations on this book (in the first part of the book a complete introduction on the notations and tables is given). One presents the more important tables, but additional tables, more complicated or not directly necessary for this work, are too in the book (see introduction to the tables of [3] for more informations).

In the first part a short description of the group is given (number of elements $|G|$, classes $|C|$) and symmetry operations are separated into the corresponding classes and graphically presented. In the first table **parameters**, the Euler angles for every symmetry operation are given (inversion is factored out).

2.5.1 Character table

In this table, the characters for every irrep are tabulated. One notes that there are two different conventions for the name of the irreps: in the book of Koster [32], the irreps are simply called $\Gamma_1, \Gamma_2, \Gamma_3, \dots$ and any information on the irrep can be obtained from the name. On the other hand in Altmann [3] some convention are made for the names.

For single group notations, one has, with eventually subscripts $i = 1, 2$ to distinguish different irreps:

- A and B represent non-degenerate irreps, symmetrical and respectively antisymmetrical with respect to the principal axis rotations

- E doubly-degenerate irrep or a pair of non-degenerate mutually conjugated irreps (left superscript $i = 1, 2$)
- T triply-degenerate irrep
- F four-fold degenerate irrep or or a pair of doubly-degenerated mutually conjugated irreps (left superscript $i = 1, 2$)
- H and I are five and six-fold-degenerate irreps

For double group, one has the same kind of notations A, \dots, I but with a half-integer subscript $n/2$, indicating that the corresponding representation is spanned by spinor basis $j = n/2$.

Finally, for both simple and double group, additional prime and second on every symbol represent symmetrical and antisymmetrical irreps with respect to a horizontal symmetry plane, and additional g and u subscript represent irrep even (gerade) or odd (ungerade) with respect to the inversion.

2.5.2 Multiplication table

For every group, one has a multiplication table $g_1 g_2 = g_3$. One recalls that, for the double group, if one associates a matrix representation to every symmetry operation g according to some convention, $g_1 g_2 = +g_3$ or $= -g_3$. In **factor table** are displayed the correct factor ± 1 to use.

2.5.3 Matrix representations

The matrix representation for a non-degenerate irrep simply correspond to the character given in the corresponding table. For the degenerate irreps, in the table **Matrix representations** a matrix representation is given for every irrep. One recalls that a specific matrix representation $\{D^\Gamma(g)\}$ is related to the choice of a set of basis functions and for another set of functions given by the unitary transformation S , as presented above, one has an equivalent matrix representation $\{S^{-1}D^\Gamma(g)S\}$.

2.5.4 Direct products of representations

In the **direct product of representation** table, the reduction of every product of representation

$$\Gamma_1 \otimes \Gamma_2 = \oplus_i \Gamma_i \quad (2.39)$$

is presented (intersection of the Γ_1 row with the Γ_2 column). For the products $\Gamma_1 \otimes \Gamma_1$, the antisymmetrical part of the reduction is listed in curly brackets.

One notes that $\Gamma_2 \otimes \Gamma_1 = \Gamma_1 \otimes \Gamma_2$, then only one is listed in the table. Finally, it's important to remark that in the product between two single group or two double group irreps, only single group irreps are involved in the reduction! In the same way, product of a simple with a double group irrep gives double group irreps.

In the table **Clebsch-Gordan (CG) coefficients**, are presented the CG coefficients corresponding to the linear transformation to obtain the new basis block-diagonalizing the reduction of the product $\Gamma_1 \otimes \Gamma_2$. One recalls that these coefficients depend on the choice of the basis functions, then for different matrix representations one has different CG coefficients!

Finally, in the **subduction (descent of symmetry)** table, the effect of a breaking of symmetry on the irreps is presented. An irrep of an higher symmetry group usually becomes a direct product of irreps of the lower symmetry group.

2.6 Effects of symmetry: illustration of group theory

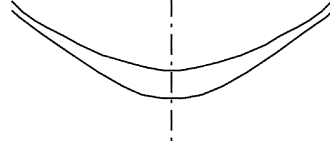
In this section, one wants to use the basic group theory concepts presented in Ch. 2 at the heterostructure level.

In the following, some group is presented in details to illustrate group theory properties and finally the effects of high symmetry are pointed out and the necessity to introduce a good formalism is emphasized.

2.6.1 C_s group

In this subsection, one illustrates the basic concept of group theory presented above with a very single group: the C_s group. This group correspond to the symmetry group of the V or T-shaped quantum wires (QWRs) and has only two symmetry operations: the identity E and a vertical symmetry plane σ as presented in Fig. 2.2.

For this group, one has two elements and two classes, then two 1D irreps, noted A' (the identity irrep, even with respect to σ) and A'' (odd). For the double group, four elements and four classes giving two additional mutually conjugated 1D irreps ${}^iE_{1/2}$ as presented in 2.1. From multiplication table 2.1 (b), one can see that $\sigma\sigma = E$, according to the character ± 1 for the single group irreps, and that $\sigma\sigma = -E$ for the double group according to character $\pm i$!

Figure 2.2: Schematic of a C_s V-shaped QWR

C_s	E	σ
A'	1	1
A''	1	-1
${}^1E_{1/2}$	1	i
${}^2E_{1/2}$	1	$-i$

(a)

C_s	E	σ
E	E	σ
σ	σ	E

(b)

C_s	E	σ
E	1	1
σ	1	-1

(c)

Table 2.1: Character (a), multiplication (b) and factor (c) tables for C_s group

Every irrep is 1D in C_s , then by taking the product of the characters, one can immediately verify table 2.2. In the same way, by complex conjugation, one immediately verifies that the ${}^iE_{1/2}$ are mutually conjugated irreps.

For the two single group irreps one obtains simply symmetry properties with the help of expression (2.19): A' are even and A'' odd states with respect to the vertical symmetry plane. In Fig. 2.3 one presents a schematic of the two kind of solution.

The double group label for the 4D valence band spinorial states are global labels not explicitly related to the different components. The symmetry of spinorial states is introduced in Ch. 6 and the necessity of a new formalism allowing to fully exploit symmetry properties is put in evidence.

C_s	A'	A''	${}^1E_{1/2}$	${}^2E_{1/2}$
A'	A'	A''	${}^1E_{1/2}$	${}^2E_{1/2}$
A''		A'	${}^2E_{1/2}$	${}^1E_{1/2}$
${}^1E_{1/2}$			A''	A'
${}^2E_{1/2}$				A''

Table 2.2: Direct product of representation table for C_s group

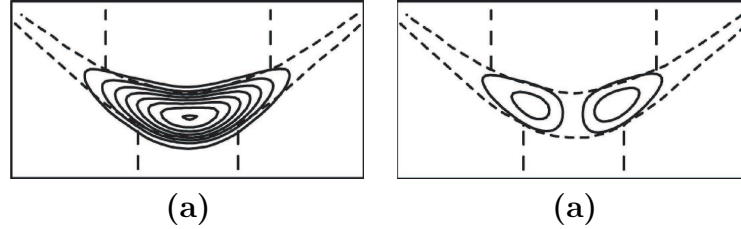


Figure 2.3: Schematic of even **(a)** and odd **(b)** functions for a C_s V-shaped QWR

2.6.2 C_{2v} group

With respect to the C_s group presented in the last subsection, a C_{2v} structure has two orthogonal vertical symmetry plane σ_x, σ_y in addition to the identity (E) and rotation of π (C_2) as presented in Fig. 2.4. For the single

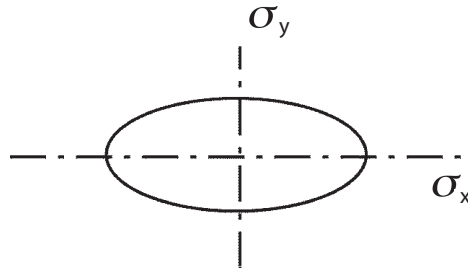


Figure 2.4: Schematic of a C_{2v} QWR

group one has four 1D irreps (A_1, A_2, B_1, B_2) and for the double group one has an additional 2D irrep (see Tab. 2.3) For the scalar functions, nothing more complicated than for the C_s case appear: one simply has four 1D irrep corresponding to the four schematics presented in Fig. 2.5.

2.6.3 C_{3v} group

The triangular C_{3v} group display more higher symmetry with respect to C_{2v} : elements of the group are the identity (E), three vertical symmetry planes σ_{vi} and two rotation of $\pm \frac{2}{3}\pi$ C_3^\pm (see Fig 2.6 for a schematic).

In Ch. 9, the new formalism is explicitly applied to the study of C_{3v} QWRs self-formed at the center of pyramidal QDs. In this subsection, one only presents the more important tables, very useful for the following, and

C_{2v}	E	C_2	σ_x	σ_y
A_1	1	1	1	1
A_2	1	1	-1	-1
B_1	1	-1	-1	1
B_2	1	-1	1	-1
$E_{1/2}$	2	0	0	0

(a)

C_s	E	C_2	σ_x	σ_y
E	E	C_2	σ_x	σ_y
C_2	C_2	E	σ_y	σ_x
σ_x	σ_x	σ_y	E	C_2
σ_y	σ_y	σ_x	C_2	E

(b)

C_s	E	C_2	σ_x	σ_y
E	1	1	1	1
C_2	1	-1	1	-1
σ_x	1	-1	-1	1
σ_y	1	1	-1	-1

(c)

Table 2.3: Character (a), multiplication (b) and factor (c) tables for C_{2v} group

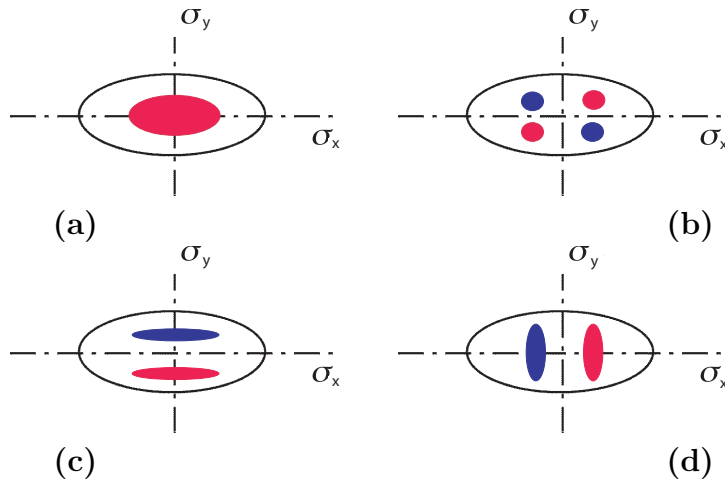


Figure 2.5: Schematic of A_1 (a), A_2 (b), B_1 (c) and B_2 (d) functions for a C_{2v} QWR

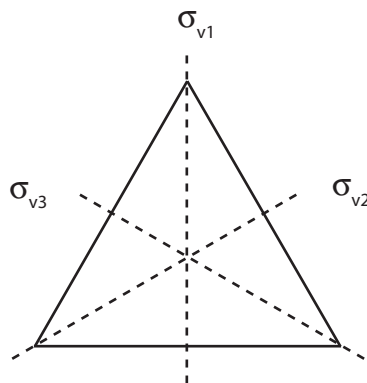


Figure 2.6: Schematic of a C_{3v} QWR

illustrate the different symmetries with the help of a schematic.

As presented in Tab. 2.4, even for the single group a degenerate irrep appear (in addition to two non-degenerates irreps) because in C_{3v} there are six elements regrouped in three classes: $C_{3v} = \{(E), (C_3^+, C_3^-), (\sigma_{v1}, \sigma_{v2}, \sigma_{v3})\}$. One recalls that elements of a same class have the same character because are mutually conjugated elements. How presented in Eqs. (2.20)-(2.21), for the 2D irrep one can not diagonalize every matrix at the same time, then one does not obtain simple symmetry properties for every operations. In particular, from multiplication table 2.4, one obtains that $[\sigma_{vi}, \sigma_{vj}] \neq 0$, then two symmetry plane do not commute and corresponding matrices cannot be diagonalized at the same time.

The matrix representation $\{D^E(g)\}$

$$\begin{aligned} D^E(E) &= \begin{pmatrix} 1 & 0 \\ 0 & 1 \end{pmatrix} & D^E(C_3^+) &= \begin{pmatrix} -\frac{1}{2} & -\frac{\sqrt{3}}{2} \\ \frac{\sqrt{3}}{2} & -\frac{1}{2} \end{pmatrix} \\ D^E(C_3^-) &= \begin{pmatrix} -\frac{1}{2} & \frac{\sqrt{3}}{2} \\ -\frac{\sqrt{3}}{2} & -\frac{1}{2} \end{pmatrix} & D^E(\sigma_{v1}) &= \begin{pmatrix} 1 & 0 \\ 0 & -1 \end{pmatrix} \\ D^E(\sigma_{v2}) &= \begin{pmatrix} -\frac{1}{2} & -\frac{\sqrt{3}}{2} \\ -\frac{\sqrt{3}}{2} & \frac{1}{2} \end{pmatrix} & D^E(\sigma_{v3}) &= \begin{pmatrix} -\frac{1}{2} & \frac{\sqrt{3}}{2} \\ \frac{\sqrt{3}}{2} & \frac{1}{2} \end{pmatrix} \end{aligned} \quad (2.40)$$

it is those explicitly used in the analytical developments of Chs. 7 8 and 9. As presented in Fig. 2.7, a particular and interesting choice consist to diagonalize σ_{v1} . Eigenvalues are ± 1 according to a zero trace (character is 0) and determinant -1 (improper rotation), then the first and second partner functions of E , noted (E, i) , $i = 1, 2$, are respectively even and odd with respect to σ_{v1} vertical symmetry plane. We recall that the two partner functions for E are closely dependent (see Eq. (2.17)) and in Ch. 9 we present a plot, obtained from numerical resolution, of real partner functions satisfying Eq. (2.17).

In the following one will introduce a novel formalism to study high symmetry structures (Ch. 8) and a Spatial Domain Reduction (SDR) technique (Ch. 7) is developed allowing to obtain a minimal domain of resolution for every irrep.

Another interesting choice for the matrix representation are those proposed by Altmann: rotations are diagonal and mirrors anti-diagonal. This equivalent representation do not mix different partner functions, but the matrices are complex and real and imaginary part are mixed by symmetry operation (phase terms are involved). One wants to compute, for the conduction band, a single band problem without spin. This problem is real, then is not

C_{3v}	E	C_3^\pm	σ_{vi}	(a)
A_1	1	1	1	
A_2	1	1	-1	
E	2	-1	0	
$E_{1/2}$	2	1	0	
${}^1E_{3/2}$	1	-1	i	
${}^2E_{3/2}$	1	-1	$-i$	

C_{3v}	A_1	A_2	E	$E_{1/2}$	${}^1E_{3/2}$	${}^2E_{3/2}$	(b)
A_1	A_1	A_2	E	$E_{1/2}$	${}^1E_{3/2}$	${}^2E_{3/2}$	
A_2		A_1	E	$E_{1/2}$	${}^2E_{3/2}$	${}^1E_{3/2}$	
E			$A_1 \oplus \{A_2\} \oplus E$	$E_{1/2} \oplus {}^1E_{3/2} \oplus {}^2E_{3/2}$	$E_{1/2}$	$E_{1/2}$	
$E_{1/2}$				$\{A_1\} \oplus A_2 \oplus E$	E	E	
${}^1E_{3/2}$					A_2	A_1	
${}^2E_{3/2}$						A_2	

C_{3v}	E	C_3^+	C_3^-	σ_{v1}	σ_{v2}	σ_{v3}	(c)	C_{3v}	E	C_3^+	C_3^-	σ_{v1}	σ_{v2}	σ_{v3}	(d)
E	E	C_3^+	C_3^-	σ_{v1}	σ_{v2}	σ_{v3}		E	1	1	1	1	1	1	
C_3^+	C_3^+	C_3^-	E	σ_{v3}	σ_{v1}	σ_{v2}		C_3^+	1	-1	1	-1	-1	-1	
C_3^-	C_3^-	E	C_3^+	σ_{v2}	σ_{v3}	σ_{v1}		C_3^-	1	1	-1	-1	-1	-1	
σ_{v1}	σ_{v1}	σ_{v2}	σ_{v3}	E	C_3^+	C_3^-		σ_{v1}	1	-1	-1	-1	1	1	
σ_{v2}	σ_{v2}	σ_{v3}	σ_{v1}	C_3^-	E	C_3^+		σ_{v2}	1	-1	-1	1	-1	1	
σ_{v3}	σ_{v3}	σ_{v1}	σ_{v2}	C_3^+	C_3^-	E		σ_{v3}	1	-1	-1	1	1	-1	

Table 2.4: Character **(a)**, direct product of irreps **(b)**, multiplication **(c)** and factor **(d)** tables for C_{3v} group

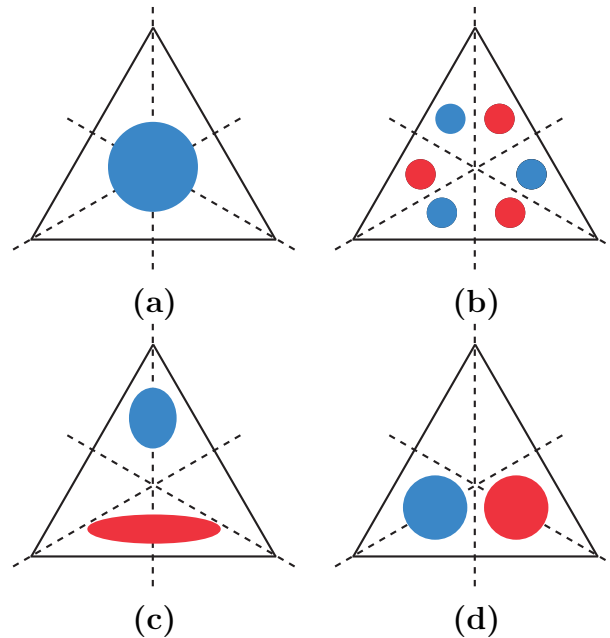


Figure 2.7: Schematic of A_1 function (a), A_2 function (b), E partner function 1 (c) and E partner function 2 (d) for a C_{3v} QWR

interesting for us to deal with complex matrices!

2.6.4 Illustration of the WET

In subsection 2.4 one has introduced the WET (2.38). Starting from the single group C_s is very easy to understand this theorem only basing on symmetry considerations. By computing two generalizations one immediately obtains the theorem for every group.

The functions given in Fig. 2.3 are even (A') and odd (A'') with respect to the symmetry plane, then the scalar product $\langle \psi^{A'} | \psi^{A''} \rangle = 0$ because there are no overlap between the functions.

- First generalization: for every group $\langle \psi_i^{\Gamma_1} | \phi_j^{\Gamma_2} \rangle = \langle \psi_i^{\Gamma_1} | \phi_i^{\Gamma_1} \rangle \delta_{\Gamma_1, \Gamma_2} \delta_{i,j}$, then there are no overlap between two function with different symmetry (different irrep or same irrep but different partner function). For C_{3v} (see Fig. 2.7) is easy to check that A_1 and $(E, 1)$ are even and A_2 and $(E, 2)$ are odd with respect to σ_{v1} (C_s is a subgroup of C_{3v} !). The zero overlap between A_i and (E, i) is not visual, but can be easily verified numerically.

This result can be demonstrated analytically using transformation law

for the functions (2.17) and the orthogonality theorem for matrix representations

$$\sum_g D_{ij}^{\Gamma_1}(g)^* D_{kl}^{\Gamma_2}(g) = \frac{|G|}{d_{\Gamma_1}} \delta_{\Gamma_1, \Gamma_2} \delta_{i,j} \delta_{k,l} \quad (2.41)$$

- Second generalization: for C_s , if $\langle \psi^{A'} | \psi^{A''} \rangle = 0$, then for every even operator $\vartheta^{A'}$ one has $\langle \psi^{A'} | \vartheta^{A'} | \psi^{A''} \rangle = 0$ because $\vartheta^{A'}$ don't change the parity of $|\psi^{A''}\rangle$. In the same way, for an odd operator $\langle \psi^{A'} | \vartheta^{A''} | \psi^{A''} \rangle \neq 0$ because $\vartheta^{A''} |\psi^{A''}\rangle$ is an even function. If one comes back to the direct product of representation table 2.2, one has $A' \otimes A'' \approx A''$ and $A'' \otimes A'' \approx A'$

Finally, with the two generalizations, for every group $\langle \psi_1^{\Gamma_1} | \vartheta^{\Gamma_3} | \psi_2^{\Gamma_2} \rangle = 0$ if Γ_1 don't appear in the reduction of $\Gamma_3 \otimes \Gamma_2$

2.7 References

Many interesting books are devoted to the application of group theory to the quantum mechanics. To give a first specific reference, I recommend the book of Cornwell [25]: in three volumes, is a very general and complete introduction of group theory and applications to the physics. Some other general references are the books of Inui [33], Lax [34], Bir-Pikus [35], Heine [36] or Wigner [37].

In addition to these general books, some useful books have to be recommended. First, Bassani [29] gives group-theory approach to solid state problems. Second, the Altmann [3] point group tables form a powerful (essential!) tool for anyone who need to deal with point groups. Most notably in the first part a very useful introduction to group theory is given. Finally, the appendices of Messiah [30,38] constitute a very concise introduction to group theory. In particular, useful analytical expressions to construct the Wigner representations are given.

Chapter 3

Band structure and heterostructures

3.1 Bulk semiconductors

In this section we recall some essentials of the crystalline structure of bulk semiconductors. The symmetry properties of the microscopic atomic structure have indeed crucial effects on the band structure and considerably simplify the theoretical description of crystals:

- translation symmetry allows to introduce the Bloch theorem (by factoring out in wave functions periodic functions with respect to the crystal structure)
- rotations (and roto-inversions) allow to introduce in a rigorous way effective mass Hamiltonians taking into account the symmetry of the crystal.

3.1.1 The crystalline structure

An ideal crystal is formed by a 3 dimensional periodic array of identical building blocks and every block, called **basis**, is formed by a an atom or a group of atoms. In addition to the basis, one has to introduce three primitive translation vectors \mathbf{a}_i (the **Bravais lattice**) in such a way that the atomic arrangement in the crystal look the same in the points \mathbf{r} and $\mathbf{r}' = \mathbf{r} + \sum_i n_i \mathbf{a}_i$ where n_i are arbitrary integers. A **crystal structure** is finally defined by adding a basis and a Bravais lattice.

Two interesting example are the diamond and zinc-blende structures. The space Bravais lattice for the diamond is face-centred cubic (fcc) (see Fig. 3.1

(a)) and the primitive basis structure has two identical atoms at $(0\ 0\ 0)$ and $(\frac{a}{4}\ \frac{a}{4}\ \frac{a}{4})$ where a is the lattice parameter. The diamond structure, presented in Fig. 3.1 (b), can be seen as two fcc structures displaced from each other by $\frac{a}{4}$ of cube diagonal. The zinc-blende structure is similar to the diamond structure, but the two fcc structure are composed of different atoms (Fig. 3.1 (c)). The more important difference between these two structures, is that zinc-blende is no more invariant with respect to the inversion, but this breaking of symmetry has only a small effect on the band structure. To simplify the analytical calculations of electronic eigenstates, zinc-blende structure like GaAs semiconductors are often modeled assuming a diamond structure. The

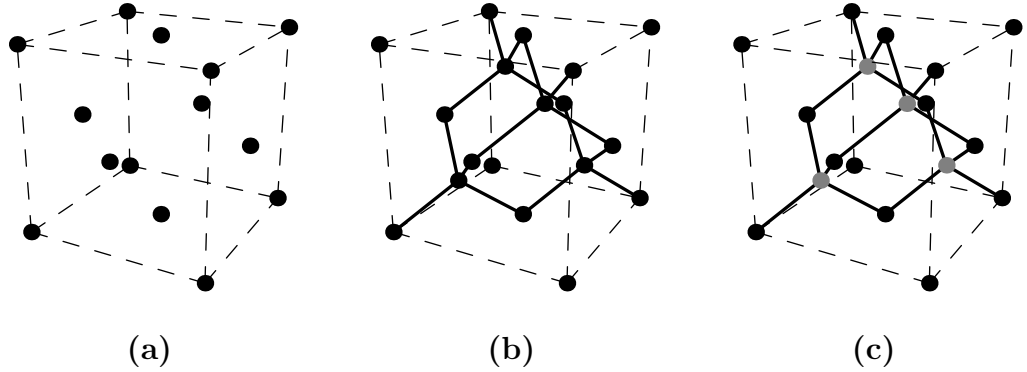


Figure 3.1: Schematic of a fcc lattice (a) and the diamond (b) and zinc-blende (c) structures

more general symmetry operation keeping the crystal invariant are given by the product of a translation τ and a rotation (or roto-inversion) g . One formally notes this operation $\{\tau|g\}$. A pure non-translation operation is simply noted $g = \{0|g\}$ and a pure translation $\tau = \{\tau|E\}$ where E is the identity rotation. The set of pure rotational symmetry operations g with respect to a fixed point is called point group.

To conclude, is interesting to note that the operation corresponding to the inversion and keeping invariant the diamond structure, is not a pure spatial inversion $i = \{0|i\}$ but the spatial inversion followed by a translation: $i = \{\mathbf{f}|i\}$, where $\mathbf{f} = (\frac{a}{4}, \frac{a}{4}, \frac{a}{4})$.

3.1.2 Translational symmetry and Bloch theorem

A crystal is invariant with respect to the pure translation $\tau_{\mathbf{n}} = \sum_i n_i \mathbf{a}_i$. For a non-infinite crystal, with dimensions $N_i a_i$, $i = 1, 2, 3$ where $N_i \gg 1 \in \mathbb{N}$ and a_i the norms of the primitive lattice vectors \mathbf{a}_i , one introduces cyclic boundary conditions $\tau_{N_1,0,0} = \tau_{0,N_2,0} = \tau_{0,0,N_3} = \mathbf{0}$ to neglect the breaking of

symmetry induced by the surfaces.

Taking into account every primitive translation, one obtains a finite $N = \prod_i N_i$ -dimensional abelian (commutative) translation group \mathcal{F} . The $\tau_{\mathbf{n}}$ translation can be represented by the character

$$\chi_{m_1, m_2, m_3}(n_1, n_2, n_3) = e^{-i\mathbf{k}\tau_{\mathbf{n}}} \quad \text{where} \quad \mathbf{k} = \sum_i \frac{m_i}{N_i} \mathbf{h}_i \quad (3.1)$$

The $\mathbf{h}_i = 2\pi \frac{\mathbf{a}_j \wedge \mathbf{a}_k}{\mathbf{a}_i \cdot \mathbf{a}_j \wedge \mathbf{a}_k}$ are the primitive reciprocal lattice vectors satisfying the condition $\mathbf{h}_i \cdot \mathbf{a}_j = 2\pi \delta_{ij}$ and the $m_i \in [0, \dots, N_i - 1]$, $i = 1, 2, 3$ label the irreducible representation.

In the following, one only considers \mathbf{k} in the first Brillouin Zone (BZ), obtained by bisecting the reciprocal lattice with perpendicular planes (and corresponding to the Wigner-Seitz cell for the reciprocal space).

From transformation law for scalar functions

$$\vartheta_{\tau_{\mathbf{n}}^{-1}} \psi(\mathbf{r}) = \begin{cases} \chi_{m_1, m_2, m_3}^*(n_1, n_2, n_3) \psi(\mathbf{r}) = e^{i\mathbf{k}\tau_{\mathbf{n}}} \psi(\mathbf{r}) \\ \psi(\mathfrak{R}_{\tau_{\mathbf{n}}} \mathbf{r}) = \psi(\mathbf{r} + \tau_{\mathbf{n}}) \end{cases} \quad (3.2)$$

one obtains the transformation rules with respect to a translation. This expression can be rewritten as

$$\psi(\mathbf{r} + \tau_{\mathbf{n}}) e^{-i\mathbf{k}(\mathbf{r} + \tau_{\mathbf{n}})} = \psi(\mathbf{r}) e^{-i\mathbf{k}\mathbf{r}} \doteq u_{\mathbf{k}}(\mathbf{r}) \quad (3.3)$$

where $u_{\mathbf{k}}(\mathbf{r})$ is a function with the periodicity of the crystal. Finally one obtains

$$\psi(\mathbf{r}) = u_{\mathbf{k}}(\mathbf{r}) e^{i\mathbf{k}\mathbf{r}} \quad (3.4)$$

corresponding to a rigorous group-theory based approach to obtain the well-known Bloch theorem. A simple way to illustrate this theorem is to consider an electron moving in a mean field potential $V(\mathbf{r})$ generated by the atomic periodic structure of the crystal. The electronic wave function correspond to a periodic function $u_{\mathbf{k}}(\mathbf{r})$ modulated by plane wave $e^{i\mathbf{k}\mathbf{r}}$ (slow variation part) as presented in Fig. 3.2, where the zeros of the periodic function correspond to the positions of the atoms.

3.1.3 Energy bands in a crystal

An effect of interaction between an electronic wave function and the periodic potential of the crystal is that energy band and band gap appear. The simplest way to understand the creation of bands is to consider the tight-binding method (molecular bonding theory).

For two independent identical atoms the energy level are exactly the same,

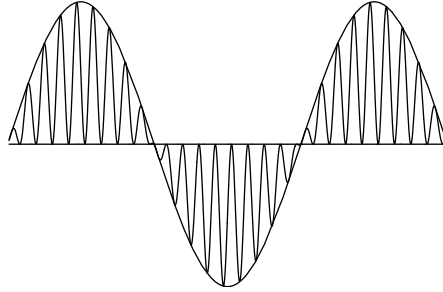


Figure 3.2: Schematic of Bloch decomposition of an electronic wave function

but when one approach the atoms (interaction) there are splitting of degeneracy: bonding, always lower in energy, and anti-bonding orbitals are generated by hybridization (see Fishman [39] for more details). A schematic is presented in Fig. 3.3 for a $A - A$ molecule, where A is an arbitrary atom. If one considers an element of the column IV, the orbitals involved are S and P . Two cases are conceivable: P_B is higher with respect to S_{AB} **(a)** and P_B is partially filled then conduction of carriers is possible and one has a metal, P_B is lower with respect to S_{AB} **(b)** and P_B is completely filled (S_{AB} empty) then conduction of carriers is not possible and one has an insulator.

A semiconductor is a particular kind of insulator with a small ($\approx 1eV$) energy gap between P_B (corresponding to the the valence band) and S_{AB} (conduction band): it is easy to excite (e.g. with a photon) a valence band electron to the conduction band obtaining two partially filled bands.

By considering a crystal as set of atoms, due to the splitting of energy levels one obtains some quasi-continuum of states corresponding to the energy bands, possibly separated by energy gaps where any electronic state can be found. An alternative interpretation can be found considering electrons in

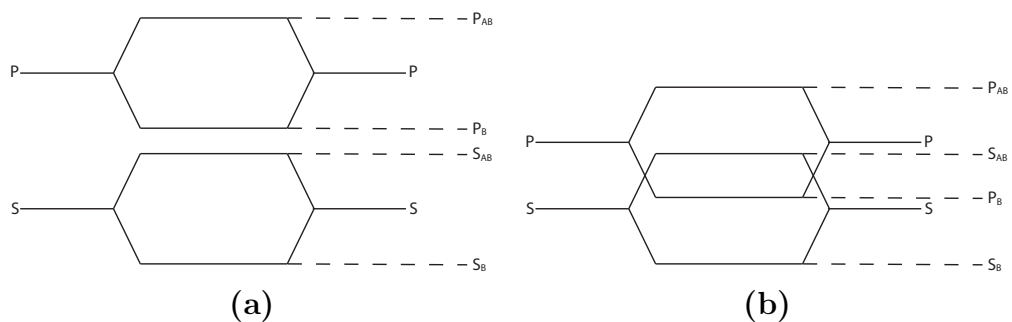


Figure 3.3: Schematic of $A - A$ hybridization model: **(a)** metal and **(b)** insulator

the weak periodic potential approximation. With this approach one obtains quadratic dispersion with respect to k energy bands and energy gaps are related to electronic wave functions with $k = \frac{\pi}{a_i}$ diffracted by the crystal and not transmitted.

3.1.4 The $Al_xGa_{1-x}As$ semiconductors

In the following we are interested to study III-V $Al_xGa_{1-x}As$ semiconductor-based heterostructures: Al and Ga are elements of column III and As of column V. In Fig. 3.4 the electronic band structures for the entire first Brillouin Zone (BZ) for GaAs and AlAs, as well as for Si and Ge, bulk semiconductor are presented and some particular high symmetry points are highlighted (Γ , X , ...).

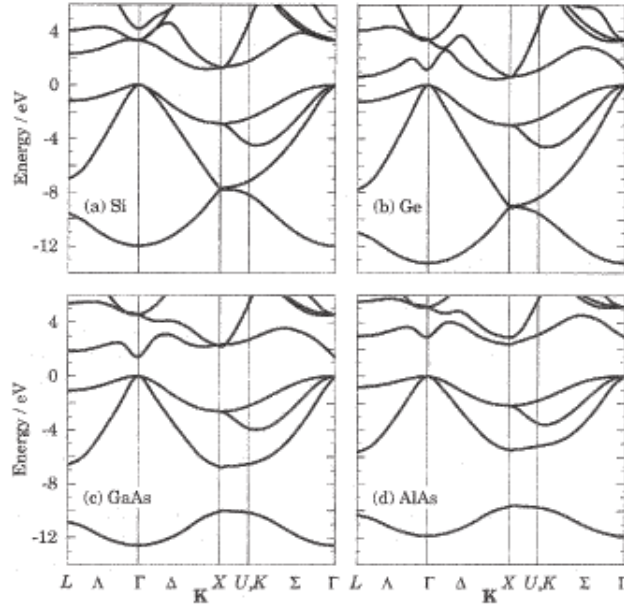


Figure 3.4: Band structure for the first BZ of Si, Ge, GaAs and AlAs [40]

With the aim to compute the optical properties of heterostructures, one needs to obtain an analytical description of the Γ point, corresponding to the center of the BZ (i.e. $k = 0$), where $Al_xGa_{1-x}As$ is a direct gap semiconductor (minimum of the upper band and maximum of lower band are at the same k) for small values of Al concentration (around $x = 0.45$).

More theoretical methods are available and in the following one explicitly

focuses on the Kane $k \cdot p$ theory allowing to obtain simple effective mass Hamiltonian near to the zone center $k = 0$ point.

3.1.5 Point groups and related definitions

In this part, one gives some group theory definitions needed to introduce the concept of point group.

First, one recalls that the crystal is invariant with respect to some symmetry operation $\{\tau|g\}$ where g is the rotational part (rotation or roto-inversion) and τ a translation. Translational part has the form $\tau = a_i + \mathbf{f}$ where \mathbf{a}_i is a primitive translation vector and \mathbf{f} a fractional translation. In $\{\tau|g\}$, one first applies rotational part, then translational part. By defining the law $\{\tau_2|g_2\}\{\tau_1|g_1\} = \{\tau_2 + g_2\tau_1 + \tau_2|g_2g_1\}$, the set of symmetry operation keeping the crystal unchanged form a group: the **space group** of the crystal.

Neglecting the translational parts, the rotational part of the space group still form a group: the **point group of the lattice**. Only 32 point groups are possible because of the limitations imposed by the translational symmetry.

For the reciprocal space, one defines the symmetry operations R_k which leave a vector \mathbf{k} in the first BZ invariant modulo \mathbf{h}

$$R_k \mathbf{k} = \mathbf{k} + \mathbf{h} \quad (3.5)$$

This operations form the **small point group of \mathbf{k}** . Finally, the group of \mathbf{k} , called **little group of \mathbf{k}** is formed by the operations $\{\tau|R_k\}$. For a general \mathbf{k} point, only the identity satisfy expression (3.5), but for some special point (the Γ , X , ... points presented in Fig. 3.4) additional symmetry operations appear. The more particular and, for us, very interesting, is the Γ point corresponding to $\mathbf{k} = \mathbf{0}$: any translation appear and the small point coincides with the point group of the crystal!

3.1.6 The $k \cdot p$ approximation

The $k \cdot p$ formalism, very useful tool to obtain effective mass Hamiltonians near to the Γ point (center of the first BZ $k = 0$), was developed by Badeen and Seitz. Finally Shokley, Dresselhaus and Kane extended the theory to the actual form and Luttinger and Kohn [41] obtain in a rigorous way effective mass equations.

In the following one presents a simplified approach (see Rosencher [42,43] for more details) to obtain effective mass Hamiltonians.

In the first part, of this subsection, one presents the theory neglecting spin of electrons. The limit of this approximation for study the valence band

is emphasized and finally the $k \cdot p$ theory for a spin-dependent problem is discussed.

Spinless problem

We consider a scalar (spinless) crystal Hamiltonian

$$H_0 = \frac{P^2}{2m} + V(\mathbf{r}) \quad (3.6)$$

for an electron moving in a periodic potential $V(\mathbf{r})$ describing the structure of the crystal. According to the Bloch theorem one formally notes an eigenstate

$$|\psi_{n,\mathbf{k}}\rangle = e^{i\mathbf{k}\mathbf{r}} |U_{n,\mathbf{k}}\rangle \quad (3.7)$$

solution of the eigenproblem

$$H_0 |\psi_{n,\mathbf{k}}\rangle = E_{n,\mathbf{k}} |\psi_{n,\mathbf{k}}\rangle \quad (3.8)$$

where $n \in \mathbb{N}$ label the energy levels.

First supposing one know the solutions $|U_{n,\mathbf{0}}\rangle$ at $\mathbf{k} = \mathbf{0}$ and related to the energy $E_{n,\mathbf{0}}$ and corresponding to the function at the top or bottom of the bands at Γ point (in the following, the index $\mathbf{k} = \mathbf{0}$ is omitted if any confusion is possible). One assumes that $\{|U_n\rangle\}$ form a complete basis and that for every \mathbf{k} near to $\mathbf{0}$ one can develop $|U_{n,\mathbf{k}}\rangle$ on the basis

$$|U_{n,\mathbf{k}}\rangle = \sum_m C_{n,m} |U_n\rangle \quad (3.9)$$

where $C_{n,m} = C_{n,m}(\mathbf{k})$.

Second, one explicitly uses the decomposition (3.7) in Eq. (3.8) to obtain

$$\left\{ H_0 + \frac{\hbar^2 k^2}{2m} + \frac{\hbar}{m} \mathbf{k} \cdot \mathbf{p} \right\} |U_{n,\mathbf{k}}\rangle = E |U_{n,\mathbf{k}}\rangle \Leftrightarrow H_{\mathbf{k}\cdot\mathbf{p}} |U_{n,\mathbf{k}}\rangle = E |U_{n,\mathbf{k}}\rangle \quad (3.10)$$

by eliminating the exponential term. One note that for $\mathbf{k} = \mathbf{0}$ we obtains again $H_0 |U_n\rangle = E |U_n\rangle$

Finally, one explicitly introduces the development (3.9) in Eq. (3.10) and projects on $\langle U_N|$ to obtain, for every N , the scalar equation

$$C_{n,N} \left(E_n + \frac{\hbar^2 k^2}{2m} - E \right) + \sum_m C_{n,m} \frac{\hbar \mathbf{k}}{m} P_{N,m} = 0 \quad (3.11)$$

where one used

$$\begin{aligned}\langle U_N | H_0 + \frac{\hbar^2 k^2}{2m} | U_m \rangle &= \left(E_N + \frac{\hbar^2 k^2}{2m} \right) \delta_{N,m} \\ \langle U_N | \mathbf{p} | U_m \rangle &\doteq P_{N,m}\end{aligned}\quad (3.12)$$

Up to now, no restriction of the dimension of the basis $\{|U_n\rangle\}$ was made. In principle, the cardinality of the basis is infinite, but the method consist to use only some mutually strong coupled bands and to take into account the eliminated band as a perturbation. Then, one defines two sets: M are the bands taken into account and M' the eliminated bands. This choice only depends on the physical problem at hand and on the accuracy needed. Eq. (3.11) can be rewritten as

$$C_{n,N} \left(E_n + \frac{\hbar^2 k^2}{2m} - E \right) + \sum_{m \in M} C_{n,m} \frac{\hbar \mathbf{k}}{m} P_{N,m} + \sum_{m' \in M'} C_{n,m'} \frac{\hbar \mathbf{k}}{m} P_{N,m'} = 0 \quad (3.13)$$

For $N = N' \in M'$, in Eq. (3.13) the last term can be neglected and one obtains an expression for the coefficients $C_{n,N'}$ (where the quadratic term in k was also neglected):

$$C_{n,N'} = \frac{\sum_{m \in M} C_{n,m} \frac{\hbar \mathbf{k}}{m} P_{N',m}}{E - E_n} \quad (3.14)$$

Finally, one inserts this expression in the equation for the relevant band (3.13) and one obtains, for all $N \in M$

$$C_{n,N} \left(E_n + \frac{\hbar^2 k^2}{2m} - E \right) + \sum_{m \in M} C_{n,m} \left(\frac{\hbar \mathbf{k}}{m} P_{N,m} + \frac{\hbar^2 k^2}{m^2} \sum_{m' \in M'} P_{N,m'} P_{m',N} \right) = 0 \quad (3.15)$$

The last set of $|M|$ equations, can be rewritten as an $|M| \times |M|$ linear matrix problem $HC = EC$ where \mathbf{C} is the vector with the coefficients. Only $|M|$ variable appear, but an infinite sum on $m' \in M'$ still appear, and one has to know every basis function $|U_n\rangle$ to analytically calculate the $P_{m,n}$ matrix elements. Nevertheless with group theory analysis of the $P_{m,n}$ matrix elements, a minimum number of independent parameter can be identified (effective masses, Luttinger parameter, ...) and appear in the equations. These essential parameters are usually obtained by fitting experimental data.

A number of multiband $k \cdot p$ model are commonly used to compute the band structure of semiconductor or heterostructures. By increasing the number of bands, a bigger part of the BZ can be described with more accuracy, but

at a numerical cost proportional to the CPU time and the required memory. To give an example we present a four band model where the $|S\rangle$ represent the conduction band function and $|iX\rangle, |iY\rangle, |iZ\rangle$ the three fold degenerate valence band functions (at $\mathbf{k} = \mathbf{0}$, without spin). Every band is obviously twice degenerate due to the spin of electrons.

One obtains the 4×4 Hamiltonian

$$H = \begin{bmatrix} E_c + \frac{\hbar^2 k^2}{2m_0} + \gamma_c k^2 & & & & \\ & \begin{matrix} |iX\rangle \\ PK_x \\ E_v + \frac{\hbar^2 k^2}{2m_0} + Lk_x^2 \\ + M(k_y^2 + k_z^2) \end{matrix} & & & \\ & & \begin{matrix} |iY\rangle \\ PK_y \\ Nk_x k_y \\ E_v + \frac{\hbar^2 k^2}{2m_0} + Lk_y^2 \\ + M(k_z^2 + k_x^2) \end{matrix} & & \\ & & & \begin{matrix} |iZ\rangle \\ PK_z \\ Nk_x k_z \\ Nk_y k_z \\ E_v + \frac{\hbar^2 k^2}{2m_0} + Lk_z^2 \\ + M(k_x^2 + k_y^2) \end{matrix} & \\ C.C. & & & & \end{bmatrix} \quad (3.16)$$

where $P = \frac{\hbar}{m_0} \langle S | P_\alpha | i\alpha \rangle$, $\alpha = X, Y, Z$ is the Kane parameter, representing the coupling between conduction and valence band. L, M, N are independent parameters (see [44] for more details). A schematic of the band structure obtained with this model is presented in Fig. 3.5 (a).

The effect of the eliminated bands is crucial for a correct description of the band structure. Neglecting the correction due to the eliminated bands (the last term Hamiltonian (3.13)), correspond to the replacement ($\gamma \rightarrow 1, L \rightarrow 0, M \rightarrow 0, N \rightarrow 0$ in Hamiltonian (3.16)). In the corresponding band structure presented in Fig. 3.5 (b), one can see a wrong curvature for the $|iX\rangle, |iY\rangle$ bands.

To conclude, if one neglects the coupling between conduction and valence band ($P \rightarrow 0$), the Hamiltonian (3.16) breaks down to a scalar Hamiltonian describing the conduction band and a 3×3 block describing the valence band. A simple band spinless scalar Hamiltonian is sufficient to obtain conduction states

$$E_n(k) = E_0 + \frac{\hbar^2 k^2}{2m^*} \quad (3.17)$$

however for a correct description of the valence band the inclusion of the spin is essential: the spin-orbit coupling split the six fold degenerate (including spin) $|i\alpha\rangle$ at $\mathbf{k} = \mathbf{0}$ to a four fold degenerate valence band and a two fold degenerate split-off band.

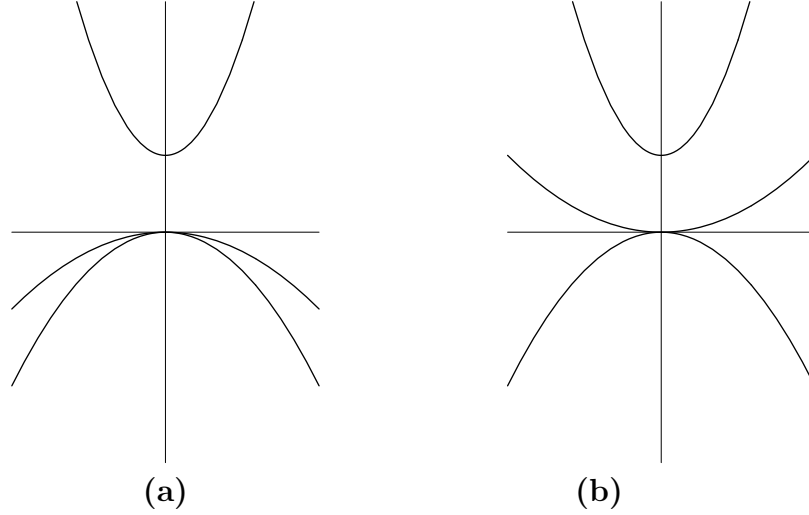


Figure 3.5: Schematic of band structure near $\mathbf{k} = \mathbf{0}$ with a spinless $k \cdot p$ model: with (a) and without (b) influence of eliminated bands

Model with Spin

In a spinless model, one started with the scalar Hamiltonian (3.6). The necessary procedure to obtain an Hamiltonian including the spin, is to use the relativistic Dirac equation for the electrons (for more details see Rose [45] or Bassani [29]). By decoupling strong and weak components of the Dirac spinor, in the non-relativistic approximation one obtains

$$\begin{aligned}
 H_0 &= \frac{P^2}{2m} + V(\mathbf{r}) + H_{so} \\
 H_{so} &\doteq \frac{\hbar}{4m^2c^2} (\nabla V \wedge \mathbf{p}) \cdot \boldsymbol{\sigma}
 \end{aligned} \tag{3.18}$$

where $\boldsymbol{\sigma}$ are the Pauli matrices [30].

H_{so} couples two components of the Dirac spinor and its origin is the interaction of the electron spin magnetic moment with the magnetic field “seen” by the electron.

The additional H_{so} gives two additional terms in the $k \cdot p$ Hamiltonian presented in Eq. (3.10):

$$H_{so} e^{i\mathbf{k}\mathbf{r}} |U_{n,\mathbf{k}}\rangle = e^{i\mathbf{k}\mathbf{r}} \left(H_{so} + \frac{\hbar^2}{4m^2c^2} (\nabla V \wedge \mathbf{k}) \cdot \boldsymbol{\sigma} \right) |U_{n,\mathbf{k}}\rangle \tag{3.19}$$

The first additional term can be incorporated in the potential by defining $\tilde{V} = V + H_{so}$ and for the second one defines

$$\boldsymbol{\pi} = \mathbf{p} + \frac{\hbar}{4mc^2} \boldsymbol{\sigma} \wedge \nabla V \quad (3.20)$$

One obtains an expression for the $k \cdot p$ Hamiltonian with identical form as the equation presented in (3.10) for the spinless problem and one applies the same procedure to obtain effective mass Hamiltonian ($P_{n,m}$ are simply replaced by $\pi_{n,m}$, matrix elements of the new potential). The four band spinless problem correspond to a eight bands problem when one includes spin:

$$\begin{aligned} |S\rangle &\rightarrow |S\rangle \otimes |+\rangle, |S\rangle \otimes |-\rangle \\ |i\alpha\rangle &\rightarrow |i\alpha\rangle \otimes |+\rangle, |i\alpha\rangle \otimes |-\rangle \end{aligned} \quad (3.21)$$

However the Hamiltonian at $\mathbf{k} = \mathbf{0}$ is no more the same and corresponding eigenstates can be formally written as linear combination of the eight functions introduced above. These functions are eigenstates of the total momentum operators J^2 and J_m and one formally notes these functions $|\frac{1}{2}, m\rangle$ for the conduction band (2D), $|\frac{3}{2}, m\rangle$ for valence band (4D) and $|\frac{7}{2}, m\rangle$ for split-off band (2D). In figure 3.6 one presents a schematic of band structure.

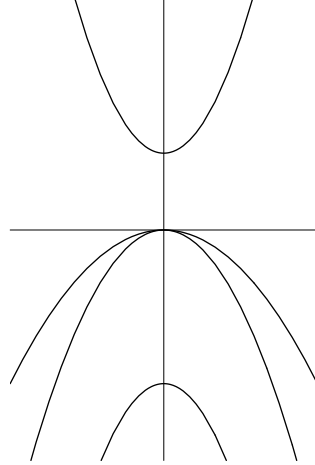


Figure 3.6: Schematic of band structure near $\mathbf{k} = \mathbf{0}$ with a $k \cdot p$ model including spin-orbit coupling

In the following, we shall use a four band model (Luttinger Hamiltonian) to describe the valence band: the conduction and split-off bands are sufficiently

well separated by the energy gaps E_g and Δ_{so} to couple weakly to the valence band in the region of interest. In the Luttinger Hamiltonian

$$H_L = -\frac{\hbar^2}{m_0} \begin{pmatrix} p+q & -s & r & 0 \\ -s^+ & p-q & 0 & r \\ r^+ & 0 & p-q & s \\ 0 & r^+ & s^+ & p+q \end{pmatrix} \quad (3.22)$$

the p, q, r, s operators depend on the choice of the corresponding $\{|\frac{3}{2}, m\rangle\}$ basis (orientation of the crystal in an active point of view) and are quadratic polynomial in k . The effective mass m^* in the conduction band is replaced by three Luttinger parameters γ_i . The Luttinger Hamiltonian describe bulk semiconductors with diamond structure, but in AlGaAs semiconductors, with zinc-blende crystal structure, the lack of inversion symmetry has only a small effect on the electronic states so that we can stay with the Luttinger Hamiltonian. A real zinc-blende Hamiltonian would include some linear terms in k related to the lack of inversion symmetry [46].

To conclude, it is important to note that the Luttinger Hamiltonian depends on the microscopic crystal structure of the bulk semiconductor [41]. Luttinger also developed an other phenomenological approach [47] solely based on group theory to obtain the general form of the Hamiltonian for diamond group.

With the help of the theory of the invariants [35], the Hamiltonian (3.22) can be expressed in the equivalent way

$$H_L = \sum_i \alpha_i f_i^{\Gamma_{i,1}}(k_x, k_y, k_z) g_i^{\Gamma_{i,2}}(J_x, J_y, J_z) \quad (3.23)$$

where f and g are polynomial functions depending only on the vector \mathbf{k} and, respectively, the J_i matrices. These functions transform like the $\Gamma_{i,1}$ and $\Gamma_{i,2}$ irreps and the reduction of $\Gamma_{i,1} \otimes \Gamma_{i,2}$ has to include the identity according to an invariant theory. The α_i constants correspond to the independent parameters appearing in the Hamiltonian.

The k_i depend on the choice of the 3D basis $\{\hat{e}_i\}$ and the J_i matrices on the Bloch function basis $\{|\frac{3}{2}, m\rangle\}$. Finally, for $\hat{e}_x = [100]$, $\hat{e}_y = [010]$, $\hat{e}_z = [001]$ and a quantization axis oriented in the \hat{e}_z direction one obtains the Hamiltonian

$$H_L = -\frac{\hbar^2}{m_0} \left\{ \frac{1}{2}(\gamma_1 + \frac{5}{2}\gamma_2)k^2 - \gamma_2 \sum_i k_i^2 J_i^2 - \gamma_e \sum_{\odot} k_i k_j (J_i J_j + J_j J_i) \right\} \quad (3.24)$$

where \sum_{\circlearrowleft} is the cyclic sum.

This Hamiltonian is the same as the one presented in Eq. (3.22), with the quadratic polynomials

$$\begin{aligned}
p &= k_x \frac{\gamma_1}{2} k_x + k_y \frac{\gamma_1}{2} k_y + k_z \frac{\gamma_1}{2} k_z \\
q &= k_x \frac{\gamma_2}{2} k_x + k_y \frac{\gamma_2}{2} k_y - k_z \gamma_2 k_z \\
r &= -k_x \frac{\sqrt{3}\gamma_2}{2} k_x + k_y \frac{\sqrt{3}\gamma_2}{2} k_y + \left\{ k_x \frac{i\sqrt{3}\gamma_3}{2} k_y + k_y \frac{i\sqrt{3}\gamma_3}{2} k_x \right\} \\
s &= \left\{ k_x \frac{\sqrt{3}\gamma_3}{2} k_z + k_z \frac{\sqrt{3}\gamma_3}{2} k_x \right\} - \left\{ k_y \frac{i\sqrt{3}\gamma_3}{2} k_z + k_z \frac{i\sqrt{3}\gamma_3}{2} k_y \right\}
\end{aligned} \tag{3.25}$$

3.2 Discussion about the inversion

Representation of the inversion is a problematic generally not treated in the literature. In particular, which is the symmetry properties of Bloch functions with respect to the inversion?

In our case, we ignore the inversion symmetry breaking of GaAs (T_d symmetry group of zinc-Blende structure), then the top valence band states of GaAs are very well represented by four functions transforming like the partner functions of a 4D irrep of the diamond group O_h . We formally note the basis function $|\frac{3}{2}, m\rangle$, where $m = \frac{3}{2}, \frac{1}{2}, -\frac{1}{2}, -\frac{3}{2}$ as

$$\begin{aligned}
\left| \frac{3}{2}, \pm \frac{3}{2} \right\rangle &= \pm \frac{1}{\sqrt{2}} (|X\rangle \pm i|Y\rangle) \otimes |\pm\rangle \\
\left| \frac{3}{2}, \pm \frac{1}{2} \right\rangle &= \pm \frac{1}{\sqrt{6}} (|X\rangle \pm i|Y\rangle) \otimes |\mp\rangle - \sqrt{\frac{2}{3}} |Z\rangle \otimes |\pm\rangle
\end{aligned} \tag{3.26}$$

We can assume, without loss of generality [29], that spinors $|+\rangle$ and $|-\rangle$ are even with respect to the inversion as presented in 2.3.5. Considering that spatially-dependent functions $|X\rangle, |Y\rangle, |Z\rangle$ are too symmetric with respect to the inversion the Bloch function basis transform like the grade 4D irrep $F_{3/2,g}$ of the diamond group O_h . The basis is then even respect the inversion and we have $W^{3/2}(i) = I_4$.

On the other hand, if we consider the spin of electrons, the corresponding 2D Bloch function basis

$$\left| \frac{1}{2}, \pm \frac{1}{2} \right\rangle = |S\rangle \otimes |\pm\rangle \tag{3.27}$$

for the conduction band model is odd with respect to the inversion ($|S\rangle$ is an odd function).

The $j = 1/2$ basis transform like the ungerade irrep $E_{1/2,u}$ of O_h and $W^{1/2}(i) = -I_2$.

To conclude this discussion about the inversion, it is important to note that the real symmetry operation leaving the diamond structure invariant with respect to the inversion is $\{i|\tau\}$, where $\{0|\tau\}$ correspond to a translation of $\frac{a}{4}(1, 1, 1)$, indeed the diamond structure is composed of two face-centred cubic structures displaced of $\frac{a}{4}(1, 1, 1)$, with a the length of the cell. In a more constructive approach, the electronic wave functions for bulk semi-conductors can be calculated including the translational part τ of the inversion as presented in [48]. However, the spatial dependence of the envelope functions is not related to the crystalline structure but to the heterostructure and for study the optical properties we are only interested on the inter-band transitions. In this case, any modification is introduced with respect to the traditional functions and in the following we still formally note $|S\rangle, |X\rangle, |Y\rangle, |Z\rangle$ the corresponding electronic functions.

3.3 Low dimensional semiconductor heterostructures

In Sec. 3.1 we have described the basics of the crystal structure for bulk semiconductors leading to $k \cdot p$ theory. In such an approach the electronic wave functions in a crystal (3.4) are decomposed in a periodic part (microscopic periodicity of the crystal) $u_{\mathbf{k}}(\mathbf{r})$ modulated by a plane wave $e^{i\mathbf{k}\cdot\mathbf{r}}$.

Let us now see how one create **quantum confinement** of the carriers by “gluing” together different crystals with similar lattice constants and band structure: the so-called **heterostructures**. Indeed bulk semiconductors with compatible crystal structure and lattice spacing can be grown on top of each other during **epitaxial** growth allowing even almost perfectly abrupt interfaces. In a theoretical model, abrupt interfaces are represented by step-functions, constant in every region with an infinite derivative at the level of the junction.

There are three types of possible heterojunction between two bulk semiconductors as presented in Fig. 3.7, where the energy gaps between the corresponding conduction and valence band for material $i = 1, 2$ are called $E_g^{(i)}$. The $Al_xGa_{1-x}As$ heterostructures considered in this thesis correspond

to type I heterojunctions and display very similar band structures (the band structures of AIAs and GaAs are presented in Fig. 3.4 (c) and (d)).

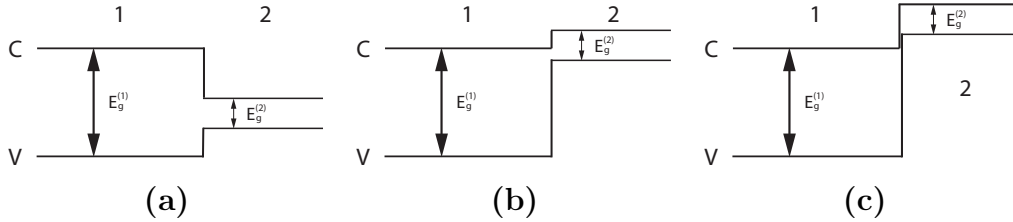


Figure 3.7: Schematic of type I (a), type II (b) and type III (c)

The heterostructures presented up to now have planar geometry, and in the case of quantum confinement of the carriers they are called Quantum Wells (QWs) and display quantum confinement in one direction. To obtain this kind of quantum confinement of the carriers, one has to wait until the end of 1960's, when novel epitaxial grown techniques appear and open the way to the fabrication of high quality low dimensional structures and still nowadays, QWs are commonly used in semiconductor lasers [49].

About fifteen years later, the improvement of fabrication techniques allow to obtain quantum structures with additional confinement: two dimensional confined Quantum Wires [50] and three dimensional confined Quantum Dots (see [51] and its references for more details).

A quantum confinement along d directions correspond to a $3 - d$ dimensions free motion of the carriers and the wave vector \mathbf{k} can always be separated into two contributions: $\mathbf{k} = \mathbf{k}_\perp + \mathbf{k}_\parallel$, where \mathbf{k}_\parallel correspond to the wave vectors for the free motion and \mathbf{k}_\perp to the confined direction. For every dimensionality, the density of states (DOS) $\rho^{dD}(E)$, corresponding to the number of quantum states per unit energy available around a given energy E , has a behavior completely different. For a direct gap bulk semiconductor (macroscopical 3D crystal without confinement, as presented in Fig. 3.8 (a)), the DOS is proportional to

$$\rho^{3D}(E) \sim \sqrt{E - E_g} \quad (3.28)$$

where E_g correspond to the energy at $\mathbf{k} = \mathbf{0}$ (see Fig. 3.8 (b)).

In the following, we quickly present the three different kind of low dimensionality heterostructures (3.3.1-3.3.3) and finally in 3.3.4 an example of complex connected structure coupling different dimensionality structures.

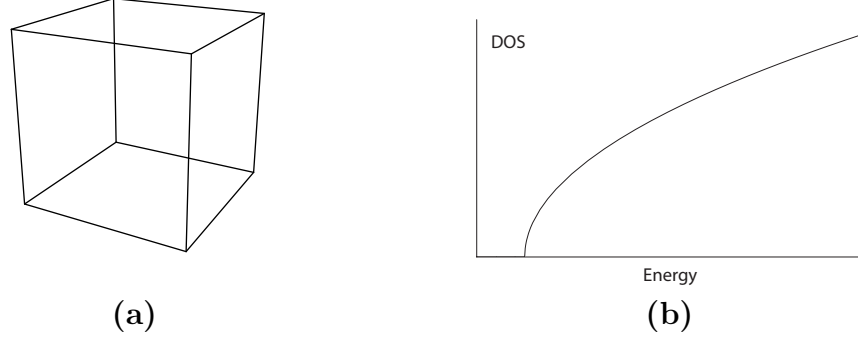


Figure 3.8: Schematic of a 3D bulk semiconductor (a) with the corresponding DOS behavior (b)

3.3.1 2D Quantum Wells (QWs)

The Quantum Wells (QWs) are heterostructures with confinement with respect to one dimension, corresponding to free motion of the carrier in 2D as presented in Fig. 3.9 (a). The thickness of the QW is of the order of magnitude of $10nm$. Respect to the macroscopical size of the bulk semiconductors, this mesoscopic dimension allow to obtain quantum effects due to the confinement of carriers. The DOS is a step function

$$\rho^{2D}(E) \sim \sum_n \Theta(E - E_n) \quad (3.29)$$

where Θ is the Heaviside function, n labelling the different energy bands and E_n correspond to the energy at $\mathbf{k} = \mathbf{0}$.

The physics of QWs was a subject of very extensive research during fifteen years (1975-1990). With respect to the bulk semiconductors, QWs have a sharper density of states and are very useful in the fabrication of quantum devices like lasers.

3.3.2 1D Quantum Wires (QWRs)

Compared to QWs, Quantum Wires (QWRs) have an additional confinement with respect to a second direction (see Fig. 3.10 (a)). Due to the translational symmetry with respect to the non-confined direction, the shape of any section is the same and strongly depend on the crystal structure of the bulk semiconductors and on the growth direction. To give a few examples, for AlGaAs heterostructures one can obtain V-shaped QWRs or triangular QWRs oriented, respectively, along the crystallographic direction $[1\bar{1}0]$ and $[111]$. It

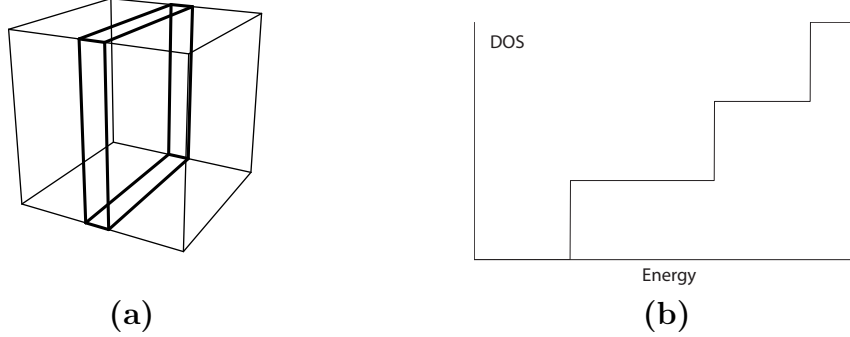


Figure 3.9: Schematic of a 2D Quantum Well (a) with the corresponding DOS behavior (b)

is important to note that for an infinite heterostructure (translational symmetry) the mesoscopic symmetry of the heterostructure is $D_{3h} = C_{3v} \otimes C_s$ because the structure is invariant with respect to an horizontal symmetry plane σ_h . From the microscopic point of view, the symmetry group of the full structure, corresponding to the small point group of the vector \mathbf{k} introduced in the Ch. 2, only display the C_{3v} symmetry operations.

For the heterostructure invariant with respect to σ_h , $+\mathbf{k}$ and $-\mathbf{k}$ are related by this additional symmetry operation and at the center of the Brillouin Zone (BZ) $\mathbf{k} \rightarrow (\mathbf{k}_0 = \mathbf{0}) \leftarrow -\mathbf{k}$ and one obtains the so-called **Zone Center (ZC) symmetry group** [17].

Finally, a QWR has a typical DOS corresponding to

$$\rho^{1D}(E) \sim \sum_n \frac{1}{\sqrt{E - E_n}} \quad (3.30)$$

and display a so called Van-Hove singularities at the band edge (see Fig. 3.10 (b)).

Application of QWRs to quantum devices allow to obtain improved lasers with higher optical gain, low threshold currents and reduced temperature sensitivity (see [52] and its references for more details).

3.3.3 0D Quantum Dots (QDs)

The Quantum Dots (QDs) are 0D structures because any free motion of the carriers is possible as presented in Fig. 3.11 (a). The QDs are often considered as artificial atoms, where the attractive positive atomic nucleus

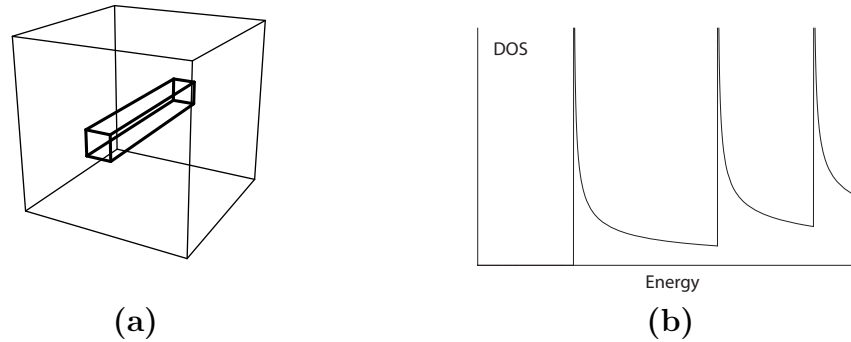


Figure 3.10: Schematic of a 1D Quantum Wire **(a)** with the corresponding DOS behavior **(b)**

is replaced by the 3D confining potential. The density of states

$$\rho^{0D}(E) \sim \sum_n \delta(E - E_n) \quad (3.31)$$

(see 3.11 **(b)**) simply represent discrete energy levels in the QD.

In addition to a reduced lasing threshold current and temperature stability, the emission energies of a QDs can be tuned in a broad range allowing to develop a new generation kind of lasers (see [51] and its references).

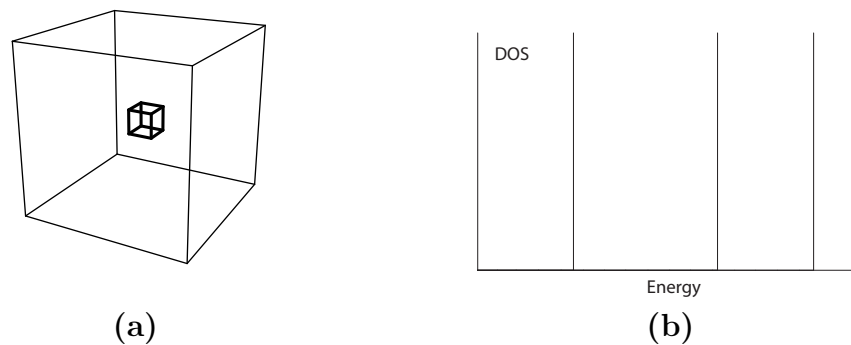


Figure 3.11: Schematic of a 0D Quantum Dot **(a)** with the corresponding DOS behavior **(b)**

3.3.4 Complex connected structures

In the last subsections one has introduced separately the different dimensionality heterostructures (QWs, QWRs, QDs). More complex structures,

involving different dimensionality can be fabricated. Some of them can be very complicated. For example the AlGaAs pyramidal QDs grown in our laboratory have a very rich environment where the dot is connected to lateral (L) and vertical (V) QWRs and QWs as presented in Fig. 3.12.

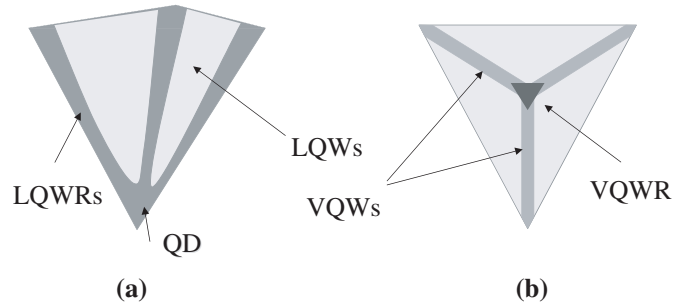


Figure 3.12: Schematic of a AlGaAs pyramidal QD with connected structures (a) and top view (b)

The theoretical and numerical modelling of this kind of structures is quite difficult because it is necessary to model 1D and 2D structures simultaneously and a brute-force approach is necessary to compute the whole structure in a superbox.

3.4 Electronic properties of semiconductor heterostructures

In order to study the electronic structure of semiconductor heterostructures many techniques have been developed (e.g. the tight binding, the orthogonalized plane wave, the pseudopotential, the cellular, the Green's function, the quantum defect or the $k \cdot p$ methods) [29]. A method which is very widespread is the envelope function approach based on the $k \cdot p$ theory.

In a first part, we shall quickly presents the historical approach [27] where one starts from the bulk semiconductor effective mass Hamiltonian and builds an heterostructure Hamiltonian with an empirical procedure. However, it is not unique and one takes care only on the hermiticity.

In a second part, we shall introduce the exact envelope function theory of Burt which is a better procedure allowing to solve all the methodological

questions of the previous approach and lead to new physics, in particular at the interfaces.

Finally, in the last part we shall present the conduction and valence band Hamiltonian used in the rest of this thesis.

3.4.1 The envelope function approximation: historical approach

The standard procedures to obtain effective mass Hamiltonians for heterostructures consists to separate slow and fast varying part of the electronic wave functions, as had been done previously for example for magnetic field. In short, it is enough to replace in the bulk effective mass equations obtained in Sec. 3.1 the wave vector by derivative applying only on slowly varying envelope functions and introducing heterostructure dependent functions:

- $\mathbf{k} = \mathbf{k}_{\parallel} + \mathbf{k}_{\perp} \rightarrow \mathbf{k}_{\parallel} - i\nabla_{\perp}$: the wave vector components in the confined directions (\perp directions) are replaced by differential operators.
- $C_{nm} \rightarrow C_{nm}(\mathbf{r}_{\perp})$: the coefficients of the development of the basis functions become spatially-dependent with respect to the confined regions.
- $E_0 \rightarrow V(\mathbf{r}_{\perp})$: the energies at the top (bottom) of the bands are replaced by the heterostructure potential.
- $m^* \rightarrow m^*(\mathbf{r}_{\perp})$: effective masses depend on the position

To give an example, one presents in the next two subsections the envelope function Hamiltonians for the conduction (spinless single) band and four band with valence band mixing (VBM) Luttinger Hamiltonian used in the following.

3.4.2 The conduction band Hamiltonian

Eq. (3.17) represent the quadratic dispersion for the conduction band energy of a bulk semiconductor. With the replacement rules presented above, one obtains the Hamiltonian for the conduction band of an heterostructure

$$H(\mathbf{r}_{\perp}, \mathbf{k}_{\parallel}) = -\nabla_{\perp} \frac{\hbar^2}{2m^*(\mathbf{r}_{\perp})} \nabla_{\perp} + \frac{\hbar^2 \mathbf{k}_{\parallel}^2}{2m^*(\mathbf{r}_{\perp})} + V_c(\mathbf{r}_{\perp}) \quad (3.32)$$

where \mathbf{k}_{\parallel} appear as parameter and $V_c(\mathbf{r}_{\perp})$ is the conduction band potential for the heterostructure (step function with the bulk value of the corresponding region). One notes that the symmetric form $\nabla_{\perp} \frac{\hbar^2}{2m^*(\mathbf{r}_{\perp})} \nabla_{\perp}$ ensure that the Hamiltonian is an hermitian operator as well as the continuity of the eigenstates.

3.4.3 The valence band Hamiltonian

For a bulk semiconductor, the valence band with mixing and spin-orbit coupling was described by the 4×4 quadratic Hamiltonian

$$H(\mathbf{r}_\perp, \mathbf{k}_\parallel) = H_L(\mathbf{r}_\perp, \mathbf{k}_\parallel) + \mathbb{I}_4 V_v(\mathbf{r}_\perp) \quad (3.33)$$

where $H_L(\mathbf{r}, \mathbf{k})$ is the Luttinger matrix given by Eq. (3.22).

With the replacement rules, one obtains the Hamiltonian for an heterostructure. The potential term is diagonal (proportional to the identity matrix \mathbb{I}_4 in our particular case) and p, q, r, s operators are quadratic in k_i . For bulk semiconductor, one has $p = \sum_{i,j=1}^3 P_{ij} k_i k_j$ (and the same for q, r, s). For an heterostructure the P_{ij} are spatially-dependent and one needs to symmetrize as presented in

$$p = \sum_i k_i P_{ii}(\mathbf{r}_\perp) k_i + \sum_{i \neq j} \frac{1}{2} (k_i P_{ij}(\mathbf{r}_\perp) k_j + k_j P_{ji}(\mathbf{r}_\perp) k_i) \quad (3.34)$$

The last step is to replace $k_i \rightarrow -i \frac{\partial}{\partial x_i}$ for the confined directions. The P_{ij}, \dots, S_{ij} coefficient depend on the choice of 3D basis and Bloch function basis. In the literature are often presented the coefficient for a [001] or, in a more general way, $[h h k]$ quantization axis direction (see [53] for example). The procedure is to start with correct coefficients and choose an optimal basis. The simple procedure to obtain the new coefficients with respect to the new basis, based on the Eq. (2.34), will be presented in details in the following (Ch. 8).

3.4.4 The exact envelope function formalism

The initial point of the Burt exact envelope function formalism is the initial Schrödinger equation with the Hamiltonian $H = -\frac{\hbar^2}{2m_0} \Delta + V(\mathbf{r})$, where $V(\mathbf{r})$ is the microscopic potential. The exact derivation of the effective mass equations for the heterostructures have more advantages:

- It is a rigorous mathematical development
- One can obtain an explicit estimation of the neglected terms
- The symmetrization of the kinetic term appear naturally.

The technical development is very similar to those presented for the bulk semiconductors $k \cdot p$ formalism, but in the exact envelope function formalism there are subtle differences concerning the starting point: in $k \cdot p$ formalism one chooses as complete basis the $\{U_{n,0}\}$ functions, corresponding to the

functions at the top or bottom of every band energy of the bulk semiconductor, and one assumes that these functions are the same in every region of the heterostructure.

In the new formalism, the starting point is more general: one assumes that the crystal has the same periodicity in every region of the heterostructure and one chooses an (arbitrary!) complete basis $\{U_n(\mathbf{r})\}$, simply noted $\{|U_n\rangle\}$ in the Dirac notation, with the crystal periodicity. In the last step of the new envelope function formalism, one will introduce again top or bottom of bands functions, to obtain again the effective mass equations, but the formalism is more general!

Every wave function $\psi(\mathbf{r})$ can be developed on the complete basis $|U_n\rangle$. One notes $F_n(\mathbf{r})$ the (unique and exact!) coefficients of the development and call them the **envelope functions**

$$|\psi\rangle = \sum_n F(\mathbf{r}) |U_n\rangle \quad (3.35)$$

Let us formulate the eigenvalues problem $H|\psi\rangle = E|\psi\rangle$, where H is the Hamiltonian presented below, and develop on the basis functions to obtain, for every n ,

$$\sum_m H_{nm} F_m = E F_n \quad (3.36)$$

where H_{nm} are the matrix elements. One recalls that $|U_n\rangle$ functions have the periodicity of the crystal, then the matrix elements are defined by taking the integrals over a unit cell (volume V_c)

$$H_{nm} = \langle U_n | H | U_m \rangle = \frac{1}{V_c} \int_{cell} U_n^*(\mathbf{r}) H U_m(\mathbf{r}) d\mathbf{r} \quad (3.37)$$

If one formally notes $H = T + V$, where T is the kinetic part, one has two term to decompose on the basis: $T|\psi\rangle$ and $V|\psi\rangle$. The first one is very simple to calculate, but for the second one needs to introduce some approximation as presented in the following.

Kinetic term $T|\psi\rangle$

For a kinetic term $T = -\frac{\hbar^2}{2m_0}\Delta$, with the decomposition (3.35) one simply obtains

$$T|\psi\rangle = -\frac{\hbar^2}{2m_0} \sum_n \{(\Delta F_n(\mathbf{r})) |U_n\rangle + 2(\nabla F_n(\mathbf{r})) \cdot (\nabla |U_n\rangle) + F_n(\mathbf{r}) (\Delta |U_n\rangle)\} \quad (3.38)$$

By introducing the closure relation $\mathbb{I} = \sum_m |U_m\rangle \langle U_m|$ and the matrix elements

$$\begin{aligned} \mathbf{P}_{nm} &= \langle U_n | \mathbf{p} | U_m \rangle = \langle U_n | \frac{\hbar}{i} \nabla | U_m \rangle \\ T_{nm} &= \langle U_n | T | U_m \rangle = \langle U_n | -\frac{\hbar^2}{2m_0} \Delta | U_m \rangle \end{aligned} \quad (3.39)$$

one finally obtains

$$T\psi = \sum_n \left(-\frac{\hbar^2}{2m_0} \Delta F_n(\mathbf{r}) - \frac{i\hbar}{m_0} \sum_m \mathbf{p}_{nm} \cdot \nabla F_m(\mathbf{r}) + \sum_m T_{nm} F_m(\mathbf{r}) \right) |U_n\rangle \quad (3.40)$$

corresponding to the envelope function expansion of T on the basis.

Potential term $V|\psi\rangle$

The expansion of the potential is more complicated with respect to the kinetic part. The reason is that the heterostructure potential does not have the crystal periodicity as $|U_n\rangle$, then the Fourier transform of the potential contain every wave vector $\mathbf{k} + \mathbf{G}$, where \mathbf{k} is vector in the first BZ and \mathbf{G} a vector of the reciprocal space.

With some tedious manipulations, presented in details in appendix 2 of Burt's article [54], one obtains

$$V\psi = \sum_n \left[\sum_m \int V_{nm}(\mathbf{r}, \mathbf{r}') F_m(\mathbf{r}') d\mathbf{r}' \right] |U_n\rangle \quad (3.41)$$

where $V_{nm}(\mathbf{r}, \mathbf{r}')$, expressed as function of the Fourier components of the potential and the basis vectors, is defined by

$$V_{nm}(\mathbf{r}, \mathbf{r}') = \frac{1}{V_c} \sum_{\mathbf{k}\mathbf{k}'} \sum_{\mathbf{G}\mathbf{G}'} U_{n,\mathbf{G}+\mathbf{G}_1}^* V_{\mathbf{k},\mathbf{G}-\mathbf{G}'} U_{m,\mathbf{G}'} e^{i(\mathbf{k}_1\mathbf{r}-\mathbf{k}'\mathbf{r}')} \quad (3.42)$$

where

$$\mathbf{k} + \mathbf{k}' = \mathbf{k}_1 + \mathbf{G}_1 \quad (3.43)$$

The effect of the non-periodicity of the heterostructure potential with respect to the crystal structure give rise to a non-local expressions of the potential $V_{nm}(\mathbf{r}, \mathbf{r}')$.

One recalls that Fourier decomposition of the basis vectors and envelope

functions give

$$\begin{aligned} |U_n\rangle &= \sum_{\mathbf{G}} U_{n,\mathbf{G}} |\mathbf{G}\rangle \\ |F_n\rangle &= \sum_{\mathbf{k}} F_{n,\mathbf{k}} |\mathbf{k}\rangle \end{aligned} \quad (3.44)$$

where \mathbf{G} is a reciprocal vector and \mathbf{k} is only in the first BZ.

To simplify the expression (3.42) for the potential, one makes the essential assumption that envelope functions are *slowly varying functions*: this means that only small values of the wave vector \mathbf{k} are involved in the Fourier decompositions. From expression (3.43) one obtains that for small values of \mathbf{k} and \mathbf{k}' , $\mathbf{k} + \mathbf{k}'$ still is in the first BZ and then $\mathbf{G}_1 = \mathbf{0}$. With this assumption, one can rewrite the non-local potential as

$$V_{nm}^{(loc)}(\mathbf{r}, \mathbf{r}') = V_{nm}(\mathbf{r}) \Delta(\mathbf{r} - \mathbf{r}') \quad (3.45)$$

where

$$\Delta(\mathbf{r} - \mathbf{r}') \doteq \frac{1}{V_c} \sum_k e^{i\mathbf{k}(\mathbf{r}-\mathbf{r}')} \quad (3.46)$$

is the plane wave expansion of the delta functions restricted to the wave vectors in the first BZ.

The expression (3.41) can then be reduced in the slowly varying approximation in the local expression

$$V\psi = \sum_n \left[\sum_m \int V_{nm}^{(loc)}(\mathbf{r}, \mathbf{r}') F_m(\mathbf{r}') d\mathbf{r}' \right] |U_n\rangle = \sum_n \left[\sum_m V_{nm}(\mathbf{r}) F_m(\mathbf{r}) \right] |U_n\rangle \quad (3.47)$$

One notes that a local potential $V(\mathbf{r})$ can always be separated in two part:

$$V_{nm}(\mathbf{r}, \mathbf{r}') = V_{nm}^{(loc)}(\mathbf{r}, \mathbf{r}') + V_{nm}^{(non-loc)}(\mathbf{r}, \mathbf{r}') \quad (3.48)$$

and, as presented in appendix 3 of [54], far from any interface, the non-local part of the potential vanishes without making any approximation, therefore *the non-local part is non-zero only in the region of an interface*.

In the following, one wants to do a last simplification to the potential: one *neglects the potential details at the interfaces*. This correspond to consider a potential

$$V(\mathbf{r}) = \sum_i \theta^{(i)}(\mathbf{r}) V^{(i)}(\mathbf{r}) \quad (3.49)$$

where $\theta^{(i)}(\mathbf{r})$ is 1 in the region (i) and 0 elsewhere. This assumption allow to approximate the local part of the potential in Eq. (3.47) by

$$V_{nm}(\mathbf{r}) = \sum_i \theta^{(i)}(\mathbf{r}) V_{nm}^{(i)} \quad (3.50)$$

neglecting small corrections due to the interfaces, where $V_{nm}^{(i)}$ are constant only depending on the bulk parameters, and the spatial dependence $\theta^{(i)}(\mathbf{r})$ only depend on the region of the heterostructure.

Envelope function equations

Finally, from Eqs. (3.40) and (3.47) one obtains rigorously the envelope function equations

$$H|\psi\rangle = E|\psi\rangle \Rightarrow \quad (3.51)$$

$$-\frac{\hbar^2}{2m_0}\Delta F_n(\mathbf{r}) - \frac{i\hbar}{m_0}\sum_m \mathbf{p}_{nm} \cdot \nabla F_m(\mathbf{r}) + \sum_m H_{nm}(\mathbf{r})F_m(\mathbf{r}) = EF_n(\mathbf{r}) \quad \forall n$$

valid in the assumption of slowly varying envelope functions and neglecting interface details. where P_{nm} and $H_{nm}(\mathbf{r}) = T_{nm} + V_{nm}(\mathbf{r})$ take the local bulk semiconductor value.

Effective mass equations

The envelope function equations (3.51) are valid for every basis $\{|U_n\rangle\}$ with the periodicity of the crystal. To obtain effective mass equation, one first makes a particular choice of basis, according to the standard envelope function formalism, by choosing eigenstates of the bulk semiconductor at $\mathbf{k} = \mathbf{0}$, with the assumption of same functions in every region of the heterostructure. Second, according to the heterostructure dimensionality, one considers envelope functions as

$$F_n(\mathbf{r}) = e^{i\mathbf{k}_{\parallel}\mathbf{r}_{\parallel}} f_{n,\mathbf{k}_{\perp}}(\mathbf{r}_{\perp}) \quad (3.52)$$

and, finally, by eliminating the non-relevant bands (details are given in Burt's paper [54]), one obtains exactly the same effective mass Hamiltonian presented above.

In the same way as for the $k \cdot p$ Hamiltonians, to take into account spin-orbit coupling one replaces \mathbf{p} by $\boldsymbol{\pi}$

3.4.5 Interface terms

As presented in the last subsection, one considers abrupt interfaces for the heterostructure and completely neglect the microscopic details at the junctions.

The effects of these interface terms, the so-called Burt-Foreman terms, are very small and add any additional theoretical or numerical difficulties (linear term in \mathbf{k} , corresponding to some new bulk parameters, are added to the

quadratic polynomial p, q, r, s). For more details, see Foreman paper [55]. Finally, in the paper of Ram-Mohan [56], the author proposes a Lagrangian formulation of the valence band structure, allowing to derive in an elegant way the interface boundary conditions.

3.5 References

Good general introductions to the crystal structure are given, for example, in the book of Kittel [57, 58] or Ashcroft [59]. In Bassani [29], a more symmetry-based approach of the crystal structure is presented (discussion on the inversion for the diamond structure, Bloch theorem justification).

For an introduction to the bulk semiconductors and low dimensional systems as well as to the resolution methods to obtain the band structure, in particular the $k \cdot p$ method, some interesting books are the Rosencher [42, 43], Bastard [27], Bassani [29], Davies [40], Harrison [60], Fishman [39] and Vasko [61]. Finally, the PhD work (in french) of Fabienne Michelini [44] was devoted to the multiband $k \cdot p$ methods.

Chapter 4

Optical properties of semiconductor heterostructures

In this chapter we introduce the study of the optical properties of heterostructures by calculating the absorption spectra for interband transitions in the dipolar approximation. In the second part, one introduces the concept of exciton, bound state of a conduction and valence band state in Coulomb interaction.

4.1 Absorption spectra

An interband transition, e.g. excitation from the valence band to the conduction band, can be induced by an incident plane wave, described by the electric field

$$\mathbf{E} = E_0 \cos(\omega t - \mathbf{q} \cdot \mathbf{r}) \boldsymbol{\epsilon} \quad (4.1)$$

where \mathbf{q} is the wave vector and $\boldsymbol{\epsilon}$ the polarization. With Coulomb gauge $\nabla \mathbf{A} = \mathbf{0}$ one has the vector potential

$$\mathbf{A} = \frac{E_0}{2\omega i} (e^{i(\mathbf{q} \cdot \mathbf{r} - \omega t)} - c.c.) \boldsymbol{\epsilon} \quad (4.2)$$

In the Hamiltonian describing an electron, the effect of electric field can be simply taken into account by a the transformation $\mathbf{p} \rightarrow \mathbf{p} + e\mathbf{A}$ to the electron Hamiltonian $H_0 = H(\mathbf{A} = \mathbf{0})$:

$$H = \frac{(P + e\mathbf{A})^2}{2m_0} + V(\mathbf{r}) = H_0 + \frac{e}{2m_0} \{\mathbf{p}, \mathbf{A}\} + \frac{e^2 \mathbf{A}^2}{m_0} \quad (4.3)$$

In the linear absorption approximation, we only take into account the linear term in \mathbf{A} . Considering that with this choice of the gauge $[\mathbf{A}, \mathbf{p}] = 0$ one

obtains the Hamiltonian

$$H = H_0 + \frac{e}{m_0} \mathbf{p} \cdot \mathbf{A} \quad (4.4)$$

The interaction with light $\mathbf{p} \cdot \mathbf{A}$ can be considered as a time dependent perturbation $W(t)$ of the electronic Hamiltonian H_0 . Using standard time-dependent approach, it is possible to obtain the probability of transition $P_{if}(t)$ between the initial state $|i\rangle$ and final state $|f\rangle$, where $\omega_{if} = \frac{E_i - E_f}{\hbar}$.

$$\begin{aligned} P_{if}(t) &= \frac{1}{\hbar^2} \left| \int_0^t e^{i\omega_{fi}t'} \langle i | W(t') | f \rangle dt' \right|^2 \\ &= \frac{1}{\hbar^2} \left(\frac{eE_0}{2m_0\omega} \right)^2 |\langle i | e^{i\mathbf{q}\cdot\mathbf{r}} \boldsymbol{\epsilon} \cdot \mathbf{p} | f \rangle|^2 \left| \int_0^t e^{i(\omega_{fi}-\omega)t'} dt' \right|^2 \end{aligned} \quad (4.5)$$

One calls

$$M_{\boldsymbol{\epsilon},if} \doteq \langle i | e^{i\mathbf{q}\cdot\mathbf{r}} \boldsymbol{\epsilon} \cdot \mathbf{p} | f \rangle \quad (4.6)$$

the optical matrix element.

One defines the density of transition probability

$$P_{if} \doteq \lim_{t \rightarrow \infty} \frac{d}{dt} P_{if}(t) \quad (4.7)$$

and by introducing the definition of the Dirac function $\lim_{t \rightarrow \infty} \frac{\sin xt}{x} = \pi \delta(x)$ one obtains

$$P_{if} = \frac{2\pi}{\hbar} \left(\frac{eE_0}{2m_0\omega} \right)^2 |M_{\boldsymbol{\epsilon},if}|^2 \delta(E_f - E_i - \hbar\omega) \quad (4.8)$$

corresponding to the Fermi gold rule ensuring the energy conservation. Finally, one defines the probability of absorption of a photon γ by time unit allowing the transition from a valence band to a conduction band by $P(\omega) = \sum_{i,j} \int d\mathbf{k} P_{ij} f(\epsilon_i)(1 - f(\epsilon_f))$, where $f(\epsilon)$ represent the occupation of energy levels. Assuming that initial energy level is full ($f(\epsilon_i) = 1$) and final level empty ($f(\epsilon_f) = 0$), one obtains

$$P(\omega) = \sum_{i,j} \int d\mathbf{k} P_{ij} = \sum_{i,j} \int d\mathbf{k} \frac{2\pi}{\hbar} \left(\frac{eE_0}{2m_0\omega} \right)^2 |M_{\boldsymbol{\epsilon},if}|^2 \delta(E_f - E_i - \hbar\omega) \quad (4.9)$$

The absorption $\alpha(\omega)$ is simply proportional to the probability of absorption (see [27] for the details)

$$\alpha(\omega) \sim P(\omega) \quad (4.10)$$

The last step is to evaluate the optical matrix elements $M_{\epsilon,if}$. Considering only small values of the wave vector \mathbf{q} ($e^{i\mathbf{q}\cdot\mathbf{r}} \cong 1$, electric dipole approximation) and supposing slowly varying envelope functions $F^{(i)}(\mathbf{r})$ and $F^{(f)}(\mathbf{r})$, for *interband transitions* one obtains

$$M_{\epsilon,if} = \sum_{nm} \langle F_n^{(i)} | F_m^{(f)} \rangle \langle U_n | \boldsymbol{\epsilon} \cdot \mathbf{p} | U_m \rangle \quad (4.11)$$

The first term, $\langle F_n^{(i)} | F_m^{(f)} \rangle$, is the spatial overlap between envelope functions and the second,

$$P_{\epsilon,nm} \doteq \langle U_n | \boldsymbol{\epsilon} \cdot \mathbf{p} | U_m \rangle \quad (4.12)$$

is called the Kane matrix.

To conclude this section, one notes that one nevertheless uses the concept of dipolar-approximation even if one includes the spin-orbit coupling (\mathbf{p} is replaced by $\boldsymbol{\pi}$).

4.2 Excitons

In this section one presents a model taking into account the Coulomb interaction between a conduction band state and a valence band state (hole). Without the electron-hole interaction, the energy E_γ of a photon necessary to excite a valence band state to a conduction band state (or in an equivalent way, to form a pair electron-hole with corresponding energies E_e and E_h) is $E_\gamma = \hbar\omega = E_e - E_h$. With the Coulomb interaction, a bound state $e-h$ is formed (center of mass and relative variables can be introduced to describe the exciton) then, taking account of the energy due to the coulomb interaction of the pair electron-hole, the energy of the photon will be smaller with respect to $E_e - E_h$.

A simple way to formulate the excitonic problem, is to obtain separately the electronic states $|\psi_i^e\rangle$, $i = 1, \dots, N_e$ and hole states $|\psi_j^h\rangle$, $j = 1, \dots, N_h$, then construct tensorial product states $|\psi_i^e \psi_j^h\rangle \doteq |\psi_i^e\rangle \otimes |\psi_j^h\rangle$ and define excitonic states as

$$|\psi^X\rangle = \sum_{ij} C_{ij} |\psi_i^e \psi_j^h\rangle \quad (4.13)$$

The corresponding Hamiltonian can be constructed from the electronic and hole Hamiltonian by adding Coulomb interaction as

$$\begin{aligned} H_X &= H_e \otimes \mathbb{I}_h + \mathbb{I}_e \otimes H_h + V_{coul}(\mathbf{r}_e, \mathbf{r}_h) \\ V_{coul}(\mathbf{r}_e, \mathbf{r}_h) &= -\frac{e^2}{4\pi\epsilon|\mathbf{r}_e - \mathbf{r}_h|} \mathbb{I}_e \otimes \mathbb{I}_h \end{aligned} \quad (4.14)$$

where $V_{coul}(\mathbf{r}_e, \mathbf{r}_h)$ is the coulomb potential.

By introducing the elements of the Coulomb matrix

$$V_{ij}^{i'j'} \doteq \langle \psi_{i'}^e \psi_{j'}^h | V_{coul} | \psi_i^e \psi_j^h \rangle \quad (4.15)$$

and the electronic and hole energies E_i^e , E_j^h one transforms the eigenvalues problem to a set of linear equations

$$H^X |\psi^X\rangle = E^X |\psi^X\rangle \Leftrightarrow (E_{i'}^e - E_{j'}^h) C_{i'j'} + \sum_{ij} V_{ij}^{i'j'} C_{ij} = E^X C_{i'j'} \quad \forall i', j' \quad (4.16)$$

The only difficulty is to simplify the matrix elements of the Coulomb potential. Finally, by solving the matrix problem one obtains the excitonic energy E^X and the coefficient C_{ij} of the development.

4.3 References

More information about the optical properties of the semiconductors and heterostructures can be found in the books of Rosencher [42,43], Bastard [29], Haug and Koch [62], Vasko [61], Harrison [60], Glutsch [63] and in the PhD work of Fabienne Michelini [44].

Finally, excitons in triangular QWRs were studied in the frame of the Master thesis, under our supervision, of Jérôme Comte and additional information about the computational method can be found in the report [64].

Chapter 5

Numerical methods

The Finite Elements Methods (FEM) is a powerful mathematical formalism allowing to transform a set of coupled partial differential equations to a generalized matrix eigenproblem, perfectly adapted in the aim of a numerical resolution.

The basic idea of the method is to decompose the spatial domain into small finite domains (meshing). To every node i of the mesh one associates a basis function $|i\rangle$ with value one on the node and zero on every other. An eigenstate $|\psi\rangle$ solution of $H|\psi\rangle = E|\psi\rangle$ can be approximated by the decomposition on the basis functions $\sum_i \psi_i |i\rangle$. Finally, the coefficient ψ_i will be solution of the matrix eigenvalue problem

$$K\underline{\psi} = EM\underline{\psi} \tag{5.1}$$

where the stiffness matrix K and mass matrix M represent the Hamiltonian and the overlap of basis functions with respect to the basis: $K_{ij} = \langle i|H|j\rangle$ and $M = \langle i|j\rangle$.

In this chapter, we quickly present the general theory of finite elements, then we introduce the particular case of linear functions on 2D triangular elements used in the following and show how to obtain stiffness and mass matrices from the basis functions and Hamiltonian introducing the very useful concept of master element (isoparametric element).

In the last part we introduce the numerical libraries used for numerical resolution of the linear problem.

5.1 The Finite Elements Method (FEM): general theory

5.1.1 Introduction to the physical problem

The FEM are very general methods well adapted to study 1D, 2D and 3D problems. In the following, one explicitly illustrates the method in the frame of the resolution of a 2D eigenvalues problem

$$H |\psi\rangle = E |\psi\rangle \quad (5.2)$$

where H is a second order differential operator and $\psi(\mathbf{r}) \in \mathcal{H} = L^2(\mathbb{R}^2)$ is an element of the Hilbert space \mathcal{H} , solution of Eq. (5.2) on the domain $\Omega \subset \mathbb{R}^2$ with boundary conditions $\nabla_{\perp} \psi(\partial\Omega) = 0$ (normal derivative zero, corresponding to Neumann conditions). One notes that in our physical problem Ω correspond to the convergence domain, to be chosen enough big to ensure convergence of eigenstates, allowing to solve the problem on Ω considering that the eigenstate is analytically zero outside. In this case, one could choose Dirichlet boundary condition $\psi(\partial\Omega) = 0$.

To gives an example, the eigenstates of a QWR surrounded by a bulk semiconductor are localized in the wire and decreasing exponentially to zero outside (tunnel effect due to finite barriers). The FEM formalism is more general and can be used to solve non-zero derivative boundary conditions or boundary conditions on the function (in particular Dirichlet conditions).

An alternative useful technique to impose $\psi(\partial\Omega) = 0$ consisting to construct the mass and stiffness matrices with Neumann conditions and eliminating the nodes corresponding to the boundary (eigenfunction is supposed to be zero!) at the time of the numerical resolution of the problem. Another method to force the value of a function to zero on a node, is the so-called penalty method and consisting to modify the final stiffness matrix obtained with the zero derivative boundary conditions by replacing the K_{ii} element by a very big element forcing the solution to converge to zero.

Finally, one has chosen to construct the matrices for Neumann conditions, and eventually apply in a second step Dirichlet conditions without modify the construction of the matrices. These techniques only impose an additional assumption on the eigenstates: every function with $\psi(\partial\Omega) = 0$ have too zero derivative. This is not restrictive considering exponential decreasing of the eigenstates!

5.1.2 Weak formulation

The first step in the FEM formulation, is the weak formulation of the problem: one chooses a set \mathbf{H} of smooth test functions satisfying the boundary conditions. One obtains a variational statement of the problem (5.2) by multiplying the equation by $v \in \mathbf{H}$ and integrating on Ω as in

$$\int d\Omega (H - E)\psi v = 0 \quad (5.3)$$

This correspond to the weak formulation because the differential equation is satisfied in the sense of weighted average (for every test function v).

In the standard formulation (5.2) of the problem, one assumed that ψ satisfy the equation in every point of Ω and that ψ, ψ', ψ'' are well defined. This is a strong assumption and not always satisfied. To give an example, for a second order differential equation with point-source $L\psi(\mathbf{r}) = \delta(\mathbf{r})$, the second derivative ψ'' is not well defined. In the weak formulation, the equation become $\int d\Omega L\psi(\mathbf{r})v(\mathbf{r}) = \int d\Omega \delta(\mathbf{r})v(\mathbf{r}) = v(\mathbf{0})$: the right-hand side is now well defined (v is a smooth function). Computing by part integration, only first order ψ' appear in the equation.

5.1.3 Galerkin approximation

The \mathbf{H} space of test functions v is an infinite dimension space (to give an example, by computing the Fourier decomposition of the function, an infinity of $e^{i\mathbf{k}\cdot\mathbf{r}}$ basis functions are involved). The Galerkin approximation consist to approximate $v \in \mathbf{H}$ by $v^N \in \mathbf{H}^N$, where \mathbf{H}^N is N -dimensional space. Let be $\hat{e}_i, i = 1, \dots, N$ a basis of \mathbf{H}^N allowing to decompose the approximate function as $v^N = \sum_i v_i \hat{e}_i$. In the same way, if one finds an approximate solution $\psi^N = \sum_i \psi_i \hat{e}_i$ of ψ one obtains the Galerkin approximation of (5.3)

$$\int d\Omega (H - E)\psi^N v^N = \sum_i v_i \left\{ \sum_j \psi_j \left(\int d\Omega \hat{e}_i H \hat{e}_j - E \int d\Omega \hat{e}_i \hat{e}_j \right) \right\} = 0 \quad (5.4)$$

Expression (5.3) stand for every $v^N \in H^N$ then for every v_i one has expression

$$\sum_j \psi_j \left(\underbrace{\int d\Omega \hat{e}_i H \hat{e}_j}_{H_{ij}} - E \underbrace{\int d\Omega \hat{e}_i \hat{e}_j}_{M_{ij}} \right) = 0 \Leftrightarrow \sum_j H_{ij} \psi_j = E \sum_j M_{ij} \psi_j \quad \forall i \quad (5.5)$$

Finally one obtains the $N \times N$ linear matrix problem

$$K \underline{\psi} = E M \underline{\psi} \quad (5.6)$$

The matrix K and M are called stiffness and mass matrices and represent, respectively, the Hamiltonian with respect to the N -dimensional basis and the non-orthogonality of the basis.

5.2 FEM: computation of matrix elements

In the following one explicitly illustrates the computation of the matrix elements H_{ij} for a scalar quadratic Hamiltonian

$$H = \sum_{\alpha,\beta} \partial_\alpha f_{\alpha,\beta}(\mathbf{r}) \partial_\beta + \sum_{\alpha} (f_\alpha(\mathbf{r}) \partial_\alpha + \partial_\alpha f_\alpha(\mathbf{r})) + f(\mathbf{r}) \quad (5.7)$$

where ∂_α are partial derivatives with respect to x_α and the $f_\bullet(\mathbf{r})$ are arbitrary functions. By computing part integrations, one can rewrite using boundary conditions

$$\begin{aligned} \int d\Omega \hat{e}_i \partial_\alpha (f_{\alpha,\beta}(\mathbf{r}) \partial_\beta \hat{e}_j) &= - \int d\Omega (\partial_\alpha \hat{e}_i) f_{\alpha,\beta}(\mathbf{r}) (\partial_\beta \hat{e}_j) \\ \int d\Omega \hat{e}_i \partial_\alpha (f_\alpha(\mathbf{r}) \hat{e}_j) &= - \int d\Omega (\partial_\alpha \hat{e}_i) f_\alpha(\mathbf{r}) \hat{e}_j \end{aligned} \quad (5.8)$$

Then the partial derivative in the Hamiltonian H , only acts on the basis vectors \hat{e}_i . To explicitly compute the stiffness matrix K and mass matrix M , one has to choose an analytical expression for the basis vectors and compute the integrations.

5.2.1 Meshing and basis function

In the following one wants to solve on a triangular domain Ω , then one chooses a regular symmetric meshing with triangular elements respecting the geometry of the problem as presented in Fig. 5.1 (the reason will appear clear in the following Ch. 7). One explicitly chooses first order (linear) basis functions \hat{e}_i : for every node i , the function \hat{e}_i is a pyramid with value 1 on i and 0 on the neighbor. The 2D basis functions are a generalization of the well know linear hat-functions of the 1D case (see Fig. 5.2). The analytical form of the basis functions is know, then a priori one can explicitly calculate every H_{ij} and M_{ij} elements, but for every node one has a different expression to calculate because the shape of the elements is not the same (already with our regular mesh but in particular for a non-regular meshing!).

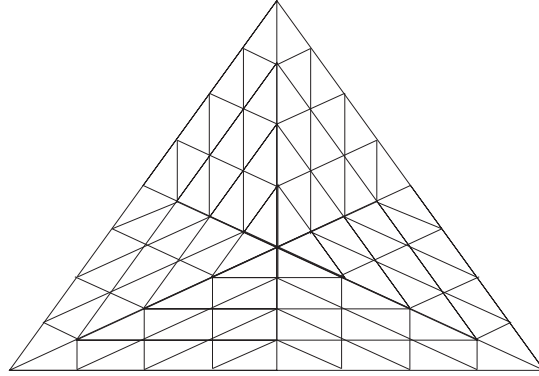


Figure 5.1: Schematic of the triangular mesh

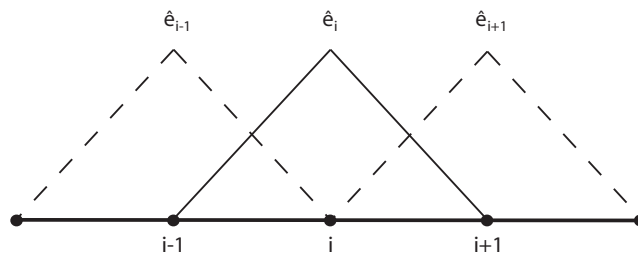


Figure 5.2: Schematic of 1D hat-functions

5.2.2 The master (isoparametric) element

To compute only one time the integrations, one introduces the concept of master element (isoparametric element) $\widehat{\Omega}$: in every element appear three sides (planes), one of every function related to a corner of the element. For every element one introduces a change of variable, translation and deformation of the shape of the element, to the master element $x = x(\eta, \mu)$, $y = y(\eta, \mu)$, where the master element is presented in Fig. 5.3. The corresponding planes have a very simple form $\pi_1(\eta, \mu) = 1 - \eta - \mu$, $\pi_2(\eta, \mu) = \mu$, $\pi_3(\eta, \mu) = \eta$ and integrals are computed once in the master elements, then with the transformation of variables one expresses the value for the specific element (details of the technique and explicit equations are given in any book of FEM, for example Becker [65] or Ram-Mohan [66]).

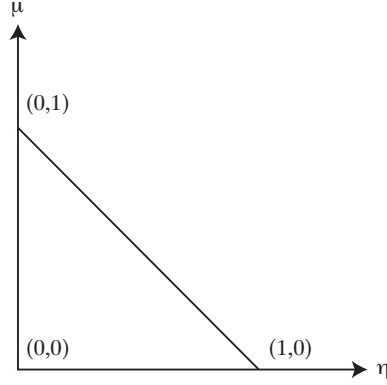


Figure 5.3: Master element for 2D triangular elements

5.2.3 Gauss-Legendre integration

In the master element one has three kind of integration to compute (where $f(\mathbf{r})$ is an arbitrary function):

- (1) $\int d\widehat{\Omega} \hat{e}_i f(\mathbf{r}) \hat{e}_j$
- (2) $\int d\widehat{\Omega} \hat{e}_i f(\mathbf{r}) (\partial_\beta \hat{e}_j)$
- (3) $\int d\widehat{\Omega} (\partial_\alpha \hat{e}_i) f(\mathbf{r}) (\partial_\beta \hat{e}_j)$

The first assumption is that finite element are enough small to consider $f(\mathbf{r}) \cong \text{const}$ in every element. Finally, \hat{e}_i is a linear basis vector, then $\hat{e}_i \hat{e}_j$ is a second order polynomial ($\hat{e}_i (\partial_\beta \hat{e}_j)$ and $(\partial_\alpha \hat{e}_i) (\partial_\beta \hat{e}_j)$ are respectively first order polynomial and constant expression). A second order polynomial can be calculated in an exact way with a third order Gauss-Legendre integration

$$\iint d\widehat{\Omega} g(\mathbf{r}) = \int_{\eta=0}^1 \int_{\mu=0}^{1-\eta} d\eta d\mu g(\eta, \mu) = \sum_{i=1}^3 p_i g(\eta_i, \mu_i) \quad (5.9)$$

where $(\eta_i, \mu_i) = \{(\frac{1}{6}, \frac{1}{6}), (\frac{1}{6}, \frac{2}{3}), (\frac{2}{3}, \frac{1}{6})\}$ are the Gauss points and $p_i = \{\frac{1}{6}, \frac{1}{6}, \frac{1}{6}\}$ are the weights.

5.3 Numerical computation and resolution of the linear problem

In the last sections 5.1 and 5.2 one has introduced the basic concepts of the finite elements computations (finite elements basis, master element, stiffness

and mass matrices, Gauss-Legendre integration) allowing to transform a differential equation $H|\psi\rangle = E|\psi\rangle$ in a linear matrix equation $K\underline{\psi} = EM\underline{\psi}$. The last step is to compute a (numerical) resolution of the linear problem. Two main artifices are necessary to optimize the computation: structure the matrices and use a well adapted algorithm (ARPACK numerical library) for the resolution.

5.3.1 Structured matrices

Two functions \hat{e}_i and \hat{e}_j have non-zero overlap only if i and j are close neighbors, then only some K_{ij} and M_{ij} can be different to zero and have to be calculated. With a judicious choice of the numbering of the nodes, the matrices M and K can be structured in the so-called band form.

$$K = \begin{pmatrix} & & & & 0 \\ & & & & \\ & & & & \\ & & & & \\ 0 & & & & \end{pmatrix}$$

This have more advantages:

- only non-zero elements have to be calculated
- the zero elements do not have to be taken into account (from the numerical point of view, one has to deal with smaller matrices)
- efficient algorithms are especially developed for matrix in band-form (smaller CPU time)

In the following, for the numerical computation one used a band storage for the matrices. An alternative storage method, indispensable if banded matrices are too big, are matrices in a sparse form: matrices are not structured but only non-zero elements are stored in a vector.

5.3.2 Resolution of a linear problem: ARPACK library

Using of an optimized and suitable algorithm, with the corresponding subroutine, it is essential to minimize the time of resolution (CPU time).

To give an example, from the analytical point of view, the simplest way to solve $H|\psi\rangle = EM|\psi\rangle$ is first to calculate the inverse M^{-1} and construct $(M^{-1}H)|\psi\rangle = E|\psi\rangle$, then to diagonalize $(M^{-1}H)$ to obtain eigenvalue and eigenstates ... but this is absolutely not optimized numerically!

Fortunately, numerical libraries allowing to compute basic linear algebra operations and solve generalized eigenproblems still exist. First, the BLAS (Basic Linear Algebra Subprograms) are optimized routines computing scalar, vector and vector-vector operations (BLAS level 1), matrix-vector operations (level 2) and matrix-matrix (level 3). Based on the BLAS 1,2 and 3, the LAPACK (Linear Algebra PACKage) library are a set of subroutines solving the most commonly linear algebra problems.

For our particular problem (large size generalized eigenproblem, with structured matrices and only some eigenstate to be calculated (lower confined energy levels)), the standard numerical libraries are not optimized and one uses the ARPACK (ARnoldi PACKage) subroutines, based on the Arnoldi implicit restarted method (iterative procedure), and allowing to considerably reduce the CPU time. The ARPACK subroutines are more complicated to use with respect to the standard LAPACK: in particular some part of the routines has to be computed by the user. This may appear penalizing, but however allow to personalize the routines for every different problem!

The general theory of the Arnoldi algorithm or numerical details on the ARPACK libraries can be found in the user guide [67].

5.4 References

The standard procedure as well as complete presentation to the Finite Elements Method (FEM) can be found, for example, in the books of Becker [65] or Ram-Mohan [66]. For a very short introduction to the 1D finite elements and more details on the standard technique on numerical integration, see the the appendix of Ram-Mohan [66] or the book of Rappaz [68].

Chapter 6

From low to high symmetries: a new formalism

The aim of this chapter is to introduce in a simple way the problematic related to the difference between low and high symmetry and demonstrate the need of our new MSR formalism.

We shall first recall fundamental results on low symmetry heterostructures [17]. They will also be of direct use in MSR. Second we will show explicitly the limitations of these techniques, in particular that they do not allow to reach *maximal* symmetrization of envelope functions in the case of higher symmetry heterostructures, which thus represent a main challenge! These results will form an essential basis for the systematic study of transformation laws presented in Ch. 2 and the development of the cornerstone of the MSR in Sec. 8.2).

Multiband $k \cdot p$ Hamiltonians (see Sec. 3.4) are very useful tools for the study of the electronic structure in semiconductor heterostructures [27]. Such models indeed allow to introduce all the relevant physics close to a high symmetry point of the band-structure, whilst keeping maximum simplicity. For III-V zincblende semiconductors like AlGaAs/GaAs it is possible for many applications to treat separately the conduction and the valence band problems. It should be stressed that the method presented in the following can be generalized to extended $k \cdot p$ models, treating simultaneously more bands (e.g. conduction and valence bands, or valence and split-off bands) or including magnetic field, Burt-Foreman terms, strain, ...

6.1 The effects of low symmetry: scalar functions

Let us now assume that we deal with a typical QWR geometry, and define the coordinate system according to $\mathbf{r}_\perp = (y, z)$ (see Fig. 6.1). The first

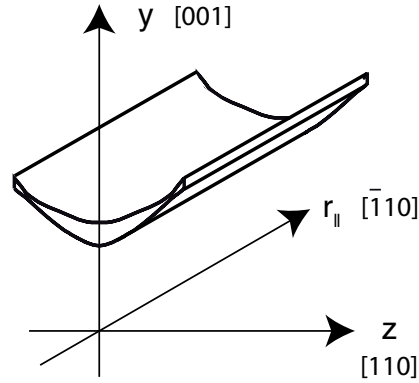


Figure 6.1: View in perspective of a typical V-shaped $Al_xGa_{1-x}As$ QWR, with coordinate system. The central part is typically pure GaAs, the surrounding bulk part is typically $x = 30\%$.

two eigenstates of the stationary solutions of the Schrödinger equation for a typical V-shaped QWR are shown on Fig. 6.2. The ground state wave

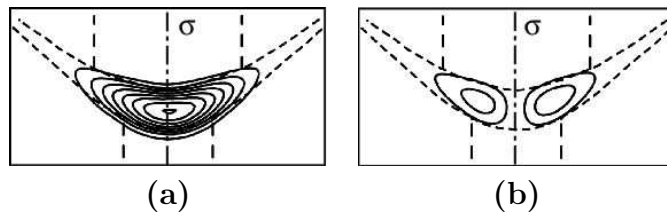


Figure 6.2: Contour plots of conduction band envelope functions of the first two electronic states in a typical V-shaped QWR (a) Even function (ground state); (b) Odd function (first excited state). The V-shaped QWR GaAs potential well is shown with a dotted line, the vertical quantum well with $x \approx 20\%$ is also visible.

function $\psi_{\mathbf{k}_\parallel}^{(e)}(\mathbf{r}_\perp)$ is *even* with respect to the symmetry plane operation $\sigma : \mathbf{r}_\perp = (y, z) \mapsto \sigma\mathbf{r}_\perp = (y, -z)$, whilst the first excited state wave function

$\psi_{\mathbf{k}_{\parallel}}^{(o)}(\mathbf{r}_{\perp})$ is *odd*, i.e.

$$\begin{aligned}\vartheta_{\sigma^{-1}}\psi_{\mathbf{k}_{\parallel}}^{(e)}(\mathbf{r}_{\perp}) &= \psi_{\mathbf{k}_{\parallel}}^{(e)}(\sigma\mathbf{r}_{\perp}) = +\psi_{\mathbf{k}_{\parallel}}^{(e)}(\mathbf{r}_{\perp}) \\ \vartheta_{\sigma^{-1}}\psi_{\mathbf{k}_{\parallel}}^{(o)}(\mathbf{r}_{\perp}) &= \psi_{\mathbf{k}_{\parallel}}^{(o)}(\sigma\mathbf{r}_{\perp}) = -\psi_{\mathbf{k}_{\parallel}}^{(o)}(\mathbf{r}_{\perp})\end{aligned}\quad (6.1)$$

Despite the trivial aspect of these observations, they are important to appreciate the case of holes that will be discussed below. It is also clear that these relations translate into stringent conditions on the wave function on the symmetry axis:

$$\begin{aligned}\partial_z\psi_{\mathbf{k}_{\parallel}}^{(e)}(y, z=0) &= 0 \\ \psi_{\mathbf{k}_{\parallel}}^{(o)}(y, z=0) &= 0\end{aligned}\quad (6.2)$$

Such relations are obviously extremely useful because they play the role of boundary conditions when solving numerically on the left or right halfplane which is the natural reduced domain of solution of the stationary Schrödinger equation. In a finite difference, or finite element approach it is easy to obtain odd and even solutions separately by solving two times the eigenproblem with different Dirichlet/Neumann boundary conditions on the symmetry axis boundary.

6.2 The effects of low symmetry: envelope functions of spinorial problems

Let us now turn to the valence band which display much less trivial behavior. In this case we shall use for illustration the minimal four band Luttinger Hamiltonian [27, 41, 47, 53] which is required when one wants to have a good estimate of the optical polarization anisotropy. It also provides a fairly good description of the QWR valence subband energy dispersion close to the Γ zone-center.

The corresponding envelope Luttinger Hamiltonian $H(\mathbf{r}_{\perp}, k)$ for the QWR valence band is given in (3.33) and in the following we simply note $k = \mathbf{k}_{\parallel} = k_x$. The corresponding eigenstates are 4D spinorial functions (related to $j = 3/2$) and each component is a k -dependent scalar function of \mathbf{r}_{\perp} (envelope functions). At this stage a few comments are in order. First the actual form of the p, q, r, s coefficients is a function of the Bloch function basis chosen. One usually define a cartesian frame with the z -axis oriented along an $[hhk]$ direction [53], and one chooses a Bloch function basis which diagonalizes the J_z component of the quasi-angular momentum. It is important to

point out that *the actual shape of each envelope function is basis-dependent even if the expectation value of any (scalar) physical quantity is basis independent*. This fact, which was not recognized for a long time, complicates a lot the question of the symmetry of the envelope functions in the presence of valence band mixing.

The existence of a symmetry group for an Hamiltonian allows to classify the eigenstates and deduce the degeneracies as well as the possible transformation properties of each kind of eigenstates. It is just a very elementary application of basic group theory to the Hamiltonian [29]. However the analysis of the symmetry of individual envelope functions requires more work. In Ch. 8 we shall examine in detail transformation properties of both scalar and spinorial sets of functions, thus it is important to give an intuitive justification and introduction to this extensive effort, and we shall first discuss in this subsection the effects of symmetry in the simplest case of a single symmetry plane (C_s symmetry), already quite well-known (see [17], and subsequent works [18, 69–71]). Then we shall enlighten in detail the difficulties involved in applying the elementary concepts to higher symmetries. This will both develop intuition and understanding, and demonstrate that one needs a completely new theory. In a spinless case like the conduction band, group theory does not bring much for the trivial C_s symmetry. As presented in the last section, the solutions classify naturally into the even and odd wave function shown in Fig. 6.2 corresponding respectively to the A' and A'' (irreps) of the C_s group.

The case of the valence band eigenstates is much more complex because of their spinorial character. Even if one knows from group theory that they classify into the two double group irreps ${}^iE_{1/2}$, $i = 1, 2$, there is no simple prescription for the envelope functions, and, indeed, even their symmetry depend on the basis chosen! In the early works on the subject [19, 21] the “standard” basis chosen was generally the one diagonalizing J_z with J_z aligned with the [001] crystalline direction as in a quantum well (i.e. the vertical direction J_y with the choice of notation in Fig. 6.1). This was quite justified since the shape of a V-shaped quantum wire is close to a deformed quantum well, and many qualitative features of the optical absorption spectrum can be understood on the basis of such an analogy [19, 21]. However with such a basis one obtains the ground state envelope functions shown in Fig. 6.3 where we clearly see that none of them is either symmetric or antisymmetric with respect to the symmetry plane!

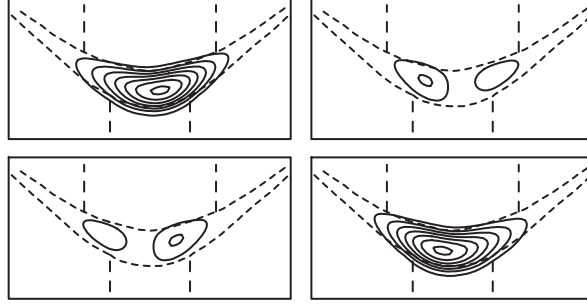


Figure 6.3: Contour plots of valence band envelope functions of the ground state of symmetry ${}^1E_{1/2}$ in a typical V-shaped QWR, when the Bloch functions diagonalize J_y corresponding to the [001] crystal direction (same QWR and same states as in Fig. 6.2 (a-d) $m = 3/2, 1/2, -1/2, -3/2$ function components respectively).

However there are still symmetry relations that can be formulated as follows:

$$\begin{aligned}\psi_{k,m}^{1E_{1/2}}(y,z) &= \psi_{k,-m}^{1E_{1/2}}(y,-z) \\ \psi_{k,m}^{2E_{1/2}}(y,z) &= -\psi_{k,-m}^{2E_{1/2}}(y,-z)\end{aligned}\quad (6.3)$$

Such symmetry relations, which only couple $\pm m$ wavefunctions, do not enforce the individual symmetry of every envelope function! Moreover they are not so convenient from the numerical point of view, in particular because they do not allow to directly reduce the domain of solution on the half-plane! The clue to this problem was found in [17] by choosing a different Bloch function basis which diagonalize J_z along the [110] crystalline direction as in Fig. 6.1. In such a case one finds the following symmetry of the envelope functions

$$\begin{aligned}\psi_{k,m}^{1E_{1/2}}(y,z) &= (-1)^{j+m} \psi_{k,m}^{1E_{1/2}}(y,-z) \\ \psi_{k,m}^{2E_{1/2}}(y,z) &= (-1)^{j+m+1} \psi_{k,m}^{2E_{1/2}}(y,-z)\end{aligned}\quad (6.4)$$

In Fig. 6.4 we display the contour plots for the same ground state as in Fig. 6.3. Although seemingly different, this representation of the eigenstate carries exactly the same physics, i.e. gives the same expectation value for any physical observable. The basic reason for the behavior as a function of m of the envelope functions in Eqs. (6.4), compared to Eqs. (6.3), which might seem surprising at first, can be explained in very simple terms by the behavior of angular momentum components through a planar reflection σ : indeed the sign of the in-plane components of the angular momentum are

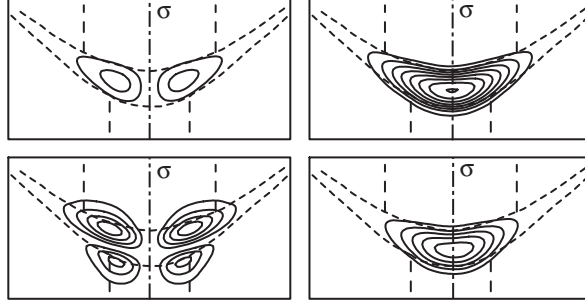


Figure 6.4: Contour plots of valence band envelope functions of the ground state of symmetry ${}^1E_{1/2}$ in a typical V-shaped QWR, when the Bloch functions diagonalize J_z corresponding to the $[110]$ crystal direction (same QWR as in Fig. 6.2 (a-d) $m = 3/2, 1/2, -1/2, -3/2$ function components respectively).

reversed, while the perpendicular component is conserved, i.e.

$$\vartheta_{\sigma^{-1}} \mathbf{J} \vartheta_{\sigma^{-1}}^{-1} = -\mathbf{J} + 2J_z \hat{e}_z \quad (6.5)$$

Therefore it is obvious that if one uses a Bloch basis that diagonalizes J_z every envelope function will be mapped onto itself (either in a symmetric way or antisymmetric way), whilst the $+m$ and $-m$ components will be mapped onto each other if one diagonalizes J_y .

Transformation rules for the envelope functions

For the spinorial states one has a global double group label and the transformation rule are given by Eq. (2.32). A spinor has then a *global symmetry but one does not have a priori symmetry properties for every scalar component!* The origin is related to the W matrix mixing different spinorial component under application of a symmetry operation. The $\{W\}$ Wigner representation depend on the choice of the basis vectors $\{|j, m\rangle\}$ and an optimal choice of the basis is essential to obtain minimal coupling schemes.

For a low symmetry group like the C_s group presented above, the concept of “optimal quantization axis” (OQA) direction allows to obtain an optimal Bloch function basis and the OQA direction is defined by the normal to the symmetry plane. With respect to this basis, every matrix W become diagonal, then the 4D Wigner representation is in the *reduced form*

$$W = {}^1E_{1/2} \oplus {}^2E_{1/2} \oplus {}^1E_{1/2} \oplus {}^2E_{1/2} \quad (6.6)$$

This is not astonishing because for the double group of C_s one has only two 1D irreps, then every 1D irrep is equivalent to ${}^1E_{1/2}$ or to ${}^2E_{1/2}$ and every degenerate irrep can be reduced.

Starting from the transformation law (2.33), for a 1D irrep and considering the W matrices in the diagonal form (6.6), one obtains transformation law for every component m

$$\underline{\psi}'(\mathbf{r}) = W^{-1}\underline{\psi}(\mathfrak{R}\mathbf{r}) = \chi^{\Gamma*}\underline{\psi}(\mathbf{r}) \quad \Rightarrow \quad \psi_m(\mathfrak{R}\mathbf{r}) = (W_{mm}^*\chi^{\Gamma})^* \psi_m(\mathbf{r}) \quad (6.7)$$

where $W = W(g)$, $\mathfrak{R} = \mathfrak{R}(g)$ and $\chi^{\Gamma} = \chi^{\Gamma}(g)$ depend on the symmetry operation g as presented in Ch. 2.

It is very simple to understand this last equation if one note that:

- In (6.7) there are no coupling between different spinorial components
- $\psi(\mathfrak{R}\mathbf{r})$ is very similar to the symmetry equation for a scalar function given in (2.19)
- According to the reduction of the Wigner representation, $W_{mm} = \chi^{iE_{1/2}}$ where $i = 1$ or 2 , then $(W_{mm}^*\chi^{\Gamma})$ is the character of the direct product of representations ${}^iE_{1/2}^* \otimes \Gamma = {}^jE_{1/2} \otimes \Gamma$, $j \neq i$ because mutually conjugated
- The direct product of two double group irreps is always reducible into single group irreps. From table 2.2:
 ${}^iE_{1/2} \otimes {}^iE_{1/2} \approx A''$ and ${}^iE_{1/2} \otimes {}^jE_{1/2} \approx A'$.

Finally, one obtains *exactly* an equation of the form (2.19) giving symmetry properties for a scalar function. Scalar components of ${}^1E_{1/2}$ and ${}^2E_{1/2}$ are alternatively (even,odd,even,odd) and (odd,even,odd,even) functions, and introducing single group labels one obtains

$$\psi^{1E_{1/2}} = \begin{pmatrix} \psi^{A'} \\ \psi^{A''} \\ \phi^{A'} \\ \phi^{A''} \end{pmatrix} \quad \psi^{2E_{1/2}} = \begin{pmatrix} \psi^{A''} \\ \psi^{A'} \\ \phi^{A''} \\ \phi^{A'} \end{pmatrix} \quad (6.8)$$

where, for every ${}^iE_{1/2}$, the ψ^{Γ} , ϕ^{Γ} are independent functions because no coupling exist. In a rigorous way, it would be necessary to introduce a ${}^iE_{1/2}$ label to the scalar functions because ψ^{Γ} and ϕ^{Γ} for ${}^1E_{1/2}$ and ${}^2E_{1/2}$ are different functions (except possibly additional degeneracy due to time reversal symmetry at the center of the zone).

Then, by explicitly consider the separation of spinorial and spatial basis,

with respect to an optimal quantization axis, in addition to a global double group label for the spinorial eigenstate, one obtains *single group classification for every component*. This is one of the more important results of this thesis work.

In Ch. 8, we shall deal in details with well-adapted bases, which simplify the problem.

In the next section, we shall quickly demonstrate the difference between low and high symmetries and show that new tools need to be found to obtain the optimal Bloch function basis.

6.3 From low to high symmetry

The previous discussion showed that a careful choice of basis allows, in the case of C_s , to symmetrize individual envelope functions. Will this be possible in the case of higher symmetry? We intend to show in this section the partial adequacy of the approach suggested in [17], where we introduced the concept of optimal quantization axis (OQA). In the previous section we considered as an example the practical case of a QWR, although similar considerations would have held for QDs. Here we shall take quantum dots as examples.

Let us first discuss the next higher symmetry, a $C_{2v} = C_2 \otimes C_s$ [3] quantum dot as depicted on Fig. 6.5 (it is a fairly common shape for pyramidal *InAs* QDs). For compatibility with the axes used in this paper we shall denote its two mutually perpendicular symmetry planes σ_y and σ_z . It is clear that since C_s is a sub-group of C_{2v} , we still can use the same basis diagonalizing σ_z , and can reduce the problem to the half-domain. However it is desirable to use the additional symmetry with respect to σ_y to further split the domain of solution. The problem do not arise with electrons, since the two sym-

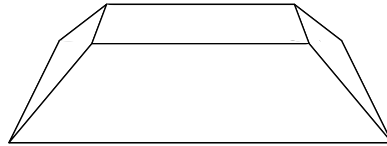


Figure 6.5: Schematic of a C_{2v} QD

metry plane operations commute (see subsection 2.6.2), and therefore one can diagonalize simultaneously the two symmetry plane operations σ_y and σ_z , and get simultaneous good quantum numbers linked with these discrete symmetries. However problems immediately arise with holes, since in the

valence-band one has no alternative but to work with a 4 band $k \cdot p$ model. From the previous qualitative discussion, we immediately see that if we take the quantization axis along z , the envelope functions of the spinor will be alternatively even/odd with respect to z , but will obey a symmetry relation coupling $+m$ and $-m$ with respect to y (c.f. Eq. (6.3)). Therefore it will not be immediately possible to solve on the half domain with respect to y . Oppositely if one chooses the y basis, the symmetry relations with respect to z will become badly behaved.

At a more fundamental point of view, such a behavior can be traced back to the fact that in this case the set of symmetry operators follow the multiplication table of the double-group. Indeed the general commutator can be written as

$$[\sigma_y, \sigma_z] = C_2 \left(1 + (-1)^{2j+1} \right) \quad (6.9)$$

Therefore when j is half-integer (here $j = 3/2$), it is *never* possible to diagonalize simultaneously both symmetry operations. This is also related to the appearance of a 2D irreps ($E_{1/2}$) for the double group and the fact that the corresponding unitary representation is not scalar but formed by 2×2 matrices $D^{E_{1/2}}(g), g \in C_{2v}$.

As a result of this analysis we suggested in [17] that the optimal basis was the one diagonalizing the projection of angular momentum along the third axis (the so-called OQA), which was along the intersection of the two planes, and which would allow to treat σ_y and σ_z on an equal footing. It turns out that it does not really solve the problem: the rotation $C_2 = \sigma_y \sigma_z$ is diagonalized in this case, but it is far from obvious how to solve on the quarter of the domain.

Even more interesting (and more problematic!) is the next higher symmetry: C_{3v} symmetry with three symmetry planes, like in Fig. 6.6. Such a case is also of practical interest [2, 23]. The reference axes of the crystal and their

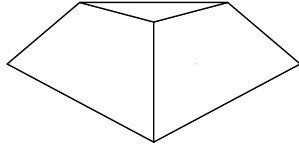
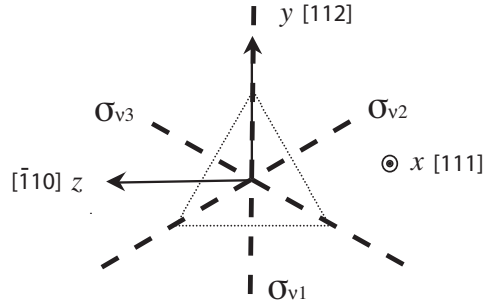


Figure 6.6: Schematic of a C_{3v} QD

x, y, z label are shown in more detail in Fig. 6.7, together with the three vertical symmetry planes $\sigma_{vi}, i = 1, 2, 3$.

As presented in subsection 2.6.3, in the C_{3v} group, there are two 1D irreps A_1 and A_2 , and a 2D irrep (E), even for the single group, adding clearly

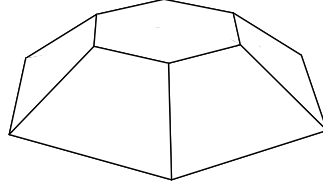
Figure 6.7: Axes and cross section of the $Al_xGa_{1-x}As$ C_{3v} QD

a supplementary difficulty: there are two basis function (partner functions) for the subspace related to degenerate eigenvalues and the corresponding 2D matrix representation explicitly depend on the basis functions. The 1D single group irreps A_1 and A_2 are respectively even and odd with respect to all the symmetry planes. Therefore, for electrons it is straightforward to see that for some eigenstate one can compute easily the solutions on $1/6$ of the domain by imposing respectively Neumann or Dirichlet boundary conditions on the two symmetry planes. However, for states belonging to the degenerate E irrep, although we can choose a representation in which any basis function is even or odd with respect to one symmetry plane, however it will not be possible to diagonalize simultaneously any two of the mirrors at the same time since none of them commute, as can be seen in the multiplication table given in Table 2.4.

Therefore in a C_{3v} heterostructure we already have for a conduction electron the same problem as we had for holes in the valence-band of a C_{2v} heterostructure: we cannot solve on a reduced domain more than one half! For holes in C_{3v} the problem is similar as for holes in C_{2v} : there are a 2D irrep among the additional double group irreps (the 1D mutually conjugated ${}^iE_{3/2}$, $i = 1, 2$ and the 2D faithful self-conjugated $E_{1/2}$).

To give a last example of an even higher symmetry group, there is also the hexagonal C_{6v} structures. A schematic of QD with C_{6v} symmetry is presented in Fig. 6.8 and a characteristic of this group is that double group display only 2D degenerate irreps. Such structures have been discussed in the literature with the help of group theory [24], however the symmetry properties of the envelope functions have not yet been studied and will be given in Sec. 10.1.

To summarize, the concept of quantization axis direction is a spatial visualization of the pure rotation of the original spinorial basis in which the Luttinger Hamiltonian was formulated: to each 3D rotation of the quantiza-

Figure 6.8: Schematic of a C_{6v} QD

tion axis direction, defined by three Euler angle α, β, γ [30], a $2j+1$ spinorial basis rotation matrix $W(\alpha, \beta, \gamma)$ can be associated. This is however a limited choice of basis, and our analysis has revealed that it was not really optimal in the sense that maximal symmetrization of the envelope functions could not be achieved in the case of higher symmetry. Moreover computation on a reduced domain did not appear possible. In the following, a radically new approach for HSH is presented which will fulfill these goals. The optimal spinorial basis is obtained by a more general unitary transformation corresponding to the reduction (block-diagonalization) of the spinorial representation and related to the choice of double group labelled basis functions.

Finally, the limit between low and high symmetry group can be identified with the presence of a 2D irrep. This require to deal with degenerate eigenstates and the Wigner representation (transformations of Bloch function basis) can not be diagonalized but only block-diagonalized.

The existence of inversion or symmetry plane is essential to have degenerate irreps for point groups, indeed the sub-groups C_n , $n \in \mathbb{N}$ of the pure rotational group $SO(3)$ are abelian (commutative) groups and every irrep is non-degenerate. In Fig. 6.9 (a) we present the more general shape of a C_{4v} quantum structure, with the four vertical symmetry planes represented by dashed lines. In Fig. 6.9 (b), a slightly deformation of the C_{4v} structure is represented. This new shape only present the C_4 symmetry group (only rotation symmetry are still displayed). Although we do not know of any real structure having such a symmetry it should be pointed out that the reduction of symmetry due to an external on-axis magnetic field in a C_{4v} structure leads also to a reduced C_4 symmetry group! This has recently been studied by [72] in the case of $InAs$ quantum dots, however here also group theory is just used to split the problem according to the main irreps, without any care about the envelope function symmetries. Moreover the problem is formulated in a plane wave basis, which give rise to full matrices during the numerical solution, which is quite a significant waste of computer time and

memory space compared to real space methods like finite difference of finite elements. In contrast, the novel MSR method, that we will present in the following chapters, also separates the eigenvalue problems associated with each irrep but also *keeps the sparse matrix structure* of the numerical problem (when formulated with a finite differences or elements approach), *moreover it reduces significantly the domain of solution*, therefore it is convenient and maximally efficient from the numerical point of view as well.

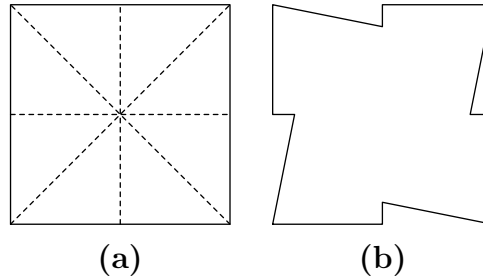


Figure 6.9: General shape of quantum structure with symmetry (a) C_{4v} ; (b) C_4

6.4 Optimal Bloch function basis

As we pointed out in the last section, high symmetry groups are related to the occurrence of degenerate irreps (for the double group of C_{2v} and even for the single group of C_{3v}). The concept of OQA direction, deriving from the physics of Quantum Wells (QWs), is useful only for study C_s QWRs like the V-shaped wires that can be seen like a deformed QW. For higher symmetry group, with additional (non-commuting!) symmetry planes, the lateral aspect is close to one and QWR cannot be considered as deformation of QWs, then any optimal direction of the quantization axis can be found.

We introduce the new concept of *fully symmetrized Bloch function basis according to the heterostructure symmetry*, the Optimal Bloch function Basis (OBB). The basic ideas and full development are presented in Ch. 8, but the core of the method consists in changing the basis so as to replace the Wigner representation by a block-diagonal representation.

With this reduced form of the “Wigner” representation the coupling between different components is minimized and simple symmetry properties for the envelope function can be found. This technique of block-diagonalization of the Wigner representation can appear a posteriori trivial but is absolutely not taken for granted without the explicit separation of spatial and Bloch

part of the operators.

The optimal basis block-diagonalizing the representation is in general not obtained by a rotation but by a more general unitary transformation and the new basis will no anymore be formed by the eigenstates of any generator of the rotations (operator J_i). This is in agreement with the fact that point group involving improper rotations are not sub-groups of $SO(3)$ and the block-diagonal representation is no more formed by Wigner matrices.

The initial basis was labelled $|j, m\rangle$, where j and m are quantum numbers for the rotations related to J^2 and J_z operators, whilst the new fully symmetrized basis with respect to the point group does not have the rotation symmetries but transform with the double group of the reduced microscopic symmetry of the heterostructure. The corresponding new quantum numbers are $j \rightarrow \Gamma$ and $m \rightarrow i$ where i is the partner function index of the double group irreps Γ .

Finally, the expression (6.7) allowing to introduce single group labels for the scalar functions can be generalized without difficulties to the HSH: the general technique is presented in Ch. 8 but the basic idea is still the reduction of the direct product of two double group irreps to single groups irreps. The choice of fully symmetrized basis according to the heterostructure symmetry group is one of the most important point of the new formalism (and of this PhD thesis) and is absolutely essential to obtain a simpler description of the physical phenomena.

6.5 High symmetry: a new formalism

In the following two chapters, we propose a general *Maximal Symmetrization and Reduction (MSR) formalism* perfectly adapted to the study of spinorial or scalar HSH problems.

The heart of the MSR formalism is threefold. First *an explicit separation of the orbital part* (spatial 3D or eventually in Fourier space) *from the spinorial part* of the states. In particular, every spinorial component can be treated as an individual scalar function. Second we choose, according to the symmetry, *the optimal fully symmetrized bases*, both for spinorial space (the Optimal Bloch function Basis (OBB)) and orbital space, which minimize the coupling between different spinorial components. Third *for every irrep* we identify the independent parameters (the orbital reduced domain) and compute a *systematic Spatial (or Fourier) Domain Reduction (SDR)* to obtain a reduced Hamiltonian with respect to the reduced domain.

Let us now shortly detail the different procedures of the proposed MSR technique.

In Ch. 7 we first treat the scalar problems, like the single band $k \cdot p$ spinless conduction band Hamiltonian. The method reduces to a systematic SDR procedure which involves two fundamental steps: first the spatial domain is decomposed into a minimal number of disjoint sub-domains which map into each other through symmetry operations (including borders as separate domains), second we project the set of domains for every irrep. This last step allows to identify for every irrep the minimal domain for any function of a given symmetry and to obtain a reduced Hamiltonian on the minimal (reduced) domain.

In Ch. 8 we present the formalism for the spin dependent problems, like the 4×4 $k \cdot p$ Luttinger Hamiltonian describing the valence band in diamond semiconductors. First we seek the optimal basis (OBB) allowing to block-diagonalize the corresponding Wigner matrix representation. Therefore by choosing the OBB, we have enforced a minimal coupling between different spinorial function components, furthermore it can be proved that every component can be decomposed in a simple way into single groups irreps labelled spinless functions. At this stage, the SDR technique is therefore applicable, and reduced Hamiltonians can be obtained for the spinorial problem.

Finally, in Ch. 9, the new formalism applied to the study of electronic and optical properties of the C_{3v} Vertical Quantum Wire (VQWR).

Chapter 7

Spatial Domain Reduction (SDR) technique for the scalar functions

We present here the general theory of the spatial domain reduction (SDR), the first part of our new MSR formalism. In this chapter the SDR technique is developed for a scalar function (the application to the spinorial problems is presented in the next chapter). This method, although completely general, is illustrated by taking the example a C_{3v} QWR (in Ch. 9 the method applied at length to a real C_{3v} structure and all relevant analytical and numerical results are discussed in detail). The generalization to other groups or other heterostructures with different dimensionality only needs some small modifications to the technique, and will be clear to the reader at the end of the section. This SDR technique is perfectly adapted to all real space methods like Finite Elements Methods (FEM) or Finite Differences (FD), however the technique can be easily adapted to perform Fourier space reductions.

We consider an arbitrary domain with the C_{3v} symmetry (see Fig. 2.6), which is the “superbox” containing the nanostructure of interest. The Hamiltonian of the system is obviously invariant under all the operations of the C_{3v} symmetry of the problem.

The presentation of the method is decomposed in three different steps. First, the spatial domain is decomposed into disjoint sub-domain according to the symmetry, then for every irrep the minimal independent sub-domains (the reduced domains) are obtained, and finally the corresponding reduced Hamiltonians are systematically constructed. Of a particular interest is the reduction for the 2D irrep E , where some additional subtleties have been addressed.

7.1 Decomposition in disjoint sub-domains

We consider an arbitrary domain of symmetry C_{3v} and represented as a triangle. Eigenstates are represented by a vector of dimension N , corresponding to the total number of nodes of the meshing (e.g. values of the states on the nodes in a FD or FEM problem with Lagrange elements). The aim of the method is to choose the best numbering of the nodes according to the decomposition of the spatial domain. The only condition we have to impose to the mesh, is to be symmetric with respect to every operation g of C_{3v} .

We obtain the decomposition of the domain in 13 disjoint parts by separating the center, the six edges and the six internal sub-domains (Fig. 7.1). In our specific 2D problem, (Fig. 7.1) correspond to the section of the QWR and for a 3D problem, (Fig. 7.1) represent the projection of the convergence domain.

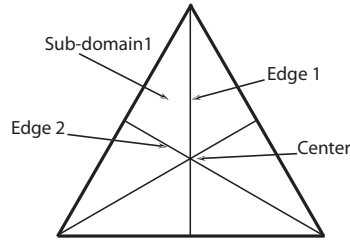


Figure 7.1: Decomposition of a spatial domain with symmetry C_{3v} in 13 disjoint parts

Every eigenstate can then be decomposed in the following vectorial form

$$\psi = \begin{pmatrix} \psi_0 \\ \psi_{Ed1} \\ \psi_1 \\ \psi_{Ed2} \\ \dots \\ \psi_6 \end{pmatrix} \quad (7.1)$$

This decomposition of the vector ψ could seem simplistic, but is essential because the independent variables appearing in the problem will be brought together into the sub-domains presented above and allow to express in a compacted form the reduced variables.

For every irreps we obtain the minimal independent parameters number and define a reduced vector ψ_{Red}^Γ on the corresponding reduced domain. For A_1 and A_2 with Eq. (7.4) we obtain

$$\psi^{A_1} = \begin{pmatrix} \psi_0 \\ \psi_{Ed1} \\ \psi_1 \\ \psi_{Ed2} \\ \psi_1 \\ \psi_{Ed1} \\ \psi_1 \\ \psi_{Ed2} \\ \psi_1 \\ \psi_{Ed1} \\ \psi_1 \\ \psi_{Ed2} \\ \psi_1 \end{pmatrix}, \quad \psi^{A_2} = \begin{pmatrix} 0 \\ 0 \\ \psi_1 \\ 0 \\ -\psi_1 \\ 0 \\ \psi_1 \\ 0 \\ -\psi_1 \\ 0 \\ \psi_1 \\ 0 \\ -\psi_1 \end{pmatrix} \quad (7.7)$$

and the corresponding reduced vectors

$$\psi_{Red}^{A_1} = \begin{pmatrix} \psi_0 \\ \psi_{Ed1} \\ \psi_1 \\ \psi_{Ed2} \end{pmatrix}, \quad \psi_{Red}^{A_2} = \psi_1 \quad (7.8)$$

For both A_1 and A_2 the minimal domain correspond to one sixth of the structure. An additional information can be found for A_2 : the function is zero on each edge, then we only need to solve the problem in the sub-domain 1. Starting from the reduced variables (7.8) we dispose of enough information to rebuilt the full eigenstates (7.7). This is the more important interest of the SDR technique: only the independent sub-domains are finally taken into account and we obtain analytical expressions for the dependent parameters. Finally, from the numerical point of view we only solve on the minimal domain.

For the 2D irrep E , the most interesting and less intuitive case, we first have to choose which equivalent matrix representation we need. The 3D rotation matrix \mathfrak{R} form a 3D reducible representation of the C_{3v} group, reducible to $A_1 \oplus E$, already in the desired block-form and we simply take this matrix representation for E (explicitly given in Eq. (2.40)). This representation is real, and the matrix representing σ_{v1} is diagonal (the first and second partner functions even and odd with respect to σ_{v1}).

For every partner function, one has a different projector operator P_1^E and

P_2^E as presented in Eq. (7.2)) which allow to obtain both partner functions:

$$\psi_1^E = \begin{pmatrix} 0 \\ \psi_{1,Ed1} \\ \psi_{1,1} \\ \psi_{1,Ed2} \\ \psi_{1,2} \\ -\frac{1}{2}\psi_{1,Ed1} \\ -\psi_{1,1}-\psi_{1,2} \\ -2\psi_{1,Ed2} \\ -\psi_{1,1}-\psi_{1,2} \\ -\frac{1}{2}\psi_{1,Ed1} \\ \psi_{1,2} \\ \psi_{1,Ed2} \\ \psi_{1,1} \end{pmatrix}, \quad \psi_2^E = \begin{pmatrix} 0 \\ 0 \\ \psi_{2,1} \\ \psi_{2,Ed2} \\ \psi_{2,2} \\ \psi_{2,Ed3} \\ -\psi_{2,1}+\psi_{2,2} \\ 0 \\ \psi_{2,1}-\psi_{2,2} \\ -\psi_{2,Ed3} \\ -\psi_{2,2} \\ -\psi_{2,Ed2} \\ -\psi_{2,1} \end{pmatrix} \quad (7.9)$$

We note that for every partner function considered separately, the reduced domain is one third, however the two partner functions can be related by the symmetry operations, therefore we need to consider one of them! The independent parameters are related to the irrep E and allow to re-build entirely each partner function.

For this 2D irrep, we shall see that non-trivial and non-intuitive boundary conditions appear. They will be systematically obtained in the following with the SDR formalism, however the simple decomposition into sub-domains (7.9) do allow to easily understand the boundary conditions on the third edge. First, for the first partner function we obtain

$$\psi_{1,Ed3} = -\frac{1}{2}\psi_{1,Ed1} \quad (7.10)$$

corresponding to a non-local boundary condition on the function.

For the second partner function there is also non-local boundary conditions but on the derivative of the function. First we note that the behavior of the normal derivative of the partner function i on an edge j can be connected to the difference between the left and right internal sub-domains: $\psi'_{i,Edj} \sim \psi_{i,j-1} - \psi_{i,j}$, where we assume $\psi_{i,0} = \psi_{i,6}$. To give an example, $\psi'_{1,Ed1} = \psi'_{1,Ed4} = 0$ because the first function is even respect to the σ_{v1} plane. Finally, for the second partner function we obtain $\psi'_{2,Ed3} = \psi_{2,1}$ and $\psi'_{2,Ed1} = -2\psi_{2,1}$ corresponding to boundary condition

$$\psi'_{2,Ed3} = -\frac{1}{2}\psi'_{2,Ed1} \quad (7.11)$$

In addition to the non-trivial boundary conditions, from Eqs. (7.9) we obtain the very nice analytical result that both partner function are analytically zero in the center $\psi_{1,0} = \psi_{2,0} = 0!$ This exact result was not recognized in the

numerics before and fully justifies our approach.

To continue with our new SDR technique, let us consider the first partner function ψ_1^E in (7.9). It would be advantageous to reduce on one sixth of the domain as for the non-degenerated A_i irreps. This can be achieved by introducing the coupling between first and second partner functions, which allows to replace the $\psi_{1,2}$ variable of the first partner function by $\psi_{2,1}$, variable of the second partner function related to the first internal domain. Such a substitution can be computed using the σ_{v3} symmetry operation and the transformation rule (2.17)

$$\psi_{1,2} \rightarrow D^E(\sigma_{v3})_{11} \psi_{1,1} + D^E(\sigma_{v3})_{21} \psi_{2,1} = -\frac{1}{2}\psi_{1,1} + \frac{\sqrt{3}}{2}\psi_{2,1} \quad (7.12)$$

Finally one obtains the vector for the first partner function on one sixth of the domain

$$\psi_1^E = \begin{pmatrix} 0 \\ \psi_{1,Ed1} \\ \psi_{1,1} \\ \psi_{1,Ed2} \\ -\frac{1}{2}\psi_{1,1} + \frac{\sqrt{3}}{2}\psi_{2,1} \\ -\frac{1}{2}\psi_{1,Ed1} \\ -\frac{1}{2}\psi_{1,1} - \frac{\sqrt{3}}{2}\psi_{2,1} \\ -2\psi_{1,Ed2} \\ -\frac{1}{2}\psi_{1,1} - \frac{\sqrt{3}}{2}\psi_{2,1} \\ -\frac{1}{2}\psi_{1,Ed1} \\ -\frac{1}{2}\psi_{1,1} + \frac{\sqrt{3}}{2}\psi_{2,1} \\ \psi_{1,Ed2} \\ \psi_{1,1} \end{pmatrix}. \quad (7.13)$$

The reduced vector for E representation on one sixth of the domain which couple both partner function components is then

$$\psi_{Red}^E = \begin{pmatrix} \psi_{1,Ed1} \\ \psi_{1,1} \\ \psi_{2,1} \\ \psi_{1,Ed2} \end{pmatrix} \quad (7.14)$$

In the same way, the second partner function can be decomposed and ex-

pressed as function of the same reduced parameters given in (7.14):

$$\psi_2^E = \begin{pmatrix} 0 \\ 0 \\ \psi_{2,1} \\ \sqrt{3}\psi_{1,Ed2} \\ \frac{1}{2}\psi_{2,1} + \frac{\sqrt{3}}{2}\psi_{1,1} \\ \frac{\sqrt{3}}{2}\psi_{1,Ed1} \\ -\frac{1}{2}\psi_{2,1} + \frac{\sqrt{3}}{2}\psi_{1,1} \\ 0 \\ \frac{1}{2}\psi_{2,1} - \frac{\sqrt{3}}{2}\psi_{1,1} \\ -\frac{\sqrt{3}}{2}\psi_{1,Ed1} \\ -\frac{1}{2}\psi_{2,1} - \frac{\sqrt{3}}{2}\psi_{1,1} \\ -\sqrt{3}\psi_{1,Ed2} \\ -\psi_{2,1} \end{pmatrix} \quad (7.15)$$

For this 2D irrep, the expression of ψ_1^E and ψ_2^E on one sixth is more complicated with respect to the 1D irreps and not intuitive, however the fact that one is able to carry out the process to the end, including the derivation of non-trivial boundary conditions, demonstrate the power of the approach.

One desires, however, to achieve more: to be able to directly solve for the relevant part only instead of solving everywhere and cutting the wave function into relevant pieces. This can be done by cutting also the Hamiltonian matrix into relevant pieces. This is what we shall achieve in the next two sections.

The last steps are then to construct the more general Hamiltonian and then, for every irrep, obtain the reduced Hamiltonian corresponding to the independent variables.

7.3 The structure of the full Hamiltonian

Let us construct the more general 13×13 block-form scalar Hamiltonian matrix applying on the vectorial expression of eigenstates (7.1). This Hamiltonian has to satisfy two conditions:

- respect the connectivity between sub-domains
- be invariant with respect to the symmetry operations of the group (operator transforming like A_1 irrep)

First, one seeks the most general matrix operator on the full domain respecting the connectivity between sub-domains H_c . Then, in the same way as for the eigenstates, an A_1 operator satisfying the connectivity rules can be found through the use of projectors on A_1 irrep since an Hamiltonian is necessary

invariant under the symmetry operations of the group:

$$H_c = \frac{1}{|\mathcal{G}|} \sum_{g \in \mathcal{G}} M(g) H_c M(g)^{-1} \quad (7.16)$$

This procedure leads to the most general Hamiltonian respecting the natural connectivity between the nodes of each domain:

$$H = \begin{pmatrix} H_0 & H_{0Ed1} & H_{01} & H_{0Ed2} & H_{01} & H_{0Ed1} & H_{01} & H_{0Ed2} & H_{01} & H_{0Ed1} & H_{01} & H_{0Ed2} & H_{01} \\ H_{0Ed1}^t & H_{Ed1} & H_{Ed11} & H_{Ed1Ed2} & 0 & 0 & 0 & 0 & 0 & 0 & 0 & H_{Ed1Ed2} & H_{Ed11} \\ H_{01}^t & H_{Ed11}^t & H_1 & H_{1Ed2} & 0 & 0 & 0 & 0 & 0 & 0 & 0 & 0 & 0 \\ H_{0Ed2}^t & H_{Ed1Ed2}^t & H_{1Ed2}^t & H_{Ed2} & H_{1Ed2}^t & H_{Ed1Ed2}^t & 0 & 0 & 0 & 0 & 0 & 0 & 0 \\ H_{01}^t & 0 & 0 & H_{1Ed2} & H_1 & H_{Ed11}^t & 0 & 0 & 0 & 0 & 0 & 0 & 0 \\ H_{0Ed1}^t & 0 & 0 & H_{Ed1Ed2} & H_{Ed11} & H_{Ed1} & H_{Ed11} & H_{Ed1Ed2} & 0 & 0 & 0 & 0 & 0 \\ H_{01}^t & 0 & 0 & 0 & 0 & H_{Ed11}^t & H_1 & H_{1Ed2} & 0 & 0 & 0 & 0 & 0 \\ H_{0Ed2}^t & 0 & 0 & 0 & 0 & H_{Ed1Ed2}^t & H_{1Ed2}^t & H_{Ed2} & H_{1Ed2}^t & H_{Ed1Ed2}^t & 0 & 0 & 0 \\ H_{01}^t & 0 & 0 & 0 & 0 & 0 & 0 & H_{1Ed2} & H_1 & H_{Ed11}^t & 0 & 0 & 0 \\ H_{0Ed1}^t & 0 & 0 & 0 & 0 & 0 & 0 & H_{Ed1Ed2} & H_{Ed11} & H_{Ed1} & H_{Ed11} & H_{Ed1Ed2} & 0 \\ H_{01}^t & 0 & 0 & 0 & 0 & 0 & 0 & 0 & 0 & H_{Ed11}^t & H_1 & H_{1Ed2} & 0 \\ H_{0Ed2}^t & H_{Ed1Ed2}^t & 0 & 0 & 0 & 0 & 0 & 0 & 0 & H_{Ed1Ed2}^t & H_{1Ed2}^t & H_{Ed2} & H_{1Ed2}^t \\ H_{01}^t & H_{Ed11}^t & 0 & 0 & 0 & 0 & 0 & 0 & 0 & 0 & 0 & H_{1Ed2} & H_1 \end{pmatrix} \quad (7.17)$$

where every H_{ij} is a block coupling the i sub-domain to j (dimension of H_{ij} depend on sub-domains i and j). The coupling H_{ii} are simply noted H_i . One notes here the natural repetition of blocks that appear due to the symmetry of the problem!

Even if the formalism is more general, in our numerics we have used only first order Lagrange finite elements, and in this case there is no coupling between the center and internal domains, therefore in the following we have used the particular case where $H_{01} = 0$ in the Hamiltonian (7.17).

7.4 The reduced Hamiltonians

The fact that for every irrep there are only a few independent sub-domains on the sixth (reduced domain) and that the Hamiltonian can be similarly broken up into pieces, let us think that it is possible to obtain a corresponding reduced Hamiltonians.

To this end, we introduce a rectangular reduction matrix S_μ^Γ in such a way that

$$\psi_\mu^\Gamma = S_\mu^\Gamma \psi_{Red}^\Gamma \quad (7.18)$$

For every irrep (and every partner functions) one has therefore a different matrix.

With finite elements one transforms a differential eigenvalues problem into

a linear equation system $H\psi_\mu^\Gamma = E^\Gamma M\psi_\mu^\Gamma$ where H and M are respectively the stiffness and mass matrices and E^Γ are the eigenvalues related the Γ irrep. The stiffness matrix H correspond to the Hamiltonian expressed in the corresponding basis (e.g. FEM basis) and has the block-form presented in (7.17). The mass matrix M represent a possible non-orthogonality of the basis vectors and has the same block-structure. The scalar product reduces to $\langle\psi|\phi\rangle = \psi^+ M\phi$, where ψ and ϕ are the vectors (7.1) corresponding to the decomposition of the scalar function with respect to the basis.

Defining a reduced mass matrix

$$M_{Red}^\Gamma = \frac{1}{d_{Red}} (S_\mu^\Gamma)^{-1} M S_\mu^\Gamma \quad (7.19)$$

where d_{Red} represent the reduction factor, we obtain that ψ_{Red}^Γ is well normalized on the reduced domain $\psi_{Red}^{\Gamma+} M\phi^\Gamma = d_{Red}\psi_{Red}^{\Gamma+} M_{Red}^\Gamma \phi_{Red}^\Gamma$. The reduction factor represent the ratio between full and reduced domain. For C_n and C_{nv} groups, simply correspond to the cardinality of the group, $d_{Red} = |\mathcal{G}|$, but for other groups can be slightly different.

According to (7.19) we define the reduced Hamiltonian on one sixth of the domain

$$H_{Red}^\Gamma = \frac{1}{d_{Red}} (S_\mu^\Gamma)^{-1} H S_\mu^\Gamma \quad (7.20)$$

and finally obtain the reduced problem on the sixth of the full domain

$$H_{Red}^\Gamma \psi_{Red}^\Gamma = E^\Gamma M_{Red}^\Gamma \psi_{Red}^\Gamma \quad (7.21)$$

This equation show that the reduction procedure not only leads to a solution of the problem on a reduced domain, but also that one obtains different eigenvalue problems for each irrep, which amounts to sort out from scratch all eigenvalues and eigenvectors according to their symmetry.

Let us now have a look at the different reduced Hamiltonians issuing from Eq. (7.21)

Reduced Hamiltonian for A_1

For A_1 we have the reduced Hamiltonian given by

$$H_{Red}^{A_1} = \begin{pmatrix} \frac{1}{6}H_0 & \frac{1}{2}H_{0Ed1} & 0 & \frac{1}{2}H_{0Ed2} \\ & \frac{1}{2}H_{Ed1} & H_{Ed11} & H_{Ed1Ed2} \\ & & H_1 & H_{1Ed2} \\ C.C. & & & \frac{1}{2}H_{Ed2} \end{pmatrix} \quad (7.22)$$

The factor 1/2 appearing in front of the H_{Ed1} and H_{Ed2} in the diagonal are simply understood: since one has a symmetric meshing of the full structure

and since we take into account only a half of a domain, there is only a half contribution to the matrix element! This correspond to a Neumann condition to the eigenfunctions (zero normal derivative). The same argument apply to the factor $1/6$ for the central element H_0 .

Reduced Hamiltonian for A_2

For A_2 irrep, the reduced Hamiltonian has obviously only one block

$$H_{Red}^{A_2} = H_1 \quad (7.23)$$

Eigenstates are zero on every edge (Dirichlet condition) and only need to solve for the first internal sub-domain.

Reduced Hamiltonian for E

Finally, let us consider the degenerate irrep E . The reduced Hamiltonian on the sixth of the domain reads

$$H_{Red}^E = \frac{1}{2} \begin{pmatrix} \frac{1}{2}H_{Ed1} & H_{Ed11} & 0 & H_{Ed1Ed2} \\ & H_1 & 0 & H_{1Ed2} \\ & & H_1 & \sqrt{3}H_{1Ed2} \\ C.C. & & & 2H_{Ed2} \end{pmatrix} \quad (7.24)$$

By far this is the less trivial case and the $\sqrt{3}H_{1Ed2}$ block represent the non-trivial coupling between the two partner functions (coupling of $\psi_{1,Ed2}$ with $\psi_{2,1}$). In the same way, one could have started with the second partner function and obtained a similar reduced Hamiltonian with respect to other reduced variables. The only important requirement is that starting from the reduced variables in ψ_{Red}^E , one should be able to reconstruct the two vectors ψ_1^E and ψ_2^E on the full domain.

7.5 Conclusion

The two Eqs. (7.22)-(7.24) represent the reduced Hamiltonians which allow to compute the electronic states of the conduction band of a triangular QWR. We restricted to first order Lagrange finite elements presented in Ch. 9, however higher order require only the consideration of H_{01} .

It should be pointed out that this new method allow to considerably reduce the size of matrices ($\sim N^2$) and CPU time ($\sim N^3$) by solving three smaller problems. The dimensions of the three matrices are $\frac{N}{6}$ for the A_i irreps and $\frac{N}{3}$ for the E irrep. The theoretical CPU time become

$$N \rightarrow \left(2\frac{1}{6^3} + \frac{1}{3^3}\right) N^3 \cong \frac{N^3}{22} \quad (7.25)$$

and is then reduced by a factor 22!

We have clearly seen that the SDR method allows to obtain in a systematical way non-trivial boundary conditions with respect to reduced (minimal!) domains for each irrep of the group. However it is not necessary to implement such boundary conditions in a non-local way as well as for the analytical conclusions about $\psi_0 = 0$ for some state.

The SDR technique, directly leads to reduce eigenvalue problems for each irreps as given in Eq. (7.21). This is very useful in computing more complex objects, since the symmetry of every state is known a priori and it becomes trivial to use selection rules!

It is important to note also that the SDR technique is very general and applies to every symmetry group, it is not dependent on the dimensionality of the problem (e.g. the previous treatment apply to C_{3v} quantum dots directly) as well as for all other real space resolution methods. For Fourier space resolution (plane wave decomposition) or Hermite FEM, some modification to the formalism have to be computed, but the general approach is the same.

Chapter 8

The MSR formalism for spinorial problems

In this chapter we develop the formalism for the spinorial-like problems.

In the first section, we present the transformation rules of the Luttinger Hamiltonian. In Sec. 8.2 we discuss the choice of the optimal Bloch function basis. We shall see that the use of a well symmetrized basis allows to exploit the SDR technique presented in Ch. 7 to compute a spatial reduction of the spinorial problem (see Sec. 8.3).

In Sec. 8.4, the advantages of the new formalism to study the optical properties of heterostructures are evidenced by computing the matrix elements of operators.

8.1 The Luttinger Hamiltonian: transformation rules

As presented in Sec. 3.4, the conduction and valence band of a semiconductor heterostructure are described by quadratic Hamiltonian in the wave vector \mathbf{k} where the components corresponding to the confined directions (y and z in Fig. 6.7) are simply replaced by a differential operator $\mathbf{k}_\perp = (k_y, k_z) = -i\nabla_\perp$ (see Eqs. (3.32) and (3.33)).

The more general form (without magnetic fields and interface terms) for a scalar quadratic Hamiltonian (e.g. Hamiltonian describing conduction band) is

$$H(\mathbf{r}, \mathbf{k}) = H_0(\mathbf{r}) + \mathbf{k}^t \mathbf{C}(\mathbf{r}) \mathbf{k} \quad (8.1)$$

where $\mathbf{C}(\mathbf{r})$ is the “matrix” (tensor) of coefficients and $H_0(\mathbf{r})$ a scalar operator. In the case of magnetic field or interface terms, the method is still valid, but some additional terms can appear in the Hamiltonian. By generalization of transformation rule (2.12) we obtain the new Hamiltonian

$$H'(\mathbf{r}, \mathbf{k}) = H(\mathfrak{R}\mathbf{r}, \mathfrak{R}\mathbf{k}) = H_0(\mathfrak{R}\mathbf{r}) + \mathbf{k}^t \mathbf{C}'(\mathbf{r}) \mathbf{k} \quad (8.2)$$

where

$$\mathbf{C}'(\mathbf{r}) = \mathfrak{R}^{-1} \mathbf{C}(\mathfrak{R}\mathbf{r}) \mathfrak{R} \quad (8.3)$$

In the following, the \mathbf{k} will be always considered as the vectorial components of the wave vector.

It is easy to understand equation (8.3) when \mathbf{C} is independent of \mathbf{r} : $\mathbf{k}^t \mathbf{C} \mathbf{k}$ is a scalar, invariant under a passive transformation and \mathbf{k} the vectorial components of wave vector, then \mathbf{C} is a tensor two times covariant and for this kind of tensors, transformation law gives $C'^{ij} = \sum_{rs} \mathfrak{R}_{ir}^{-1} \mathfrak{R}_{js}^{-1} C^{rs} = \sum_{rs} \mathfrak{R}_{ir}^{-1} C^{rs} \mathfrak{R}_{sj}$.

For the 4D Luttinger Hamiltonian describing the valence band $H(\mathbf{r}, \mathbf{k})$, every component $H_{ij}(\mathbf{r}, \mathbf{k})$ is a quadratic scalar operator in \mathbf{k} transforming like Eq. (8.2)

$$\begin{aligned} H'(\mathbf{r}, \mathbf{k}) &= W^{-1} H(\mathfrak{R}\mathbf{r}, \mathfrak{R}\mathbf{k}) W \\ \Rightarrow H'_{ij}(\mathbf{r}, \mathbf{k}) &= \sum_{r,s} W_{ir}^{-1} H_{rs}(\mathfrak{R}\mathbf{r}, \mathfrak{R}\mathbf{k}) W_{sj} \end{aligned} \quad (8.4)$$

where, as usually, the dependence on the symmetry operation $W = W(g)$ and $\mathfrak{R} = \mathfrak{R}(g)$ is omitted.

8.2 The fully symmetrized basis and the separation of spinorial and spatial parts

In this section we introduce the concept of fully symmetrized basis related to the explicit separation of orbital and spinorial part for operators and eigenstates. How introduced in Ch. 6, with an Optimal Bloch function Basis (OBB) respecting the symmetry of the group, the coupling between different envelope functions can be minimized and one can decompose in the simplest way every scalar component into single group irreps.

We recall that for a spin dependent problem, like the valence band with valence band mixing (VBM) Luttinger problem, we have to define two basis: the 3D basis $\{\hat{e}_i\}$ and the Bloch function spinorial basis $\{|j, m\rangle\}$. Question

is: how to choose the best Bloch function basis? Or in an equivalent way, how to choose the best equivalent matrix representation?

Defining a unitary matrix S in such a way that new basis vector are given by $|j, m\rangle' = \sum_n S_{nm} |j, n\rangle$, the new Wigner operators and the new Hamiltonian respect the new basis become

$$\begin{aligned} W'(g) &= S^{-1}W(g)S \\ H'(\mathbf{r}, \mathbf{k}) &= S^{-1}H(\mathbf{r}, \mathbf{k})S \end{aligned} \quad (8.5)$$

Up to now, one simply considered the concept of optimal quantization axis direction, well adapted only to the study of quantum wells (QWs) and low symmetry C_s QWRs. In our approach, we want to choose the new basis explicitly in according to the symmetry of the quantum structure by introducing a double group label for every basis vector (the fully symmetrized basis), then we need more general unitary transformation than a rotation and the new fully symmetrized basis functions are no more eigenstates of any generator of the rotations (operator J_i) but transform with the double group irreps. We make a unitary transformation which goes from basis functions labelled by (j, m) towards new basis functions labelled by true quantum numbers (Γ, μ) , where Γ and μ are the double group irrep and partner function index for the Hamiltonian symmetry group. The Wigner representation is in a completely reduced form, then every matrix is block-diagonal and the couplings between different spinorial components under symmetry operations are minimized according to Eq. (2.32).

For the C_{3v} group, the eigenstates describing the conduction band in a model including spin of the electrons are 2D spinors related to $j = 1/2$. The corresponding Wigner representation is then 2D and equivalent to the $E_{1/2}$ irrep (then is no more reducible and the corresponding Bloch basis is already fully symmetrized with respect to the symmetry). For the Luttinger problem, describing the valence band, eigenfunctions transform like a spinor with $j = 3/2$: the Wigner representation is 4D and from the traces of the matrices we deduce that the representation is reducible to ${}^1E_{3/2} \oplus E_{1/2} \oplus {}^2E_{3/2}$. With respect to the fully symmetrized Bloch function basis

$$\{|{}^1E_{3/2}\rangle, |E_{1/2}, 1\rangle, |E_{1/2}, 2\rangle, |{}^2E_{3/2}\rangle\} \quad (8.6)$$

where the partner function index is implicit for non-degenerate irreps ${}^iE_{3/2}$, the matrices have the reduced block-diagonal form given by

$$W_{Red}(g) = \begin{pmatrix} \chi^{1E_{3/2}}(g) & & \mathbf{0} \\ & D^{E_{1/2}}(g) & \\ \mathbf{0} & & \chi^{2E_{3/2}}(g) \end{pmatrix} \quad (8.7)$$

$\chi^{iE_{3/2}}(g)$ are the characters of the 1D irrep ${}^iE_{3/2}$ and $D^{E_{1/2}}(g)$ a 2D matrix representation for $E_{1/2}$ that we can fix without restraint by choosing the two partner functions. In the following we explicitly choose, according to the product of representations $E \otimes {}^2E_{3/2} \approx E_{1/2}$

$$D^{E_{1/2}}(g) = D^E(g)\chi^{2E_{3/2}}(g) \quad (8.8)$$

where $D^E(g)$ is the 2D representation for the single group irrep E presented in (2.40) (motivation will appear clear in the following).

An alternative way to understand the decomposition of the Wigner representation into the block-diagonal form (8.7), is to consider the diamond group O_h , symmetry group of the Luttinger Hamiltonian for the underlying bulk semiconductor. With respect to O_h , a spinor $j = 3/2$ transform like the 4D $F_{3/2,g}$ irrep. However C_{3v} is a sub-group of O_h and subduction tables (see Sec. 2.5) from O_h to C_{3v} gives [3] $F_{3/2,g} \rightarrow {}^1E_{3/2} \oplus E_{1/2} \oplus {}^2E_{3/2}$.

Finally, we note that the 3D matrix representation $\{\mathfrak{R}\}$ is already in a reduced block-diagonal form $A_1 \oplus E$ for C_{3v} with the basis presented in Fig. 6.7 (\hat{e}_x is invariant with respect to every symmetry operations of the group and \hat{e}_y, \hat{e}_z are mutually coupled according to E irrep), then we implicitly have chosen the basis according to the symmetry of the heterostructure in the same way as for the Bloch function basis!

The fully symmetrized 3D and Bloch function basis (with corresponding matrix representation completely reduced), are the well adapted basis to study the electronic properties of heterostructures. In particular, as presented in the following, every component of a spinorial state can be decomposed in the simplest way with respect to the symmetry (single group-labelled scalar functions) because the Block-diagonal Wigner operators minimize the coupling between different components.

The 4×4 Luttinger matrix (3.22) describing the $j = 3/2$ valence band depend on some p, q, r, s scalar operators quadratic in \mathbf{k} .

With respect to the fully symmetrized basis, the Luttinger Hamiltonian is expressed in a very simple form. In particular, every p, q, r, s operator transform like single group representations: p and q are scalar operators transforming like A_1 and (r, s) form a set of irreducible tensorial operator (ITO) transforming with the irrep E (see Ch. 9 for more details and explicit form of the operators).

To obtain these decompositions, we start from the invariance law under symmetry operations for the Hamiltonian (2.14) and, with expression (2.34)

where the spinorial and spatial part of the operators are explicitly separated, (8.4) allow to obtain

$$\begin{aligned} \vartheta_{g^{-1}}^{(3D)} H(\mathbf{r}, \mathbf{k}) \vartheta_{g^{-1}}^{-1(3D)} &= \vartheta_{g^{-1}}^{-1(j)} H(\mathbf{r}, \mathbf{k}) \vartheta_{g^{-1}}^{(j)} \\ \Leftrightarrow H(\mathfrak{R}\mathbf{r}, \mathfrak{R}\mathbf{k}) &= W H(\mathbf{r}, \mathbf{k}) W^{-1} \end{aligned} \quad (8.9)$$

The left hand side of (8.9) corresponds to a single group transformation and allows to obtain the desired symmetry properties for the components.

In the same way, from the symmetry properties for spinor (2.33) we obtain again scalar function transformation laws for every component

$$\begin{aligned} \vartheta_{g^{-1}}^{(3D)} \underline{\psi}_{\mu}^{\Gamma}(\mathbf{r}) &= \sum_{\nu=1}^{d_{\Gamma}} [D^{\Gamma}(g^{-1})]_{\nu\mu} \vartheta_{g^{-1}}^{-1(j)} \underline{\psi}_{\nu}^{\Gamma}(\mathbf{r}) \\ \Rightarrow \psi_{\mu,i}^{\Gamma}(\mathfrak{R}\mathbf{r}) &= \sum_{\nu=1}^{d_{\Gamma}} \sum_{j=1}^d [D^{\Gamma}(g^{-1})]_{\nu\mu} W_{ij} \psi_{\nu,j}^{\Gamma}(\mathbf{r}) \end{aligned} \quad (8.10)$$

where $i = 1, \dots, 4$ are the components related to the basis

$$\{|^1E_{3/2}\rangle, |E_{1/2}, 1\rangle, |E_{1/2}, 2\rangle, |^2E_{3/2}\rangle\} \quad (8.11)$$

The effects of the minimal coupling schema of W_{Red} due to a fully symmetrized basis appear evident.

To illustrate this last essential expression, we consider the first component (related to $|^1E_{3/2}\rangle$ basis function) of the non-degenerate irrep $\Gamma = ^2E_{3/2}$. Eq. (8.10) reduce to the simple uncoupled expression

$$\psi_1^{^2E_{3/2}}(\mathfrak{R}\mathbf{r}) = \chi^{^2E_{3/2}}(g)^{\star} \chi^{^1E_{3/2}}(g) \psi_1^{^2E_{3/2}}(\mathbf{r}) = \left(\chi^{^2E_{3/2}}(g) \chi^{^1E_{3/2}}(g)^{\star} \right)^{\star} \psi_1^{^2E_{3/2}}(\mathbf{r}) \quad (8.12)$$

Considering that $^iE_{3/2}$ are mutually conjugated irreps and $^2E_{3/2} \otimes ^1E_{3/2}^{\star} \equiv A_2$ (see table 2.4), we obtain that $\psi_1^{^2E_{3/2}}(\mathbf{r})$ transform like the single group irrep A_2 . In a similar way, we obtain that the last component transform like A_1 and the two central functions like the 2D E

$$\underline{\psi}^{^2E_{3/2}}(\mathbf{r}) = \begin{pmatrix} \psi^{A_2}(\mathbf{r}) \\ \psi_1^E(\mathbf{r}) \\ \psi_2^E(\mathbf{r}) \\ \psi^{A_1}(\mathbf{r}) \end{pmatrix} \quad (8.13)$$

To generalize, for each irrep Γ , the scalar component related to the Bloch functions $|\tilde{\Gamma}, \mu\rangle$ transform like $\Gamma \otimes \tilde{\Gamma}^*$ and the introduction of the generalized Clebsch-Gordan coefficients allows to write

$$\psi_{\mu,i}^{\hat{\Gamma}}(\mathbf{r}) = \sum_{\Gamma_s, \mu_s} C_{\mu, \tilde{\mu}^*, \mu_s}^{\Gamma, \tilde{\Gamma}^*, \Gamma_s} \psi_{\mu_s}^{\Gamma_s}(\mathbf{r}) \quad (8.14)$$

where $\psi_{\mu_s}^{\Gamma_s}$ are scalar functions transforming like the single group irrep (Γ_s, μ_s) . In an equivalent way, this correspond to a fixed variance development: $\hat{\Gamma}$ is a possible symmetry of the envelope functions related to a $|\tilde{\Gamma}, \mu\rangle$ basis function only if Γ belong in the reduction of $\hat{\Gamma} \otimes \tilde{\Gamma}$.

For the ${}^1E_{3/2}$ irrep we obtain the similar decomposition

$$\underline{\psi}^{{}^1E_{3/2}}(\mathbf{r}) = \begin{pmatrix} \psi^{A_1}(\mathbf{r}) \\ -\psi_2^E(\mathbf{r}) \\ \psi_1^E(\mathbf{r}) \\ \psi^{A_2}(\mathbf{r}) \end{pmatrix} \quad (8.15)$$

For the double group irrep $E_{1/2}$ it is a little more complicated to introduce a single group label for every component due to the two-dimensionality of the irrep.

For the first components: Wigner operators are block-diagonal with dimensions of blocs 1, 2, 1, then from (8.10) we obtain that $(\psi_{\mu=1,1}^{E_{1/2}}, \psi_{\mu=2,1}^{E_{1/2}})$ form a pair of two partner function for the irrep E (and we have exactly the same for the fourth components $\psi_{\mu,4}^{E_{1/2}}$). This result can be easy understood considering that the representation product ${}^iE_{3/2} \otimes E_{1/2} \approx E$, for $i = 1, 2$.

In the same way, the four functions $\psi_{1,2}^{E_{1/2}}, \psi_{1,3}^{E_{1/2}}, \psi_{2,2}^{E_{1/2}}, \psi_{2,3}^{E_{1/2}}$ form a basis for the 4D representation $E_{1/2} \otimes E_{1/2}$ and this representation can be reduced as $E_{1/2} \otimes E_{1/2} \approx E \otimes E \approx A_1 \oplus A_2 \oplus E$. In others words, this representation reduction correspond to decompose the central components, using projector operators, into the corresponding single group irreps.

Finally, by introducing the corresponding Clebsch-Gordan coefficients of the

reduction we obtain

$$\begin{aligned} \underline{\psi}_1^{E_{1/2}}(\mathbf{r}) &= \begin{pmatrix} -\phi_2^E(\mathbf{r}) \\ \frac{1}{\sqrt{2}}(\psi^{A_1}(\mathbf{r}) + \psi_1^E(\mathbf{r})) \\ \frac{1}{\sqrt{2}}(\psi^{A_2}(\mathbf{r}) - \psi_2^E(\mathbf{r})) \\ \varphi_1^E(\mathbf{r}) \end{pmatrix} \\ \underline{\psi}_2^{E_{1/2}}(\mathbf{r}) &= \begin{pmatrix} \phi_1^E(\mathbf{r}) \\ -\frac{1}{\sqrt{2}}(\psi^{A_2}(\mathbf{r}) + \psi_2^E(\mathbf{r})) \\ \frac{1}{\sqrt{2}}(\psi^{A_1}(\mathbf{r}) - \psi_1^E(\mathbf{r})) \\ \varphi_2^E(\mathbf{r}) \end{pmatrix} \end{aligned} \quad (8.16)$$

As presented above, C_s is a sub-group of C_{3v} . A_1 and $(E, 1)$ are even irreps and A_2 and $(E, 2)$ odd irreps with respect to the σ_{v1} symmetry plane and the spinor components still are (even,odd,even,odd) or (odd,even,odd,even) with respect to this plane. This is related to the particular choice of basis functions diagonalizing $D^E(\sigma_{v1})$. In this section, we have introduced the concept fully symmetrized basis corresponding to the basis reducing the Wigner representation. With respect to an optimal spinorial basis, every component can be decomposed in a simple way introducing single group labels. To continue from this point, we have to couple the choice of optimal basis with the Spatial Domain Reduction technique developed in Ch. 7: each single group function appearing in the double group spinors decompositions (8.13)-(8.16) can be treated as an independent scalar function.

8.3 Reduction of a spinorial sets of functions

In Ch. 7, we presented the methods to compute a spacial domain reduction for a spinless problem and in the last section how to choose an optimal bloch function basis for a spin dependent problem.

In this, we finally apply the SDR to a spin dependent problem. Spinorial components of the double group irreps are labelled with single group irreps as presented in Eqs. (8.13)-(8.16).

In a FEM decomposition of the spinorial problem, the vector representing a Γ eigenstate $\psi^\Gamma = (\psi_1, \psi_2, \psi_3, \psi_4)$ is composed by 52 blocks (four scalar vectors with 13 blocks corresponding to four vectors (7.1)). To reach the SDR, we construct the reduced vector on a sixth of the structure taking into account reduced variables for every functions (single group irreps labelling)

appearing in the spinor

$$\begin{aligned} \psi_{Red}^{2E_{3/2}} &= \begin{pmatrix} \psi_{Red}^{A_2} \\ \psi_{Red}^E \\ \psi_{Red}^{A_1} \end{pmatrix} & \psi_{Red}^{1E_{3/2}} &= \begin{pmatrix} \psi_{Red}^{A_1} \\ \psi_{Red}^E \\ \psi_{Red}^{A_2} \end{pmatrix} \\ \psi_{Red}^{E_{1/2}} &= \begin{pmatrix} \phi_{Red}^E \\ \psi_{Red}^{A_1} \\ \psi_{Red}^E \\ \psi_{Red}^{A_2} \\ \varphi_{Red}^E \end{pmatrix} \end{aligned} \quad (8.17)$$

For the degenerate $E_{1/2}$ irrep, E appear three times, then $\phi_{Red}^E, \varphi_{Red}^E, \psi_{Red}^E$ are independent (uncoupled) variables and in Eq. (8.17), the reduced variables of E obviously appear three times.

The last step before carrying out reduced Hamiltonians is to construct the more general valence band Luttinger Hamiltonian (i.e. A_1 operator respecting the connectivity of the spatial domain). We showed in Sec. 8.2 that in Luttinger Hamiltonian p, q, r, s operators can be decomposed, in a similar way as for the spinorial states, with respect to the single group irreps. In particular, for C_{3v} , p, q are A_1 operator and (r, s) an ITO transforming with E irrep.

The most general form for p and q operators are then given by Eq. (7.17) with the replacement $H_{ij}^t \rightarrow H_{ij}^+$ considering that our valence band Luttinger Hamiltonian is a complex operator. To obtain r and s operators, we start from the scalar connectivity Hamiltonian and apply the projectors on E :

$$H_c = \frac{2}{|\mathcal{G}|} \sum_{g \in \mathcal{G}} D_{ii}^{\Gamma*}(g) M(g) H_c M(g)^{-1} \quad (8.18)$$

with $i = 1, 2$ for r, s respectively.

We construct the 52×52 block-form Hamiltonian, then, as for the scalar functions, we determine the reduction matrices S_i^Γ (7.18) and obtain reduced matrices $M_{Red}^\Gamma, H_{Red}^\Gamma$ given by Eqs. (7.19) and (7.20).

Reduced Hamiltonians for the non-degenerate irreps ${}^iE_{3/2}$

For the non-degenerate irreps ${}^iE_{3/2}$ we obtain the reduced Hamiltonians

$$H_{Red}^{2E_{3/2}} = \begin{pmatrix} H_{Red}^{A_2}(p+q) & C_{A_2-E}(r, s) & 0 \\ & 2H_{Red}^E(p-q) & C_{E-A_1}(r, s) \\ C.C. & & H_{Red}^{A_1}(p+q) \end{pmatrix} \quad (8.19)$$

$$H_{Red}^{1E_{3/2}} = \begin{pmatrix} H_{Red}^{A_1}(p+q) & C_{A_1-E}(r, s) & 0 \\ 2H_{Red}^E(p-q) & C_{E-A_2}(r, s) & \\ C.C. & H_{Red}^{A_2}(p+q) & \end{pmatrix} \quad (8.20)$$

where in the diagonal, $H_{Red}^{A_1}$, $H_{Red}^{A_2}$, H_{Red}^E are the same reduced Hamiltonians as for the conduction spinless problem and only depend on $p+q$ or $p-q$.

The non-diagonal coupling terms

$$C_{E-A_1}(r, s) = \begin{pmatrix} \frac{1}{2}r_{Ed10} & \frac{1}{2}r_{Ed1} & r_{Ed11} & r_{Ed1Ed2} \\ 0 & r_{1Ed1} & r_1 & r_{1Ed2} \\ 0 & s_{1Ed1} & s_1 & s_{1Ed2} \\ 2r_{Ed20} & r_{Ed2Ed1} + \sqrt{3}s_{Ed2Ed1} & r_{Ed21} + \sqrt{3}s_{Ed21} & 2r_{Ed2} \end{pmatrix} \quad (8.21)$$

$$C_{E-A_2}(r, s) = \begin{pmatrix} -s_{Ed11} \\ -s_1 \\ -r_1 \\ \sqrt{3}r_{Ed21} - s_{Ed21} \end{pmatrix} \quad (8.22)$$

only depends on the r and s operators and reflect the coupling between the different envelope functions still present in the Luttinger Hamiltonian (3.22). If we neglect this coupling, the reduced Hamiltonian is block-diagonal and each block is a scalar Hamiltonian.

We note that r and s are not self-adjoint operator, then $C_{A_i-E} \neq C_{E-A_i}^+$ but $C_{A_i-E} = C_{E-A_i}(r_{ij} \rightarrow r_{ji}, s_{ij} \rightarrow s_{ji})$, where r_{ij} and s_{ij} are the blocs appearing in the r, s operators.

Reduced Hamiltonian for the degenerate irrep $E_{1/2}$

With the same reduction technique, for the 2D $E_{1/2}$ irrep we obtain the reduced Hamiltonian

$$H_{Red}^{E_{1/2}} = \frac{1}{2} \begin{pmatrix} 2H_{Red}^E(p+q) & \frac{1}{\sqrt{2}}C_{E-A_1} & -\frac{1}{\sqrt{2}}C_{E-E} & \frac{1}{\sqrt{2}}C_{E-A_2} & 0 \\ & H_{Red}^{A_1}(p-q) & 0 & 0 & \frac{1}{\sqrt{2}}C_{A_1-E} \\ & & 2H_{Red}^E(p-q) & 0 & \frac{1}{\sqrt{2}}C_{E-E} \\ & & & H_{Red}^{A_2}(p-q) & -\frac{1}{\sqrt{2}}C_{A_2-E} \\ c.c. & & & & 2H_{Red}^E(p+q) \end{pmatrix} \quad (8.23)$$

The coupling terms $C_{E-\Gamma}$ and corresponding $C_{\Gamma-E}$ are the same appearing in the reduced Hamiltonians (8.19) and (8.20). The additional block C_{E-E} is given by

$$C_{E-E}(r, s) = \begin{pmatrix} \frac{1}{2}r_{Ed1} & r_{Ed11} & -s_{Ed11} & r_{Ed1Ed2} - \sqrt{3}s_{Ed1Ed2} \\ r_{1Ed1} & r_1 & -s_1 & r_{1Ed2} - \sqrt{3}s_{1Ed2} \\ -s_{1Ed1} & s_1 & -r_1 & -s_{1Ed2} - \sqrt{3}r_{1Ed2} \\ r_{Ed2Ed1} + \sqrt{3}s_{Ed2Ed1} & r_{Ed21} - \sqrt{3}s_{Ed21} & -s_{Ed21} - \sqrt{3}r_{Ed21} & -4r_{Ed2} \end{pmatrix} \quad (8.24)$$

Finally we note that, by coupling the choice of optimal Bloch function basis and spatial domain reduction technique, from the decomposition of envelope

functions with respect to the symmetry we can introduce reduced domains and finally obtain reduced Hamiltonians for double group problems. The reduced Hamiltonians are block-diagonal and their structure is as follows: diagonal blocks correspond to scalar Hamiltonians $H^\Gamma(p \pm q)$ and off-diagonal coupling blocks $C_{\Gamma_1, \Gamma_2}(r, s)$ only depend on the operators (r, s) . Irreps Γ_1, Γ_2 represent a coupling between a scalar function with symmetry Γ_1 with a Γ_2 function.

As result of the explicitly separation of spinorial and spatial part, in the double group Hamiltonians, everything depend only on the single group irreps A_1, A_2 and E .

The analytical developments can appear tedious, but correspond to a systematic procedure that can be easily computed and automated on a personal computer with a program like Mathematica [73].

In the next section, we present an interesting physical application of the new MSR formalism: computation of the matrix elements of an operator. The effects of a decomposition of envelope functions with respect to the symmetry will appear evident and allow to obtain simple analytical expression for the matrix elements.

8.4 Selection rules and matrix elements with the MSR formalism

In this section, we apply the MSR formalism to the computation of matrix elements of operators. The Wigner-Eckart Theorem (WET) presented in Sec. 2.4 allow to obtain the selection rules for operators. With our formalism, we obtain the same selection rules predicted by WET, but in addition we obtain simple expressions for the amplitude of transitions by introducing single group decomposition of the envelope functions.

The WET gives selection rules for an operator transforming like an irreducible representation Γ of a group A_μ^Γ , where μ is the partner operator index of the ITO (see Eq. (2.37)). The generalized Wigner-Eckart Theorem (gWET) gives information about the amplitudes by factorizing $\langle \psi_i^{\Gamma_2} | A_k^\Gamma | \psi_j^{\Gamma_1} \rangle$ into “reduced matrix elements” only dependent on the the irreps and the Clebsch-Gordan (CG) coefficients (see 2.5.4).

With our formalism, we separate the spinorial and spatial part of $\langle \psi_i^{\Gamma_2} | A_k^\Gamma | \psi_j^{\Gamma_1} \rangle$ and refine the result using additional single group selections rules.

In the following, we formally note a spinor

$$|\psi^\Gamma\rangle = \sum_i |\psi_i\rangle \otimes |\Gamma_i, \mu_i\rangle \quad (8.25)$$

where $\{|\Gamma_i, \mu_i\rangle\}$ correspond to the fully symmetrized Bloch function basis and $|\psi_i\rangle$ are the corresponding envelope functions.

As presented in Sec. 8.2, every envelope function can be systematically decomposed into a set B_i^Γ of single group irreducible representations:

$$|\psi_i\rangle = \sum_{\Gamma_j \in B_i^\Gamma} b_i^{\Gamma_j} |\psi_i^{\Gamma_j}\rangle \quad (8.26)$$

where $b_i^{\Gamma_j}$ are some constant related to the CG coefficients and the partner function label μ_j is omitted.

A matrix element of an operator A^Γ (the μ label is understood in the following) can be expressed as

$$\langle \phi^{\Gamma_2} | A^\Gamma | \psi^{\Gamma_1} \rangle = \sum_{i,j} \langle \phi_i | A_{ij}^\Gamma | \psi_j \rangle \quad (8.27)$$

where $A_{ij}^\Gamma = \langle \Gamma_i, \mu_i | A^\Gamma | \Gamma_j, \mu_j \rangle$ is a matrix operator transforming like Γ and representing A^Γ in the Bloch function basis.

Every scalar component A_{ij}^Γ can be labelled with a single group irrep and according to a fixed variance development, each scalar term $\langle \phi_i | A_{ij}^\Gamma | \psi_j \rangle$ of Eq. (8.27) have to be zero or belong to the identity representation A_1 .

To illustrate this last argument, one can consider the Luttinger Hamiltonian (3.22): it is a matrix operator expressed with respect to the Bloch function basis representing an Hamiltonian. Each component depend on the p, q, r, s scalar operators and present the corresponding single group symmetry. The symmetry of the envelope functions of the eigenstates of the Luttinger Hamiltonian are in agreement with a fixed variance development (for C_{3v} , see Eqs. (8.13)-(8.16)).

A more particular and interesting case is when every A_{ij}^Γ is simply a constant. This allow to introduce in expression (8.27) the overlap of spatial function belonging to the same irrep according to the representation orthogonality rule

$$\langle \phi_i^{\Gamma_1} | \psi_j^{\Gamma_2} \rangle = \delta_{\Gamma_1, \Gamma_2} \langle \phi_i^{\Gamma_1} | \psi_j^{\Gamma_1} \rangle \quad (8.28)$$

where $\delta_{\Gamma_1, \Gamma_2}$ is intended as $\delta_{\Gamma_1, \Gamma_2} \delta_{\mu_1, \mu_2}$.

Finally, we obtain

$$\begin{aligned} \langle \phi^{\Gamma_2} | A^\Gamma | \psi^{\Gamma_1} \rangle &= \sum_{i,j} A_{ij}^\Gamma \langle \phi_i | \psi_j \rangle \\ &= \sum_{i,j} A_{ij}^\Gamma \sum_{\Gamma_k \in (B_j^{\Gamma_1} \cap B_i^{\Gamma_2})} b_i^{\Gamma_k} b_j^{\Gamma_k} \langle \phi_i^{\Gamma_k} | \psi_j^{\Gamma_k} \rangle \end{aligned} \quad (8.29)$$

With the new MSR formalism, the expression for the matrix elements of an operator take then a very simple analytical form because only overlap of scalar functions with the same symmetry are involved and usually $B_j^{\Gamma_1} \cap B_i^{\Gamma_2} = \emptyset$ or contain only a very small number of terms.

In 9.2.3 the dipolar matrix elements are computed in the frame of the C_{3v} symmetry group and the expression (8.29) allow to considerably simplify the expression of the polarization isotropy. A perfect polarization isotropy in the plane can be analytically proven and some analytical ratio between parallel and orthogonal directions are obtained.

8.5 Discussion

In this chapter we tackled the spinorial problem by showing that an optimal chosen fully symmetrized basis allows to apply the SDR to every component. This technique, called MSR, was illustrated with the case of C_{3v} symmetry and in the next chapter we apply the new formalism to study a real C_{3v} VQWR numerically.

Nevertheless it is important to note that the MSR formalism is not restricted to this problem but can be easily generalized to any other more general vectorial, spinorial or tensorial-like problem, also with different dimensionality (3D QDs), different symmetry groups. It is also applicable to various numerical methods, whether they would be in the spatial domain (e.g. finite differences) or the Fourier domain, or any other basis. The approach is even not limited to linear problems provided one accounts for proper products of representations. The essence is to symmetrize separately the bases in the spinorial-like space and the real-coordinate-like space.

In our frame (electronic structure of heterostructures), it is clear that any number of bands can be accounted for. Similarly, strain (including the separate strain equations), Burt-Foreman interface terms [54, 55, 74], or the presence of an external field like a magnetic field can be also taken into account. The choice of fully symmetrized basis presented in Sec. 8.2 only depends on the symmetry group considered (some additional illustrative examples will

be given in Ch. 10).

Let us now compare in more details our method with the work of Vukmirovic et al. [72, 75]. In [72], a method for resolution into symmetrized plane waves decomposition is suggested for a C_4 pyramidal QD, however this is most useful for strongly coupled periodic structures like found for example in [75] for C_6 hexagonal QD superlattices. In this paper the author define N-dimensional representation of the rotation operators on the full coupled Fourier-Spin space (no separate symmetrization). With projection operators a “symmetry adapted basis” can be found (diagonalization of the representation) and as expected in this basis, the Hamiltonian can be block-diagonalized. For a C_n group, this method allow to separate the Hamiltonian into n blocks of equivalent sizes and reduce the necessary computation time. The limitations of this approach are however evident. First, it is well adapted only for the rotation sub-groups C_n where every irrep of the simple and double group are 1D. As we have seen earlier even for small groups like C_{2v} , degenerate eigenvalues could appear. Indeed in [75] the author study a C_{6v} problem (every double group irreps is 2D) but only exploit the C_6 symmetry (with only 1D irreps) by neglecting the vertical symmetry planes and they cannot describe in this frame optimally the degeneracy of eigenstates. Of course in the presence of a magnetic field this would be the correct approach, but additional lifting of degeneracies would occur. Second, the approach of [72, 75] does not separate orbital and spinorial contributions (double group irreps appear in the reduction). Therefore the symmetry properties of the structure are taken into account only at the last step before numerical resolution and no single group classification of envelope functions can be obtained or a domain reduction achieved. The new MSR method is however also applicable in this case. For a $k \cdot p$ Hamiltonian the optimal Bloch function basis is of course the same and only the spatial domain reduction has to be replaced by introducing the concept of a “reduced plane waves basis”. In [76], we have introduced such a procedure to work with a reduced domain in Fourier space (see Fig. 6c of [76] for the reduced Fourier domain for every irreps of the C_{3v} group).

We would like to end by stressing that the advantages of the new MSR formalism are manifold and have been found to be greater than originally anticipated. Indeed besides the possibility of performing SDR we have found that there were many advantages gained from the analytical point of view: first the Hamiltonian operator usually takes a simpler form in the adapted fully symmetrized basis, second the spinorial components of eigenstates (as well as the components of any operator in the spinorial basis) can be treated in the same way and easily decomposed into parts to which simple group

irreps can be associated (and for which “sub-selection rules” can be applied at an intermediate calculational level, further simplifying and enlightening the various couplings).

Chapter 9

Application to C_{3v} vertical quantum wires: analytical and numerical results

A novel formalism, presented in Chs. 7 and 8, has been developed with the aim of study a C_{3v} Vertical Quantum Wire (VQWR).

The basic concepts related to the semiconductor heterostructures and C_{3v} group were introduced in the preceding chapters (Chs. 3 and 2).

In this chapter, we first introduce more in detail the quantum structure studied and the analytical model used, then the more important analytical and numerical results are presented.

9.1 C_{3v} VQWR and pyramidal QDs

Among the different types of QDs, tetrahedral QDs grown by organometallic chemical vapor deposition (OMCVD) in inverted tetrahedral pyramids patterned onto (111)B GaAs substrate occupy a special position: it is possible to make regular arrays, they have a high ground to first excited states separation energy, and display a simultaneous low inhomogeneous broadening. The way in which they are incorporated in a solid state matrix gives a rich environment (see Fig. 3.12 for a schematic), consisting of many quantum structures connected to the dot (a vertical and three lateral QWRs, three lateral and three vertical QWs), which strongly influences the electronic and optical properties.

9.1.1 Motivation for the study

A complete study of the pyramidal QD taking into account the real geometry and the connected structures was performed by Fabienne Michelini [2], but any rigorous study of the VQWR, that serves as main channel for QD carrier capture and is the most influential for the electronic properties of the QD, was up to now at our knowledge never computed. As presented above, a beautiful feature of the VQWR is its high symmetry: three symmetry planes intersecting on the same vertical axis, leading to a “triangular” C_{3v} symmetry.

The study of the C_{3v} VQWR, envisaged as a small and original exercise to improve calculations techniques for this PhD thesis, showed a more interesting problem that conceived and finally allowed to:

- show the limit of the current resolution technique in the case of an High Symmetry Heterostructure (HSH)
- develop a new very general Maximal Symmetrization and Reduction (MSR) formalism for study HSH (see Chs. 7 and 8)

In addition, a new analytical and numerical method [77] for study coupled structures with different dimensionality like (0D QDs-1D VQWRs) has been developed in the frame of a Master thesis under our supervision (see the Master thesis of Guillaume Tarel [78] for an introduction of the method).

9.1.2 Fabrication of pyramidal QDs

Pyramidal QDs are, with the complex connected quantum structures, self-formed structures grown by OrganoMetallic Chemical Vapor Deposition (OMCVD) in inverted tetrahedral pyramid patterned onto (111) B GaAs substrate.

The first step is to construct a mask on the substrate and by anisotropic chemical attack, inverted pyramids are obtained. The second step is to grow the heterostructure by MOCVD: the constituents, in the vapor phase, are deposited in atomic layers to form the quantum structure.

For a review of details about grown and experimental techniques see for example [79, 80] or the experimental PhD thesis reports at EPFL of Ducommun [51] or Baier [81]. For more information about structural and optical properties of a pyramidal QD see Hartmann [23], and for a theoretical model of the structure Michelini [2].

9.1.3 Model of VQWR

We explicitly model the 2D $Al_xGa_{1-x}As$ C_{3v} QWR structure corresponding to a triangular-like vertical quantum wire (VQWR) (6% concentration of aluminium) connected to three vertical quantum wells (VQWs) (20%Al, width $L = 22/\sqrt{2} nm \cong 15.55 nm$) where the VQWR electronic wavefunctions may spill out. Outside there is a barrier containing 30% of Al. We note that the concentration of Al in the different parts of the quantum structure are determined by the growth mechanism.

The model for the complex C_{3v} -QWR cross section is shown in Fig. 9.1.

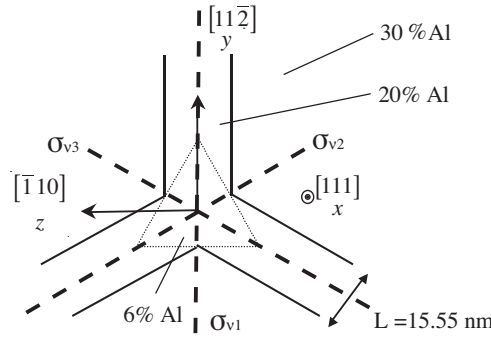


Figure 9.1: Model of the cross section of the $Al_xGa_{1-x}As$ C_{3v} -QWR

Conduction and valence band

To compute electronic properties, we solve separately in the frame of the $k \cdot p$ approximation the Γ_6 conduction band (single band spinless problem, see 3.4.2) and the Γ_8 valence band (four band with mixing Luttinger Hamiltonian, see 3.4.3).

As presented in Fig. 9.1, the $x = [111]$ direction correspond to the parallel direction and the confined orthogonal directions are $y = [11\bar{2}]$ and $z = [\bar{1}10]$. For the valence band, the p, q, r, s quadratic polynomials, function of the Luttinger parameters $\gamma_i = \gamma_i(\mathbf{r}_\perp)$, explicitly depend on the 3D basis and Bloch functions basis: for $x = [100]$, $y = [010]$, $z = [001]$ and quantization axis in the z direction, we have the parameters given in Eq. (3.25), still in the symmetrized form, where $k_x \rightarrow k$, $k_y \rightarrow -i\partial_y$, $k_z \rightarrow -i\partial_z$.

As presented in Ch. 3, the eigenstates of the $k \cdot p$ conduction band Hamiltonian are the envelope functions $\psi(\mathbf{r}_\perp)$. In a more rigorous way, we should introduce a subband index n and the $k = k_x$ as parameter: $\psi_k^n(\mathbf{r}_\perp)$ (in the following, these index will be omitted if not explicitly necessary). Finally,

the full electronic conduction band wave function is given by

$$\Psi_{C,k}^n(\mathbf{r}) = \psi_k^n(\mathbf{r}_\perp) e^{ikx} u_C(\mathbf{r}) \quad (9.1)$$

where $u_C(\mathbf{r})$ is the corresponding Bloch function.

In a similar way, for the valence band we have four envelope functions $\psi_{k,m}^n(\mathbf{r}_\perp)$ and the wave functions reads

$$\Psi_{V,k}^n(\mathbf{r}) = \sum_{m=3/2}^{-3/2} \psi_{k,m}^n(\mathbf{r}_\perp) e^{ikx} u_{V,m}(\mathbf{r}). \quad (9.2)$$

For any other 3D or Bloch function basis, the new coefficient can be obtained with the rigorous procedure introduced in details in Eq. (8.4).

Finally, in Table 9.1 we present the numerical values for the effective mass, Luttinger parameter and band parameters (bulk parameters) as function of the aluminium concentration x . The conduction and valence band confine-

Table 9.1: Material parameters used in the calculation [19]

Symbol	Parameter	Unit	$Al_xGa_{1-x}As$
E_g	energy gap	eV	$1.519 + 1.247x$
$\Delta E_c/E_v$	band offsets		$68/32$
m_e	electron mass	m_0	$0.0665 + 0.0835x$
γ_1	Luttinger parameter		$6.790 - 3.000x$
γ_2	Luttinger parameter		$1.924 - 0.694x$
γ_3	Luttinger parameter		$2.681 - 1.286x$

ment scalar potentials are obtained from the energy gap and band offset: $V_c(x) = \frac{68}{100}1.247x$ and $V_v(x) = -\frac{32}{100}1.247x$. The energies obtained from these Hamiltonians correspond to the confinement energies of the electrons and holes. We fix the zero of the energies at the top of the valence band, then energies of the holes are negative and we have to add the constant energy gap 1.519 eV to obtain the energy of the electrons in the conduction band.

Analytical computation

The matrix (analytical) manipulations presented in the last two chapters can appear very tedious but can be computed and automated in a simple way using, for example, a program like Mathematica (see Wolfram [73] for an introduction). For different groups, there are only some small and non-fundamental modification to do to the analytical code (notebook).

Numerical computation

The numerical computation of the electronic states was done by writing a Fortran 90 finite elements code (see for example Delannoy [82] for an introduction to the numerical techniques in Fortran 90). As introduced in the following, symmetry properties of the structure are explicitly taken into account in the numerical resolution by a rigorous theoretical study (MSR formalism in Chs. 7 and 8). Finally, numerical resolution of the linear problem is computed with the help of the ARPACK library using banded matrices.

9.2 Analytical and numerical results

In this section we present the most important analytical and numerical results of the study of the C_{3v} quantum structure presented in the last section. First, in 9.2.1 we discuss the effects on the Luttinger Hamiltonian of the choice of an optimal basis and the additional time-reversal symmetry as well as its effects on the spinorial states.

Second, in 9.2.2 the band structures and eigenstates for both conduction and valence band problem are given.

Subsection 9.2.3 is dedicated to the optical properties: two main features will be of interest: 1) spectra of interband dipolar transition matrix elements at Zone center (ZC), 2) complete absorption spectra for free (non-interacting) carriers. Matrix element spectra (at $k = 0$) are known to give a very good understanding of the general shape of experimental PLE absorption spectra [19] but we will see that matrix element spectra at $k = 0$ are not so good in C_{3v} quantum wires, since some lines may be missing. We will show that the absent peaks are justified theoretically when one accounts for an approximate ZC symmetry (σ_h operation). This result opens a novel question which are treated in the subsequent subsection 9.2.4: what is the degree of validity of the Hamiltonian obtained neglecting ZC symmetry breaking? We will too putting in evidence the advantages of our new formalism to understand the effects of a breaking of symmetry or additional symmetries.

Finally, in 9.2.5 the properties of a (hypothetic) similar structure such that the C_{3v} VQWR profile is oppositely oriented with respect to the bulk crystal structure, a parametric study as a function of the wire width and a comparison with the experience are presented.

9.2.1 The Luttinger Hamiltonian and additional time-reversal symmetry

OBB and Luttinger Hamiltonian

In the last chapter we have introduced the optimal Bloch function basis for a C_{3v} structure (8.6). With respect to this basis, the Wigner operators have the block-diagonal form presented in (8.7) and the p, q, r, s polynomial take the simple form

$$\begin{aligned}
 p &= k_x \frac{\gamma_1}{2} k_x + k_y \frac{\gamma_1}{2} k_y + k_z \frac{\gamma_1}{2} k_z \\
 q &= -k_x \gamma_3 k_x + k_y \frac{\gamma_3}{2} k_y + k_z \frac{\gamma_3}{2} k_z \\
 r &= k_y b k_y - k_z b k_z + (k_x a k_y + k_y a k_x) \\
 s &= -(k_y b k_z + k_z b k_y) + (k_z a k_x + k_x a k_z)
 \end{aligned} \tag{9.3}$$

where

$$\begin{aligned}
 a &= \frac{(2i + \sqrt{2}) \gamma_2 + (i - \sqrt{2}) \gamma_3}{2i\sqrt{3}} \\
 b &= \frac{(2i + \sqrt{2}) \gamma_3 + (i - \sqrt{2}) \gamma_2}{2\sqrt{3}}
 \end{aligned} \tag{9.4}$$

With respect to the fully symmetrized Bloch function basis, the Luttinger Hamiltonian is considerably simpler than what a straightforward choice of basis would give, for example Eq. (3.25). In particular, (r, s) operators transform like the E irrep, then only two independent parameters a and b can appear.

We note that in Eqs. (9.3) and (9.4) we omitted the spatial dependence of the Luttinger parameters $\gamma_i = \gamma_i(\mathbf{r}_\perp)$. In a problem including magnetic field or Burt-Foreman interface effects, additional terms in the Hamiltonian appear.

Time reversal symmetry

It is well-known [34] that time-reversal symmetry is responsible for the symmetry of the bulk valence-band structure around zone-center $E(k) = E(-k)$, and in particular of the degeneracy at zone-center (ZC) where two bands always cross. This is a consequence of Kramers two-fold degeneracy for half integer spin particles. Time reversal symmetry is necessarily represented by an antiunitary operator which we formally write as $K = UK_0$ where K_0 is the complex conjugation operator and U a unitary 4×4 operator. Starting

from a quantization axis direction $[\bar{1}10]$ (see Fig. 9.1), we can construct the time reversal operator using the properties $K^{-1}\mathbf{J}^{(j)}K = -\mathbf{J}^{(j)}$. We obtain an antidiagonal matrix operator K represented by

$$K = \begin{pmatrix} 0 & 0 & 0 & 1 \\ 0 & 0 & -1 & 0 \\ 0 & 1 & 0 & 0 \\ -1 & 0 & 0 & 0 \end{pmatrix} K_0 \quad (9.5)$$

In the same way, the form of the U operator can be obtained from the action of $-i\sigma_y K_0$ on the Bloch function basis (3.26).

In a new Bloch function basis, the p, q, r, s structure of the Luttinger Hamiltonian is preserved if the time reversal operator keeps the same form. To obtain the OBB, we need to block-diagonalize the Wigner representation. In the corresponding reduction matrix free parameters can appear, corresponding to the phase of some terms, that we have to fix in order to take invariant the form of time reversal operator K .

It is then easy to check that similarly the QWR Luttinger Hamiltonian satisfies the expected symmetry

$$K^{-1}H(\mathbf{k}, \mathbf{r})K = H(-\mathbf{k}, \mathbf{r}) \quad (9.6)$$

where we have explicitly separated the k component along the wire axis. The main interest is that time reversal symmetry applied to the envelope functions of *any* eigenstate (defined by the four quantum numbers n, Γ, μ, k) leads to the symmetry relation

$$\vartheta_{K^{-1}}\psi_{(\mu,k),m}^{(\Gamma,n)}(\mathbf{r}) = (-1)^{m+\frac{1}{2}} \left(\psi_{(\mu^*,-k),-m}^{(\Gamma^*,n)}(\mathbf{r}) \right)^* \quad (9.7)$$

where (Γ, μ) and (Γ^*, μ^*) are defined as *conjugate subbands* under time-reversal. ${}^1E_{3/2}$ and ${}^2E_{3/2}$ are 1D mutually conjugated irreps and the functions cross at $k = 0$. The 2D self-conjugated irrep $E_{1/2}$ is degenerate for every k due to the spatial C_{3v} symmetry and the two partner functions cross at $k = 0$. Finally, at ZC, every eigenvalue is degenerate due to the additional time-reversal symmetry.

9.2.2 Band structure and electronic states

Electronic states

The conduction band structure of our typical C_{3v} QWR is presented in Fig. 9.2, where the origin for the energies is set at the top of the valence band. As introduced in the theoretical part, we obtain the energy subbands corresponding to each irrep by solving the corresponding eigenproblem. The

A_1 and A_2 subbands are non degenerate, and the E subbands are twice degenerate. In this simple model without spin-orbit coupling in the conduction band the electron spin simply doubles further the degeneracy of each subband. The ground state is naturally an A_1 state and the first excited state

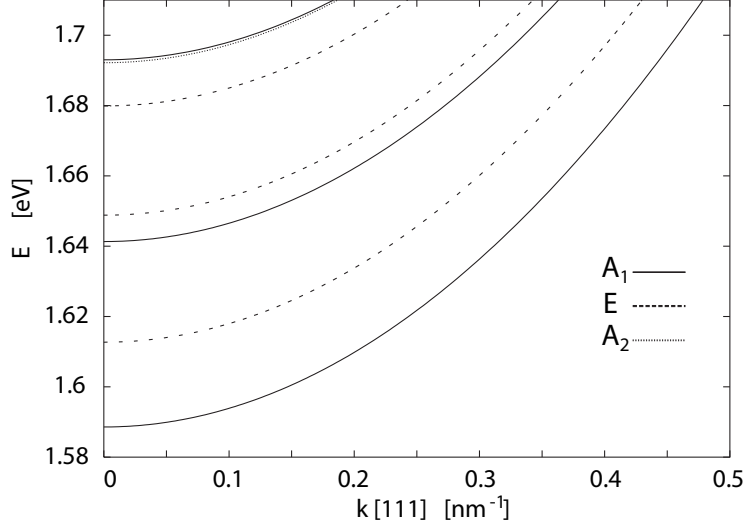


Figure 9.2: Conduction band for the AlGaAs C_{3v} -QWR

a degenerate E state. Fig. 9.3 (a) displays a contour plot of the ground state (A_1) at the center of the Brillouin zone $k = 0$, Fig. 9.3 (b) display the first A_2 state, and Fig. 9.3 (c)-(d) the two basis functions of the degenerate first excited state (E). We highlighted the sixth of the structure (minimal domain) used in the numerical resolution.

As presented in Eqs. (7.7), it is easy to rebuild, according to the symmetry properties, the functions related to the 1D irreps A_i on the full domain starting from the sixth. For the degenerate irrep E , this procedure is not intuitive, but can be analytically computed with the help of the expressions obtained in (7.13) and (7.15) during the reduction computed with the SDR technique.

The position of the continuum linked with *delocalized states in the three vertical QWs* is around 1.6998 eV: its symmetry is associated with degenerate $A_1 \oplus E$ representations, due to the natural 3-fold degeneracy of the unconfined QW states. The 3-fold degenerate state cannot be converged with a 2D code, however a simple way to obtain an approximation of the limit of the continuum is to enlarge the numerical convergence domain. The A_1 and E eigenvalues converge asymptotically to the correct value as presented in Fig. 9.4. It is interesting to note that the confined A_2 state appears only at

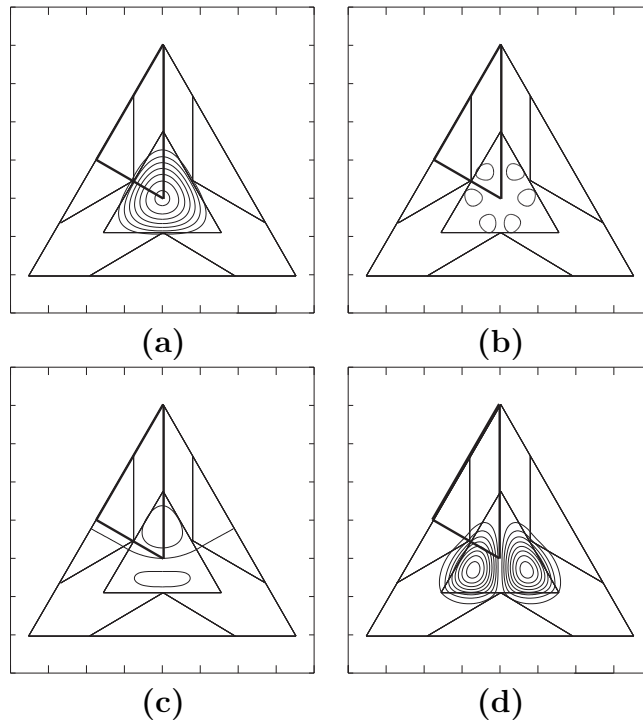


Figure 9.3: **(a)** First A_1 state (ground state), **(b)** First A_2 state, and **(c)**, **(d)** first degenerate E state (first excited electronic state)

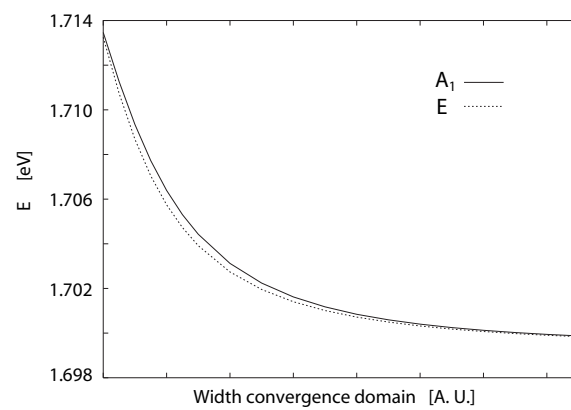


Figure 9.4: Convergence of the 3-fold QW state corresponding to the limit of the continuum

relatively high energy. A_2 state appears at high energy because the symmetry of A_2 corresponds to relatively high azimuthal oscillation of the wavefunction and there is a significant amount of *azimuthal confinement* due to the lateral QWs.

Hole states

In Fig. 9.5 (a) we show the valence band structure of the C_{3v} -QWR. The bands corresponding to the $E_{1/2}$ irrep are of course degenerate for every value of k and those belonging to (${}^1E_{3/2}$, ${}^2E_{3/2}$) are mutually degenerate at the center of Brillouin zone due to the time reversal symmetry. Every com-

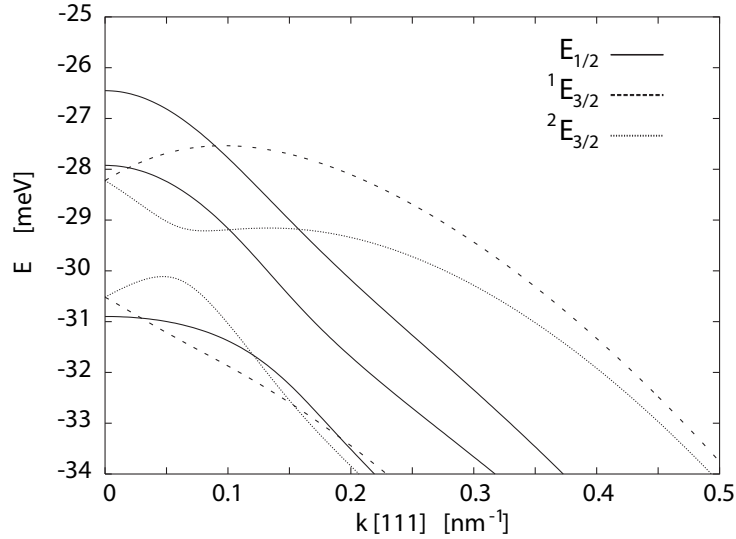


Figure 9.5: Valence band (only first energy levels) for the AlGaAs C_{3v} -QWR

ponent of the eigenstates ${}^1E_{3/2}$, ${}^2E_{3/2}$ and $E_{1/2}$ can be separated into single group A_1 , A_2 and E functions as presented in Eqs. (8.13), (8.15) and (8.16). For the conduction band, we obtained that ground state have A_1 symmetry and first excited state E symmetry. For hole states, ground state and first excited state are both $E_{1/2}$. Eigenstates are of course normalized to one, but if we calculate the relative contributions to the norm due to each single group irreps, we obtain that for ground state the norm of the A_1 component is around 0.957 and for the first excited state, norm of the E components is 0.999. Up to now, the concept of Heavy Holes (HH) and Light Hole (LH) character, related to the choice of an optimal quantization axis (OQA), was routinely used to describe a valence band state, but this HH/LH character

explicitly depend on the Bloch function basis and take a physical sense only if a convention for the Bloch function basis is imposed. With our new MSR formalism, for the high symmetry heterostructures convention is given by taking the fully symmetrized basis and the single group norm ratio naturally appear as characterization of the spinorial state imposed by the symmetry of the heterostructure. However, in low dimension structures like the V -shaped quantum wires, the HH-LH character remains an interesting concept when the vertical quantization axis, corresponding to the OBB, is used. These structure is reminiscent of a deformed quantum well, and the mixing can be directly related to the lateral deformation (pinching) effect in the V -wings [19].

The shape of the corresponding A_i and E functions for the ground and first excited state are very similar to the firsts A_i and E electronic states presented in Fig. 9.3.

Time reversal symmetry gives an addition degeneracy for the mutually conjugated ${}^iE_{3/2}$ eigenstates at the ZC and obviously connects the envelope functions at $k = 0$ according to Eq. (9.7).

In the same way as for the conduction band, we can determine the first non-confined state (continuum QWs states) for a spin dependent problem considering the representation product of $A_1 \oplus E$ with $E_{1/2}$. We obtain a six-fold degenerate state ${}^1E_{3/2} \oplus {}^2E_{3/2} \oplus E_{1/2} \oplus E_{1/2}$ with energy around -49 meV . There are 48 confined subbands (8 ${}^1E_{3/2}$, 8 ${}^2E_{3/2}$ and 16 degenerate $E_{1/2}$). The first bands are represented in Fig. 9.5.

9.2.3 Optical properties

Dipolar transitions

We are now interested on the study of the optical properties and optical selection rules. The oscillator strength of any interband dipolar optical transition is proportional to the square of the momentum matrix elements in direction d ($d = x, y$ or z). From Eqs. (4.11) and (8.29) we express the square of optical matrix element as

$$\begin{aligned}
 M_d^{n_c, n_v}(k) &= \left| \langle \Psi_{C,k}^{n_c} | \hat{P}_d | \Psi_{V,k}^{n_v} \rangle \right|^2 = \left| \sum_{i_c, i_v} \langle \psi_{C,k,i_c}^{n_c} | \psi_{V,k,i_v}^{n_v} \rangle (P_d)_{i_c, i_v} \right|^2 \\
 &= \left| \sum_{\Gamma_i, \mu_i} \sum_{i_c, i_v} \langle \psi_{C,\mu_i,k,i_c}^{\Gamma_i, n_c} | \psi_{V,\mu_i,k,i_v}^{\Gamma_i, n_v} \rangle (P_d)_{i_c, i_v} \right|^2 \quad (9.8)
 \end{aligned}$$

where \widehat{P}_d is the d -component of the momentum operator and $(P_d)_{i_c, i_v}$ are the elements of the Kane matrix for the corresponding d direction. To study the optical properties we need to take into account of the spin $j = 1/2$ for the conduction band and the technique for construct $j = 1/2$ spinors from our spinless model is presented in the following. The envelope functions related to the symmetrized basis are simply labelled by $i_c = 1, 2$ for the conduction states and $i_v = 1, 2, 3, 4$ for the valence states. Finally

$$\left\langle \psi_{C, \mu_i, k, i_c}^{\Gamma_i, n_c} \left| \psi_{V, \mu_i, k, i_v}^{\Gamma_i, n_v} \right. \right\rangle = \int d^2 \mathbf{r}_\perp \left(\psi_{C, \mu_i, k, i_c}^{\Gamma_i, n_c}(\mathbf{r}_\perp) \right)^* \psi_{V, \mu_i, k, i_v}^{\Gamma_i, n_v}(\mathbf{r}_\perp) \quad (9.9)$$

represent the overlap integrals between conduction and valence envelope functions. In the following we use the shorthand notation $\psi_{C, \mu_i, k, i_c}^{\Gamma_i, n_c} = \psi_{C, \mu_i}^{\Gamma_i}$ for the scalar functions and, in the same way as in Eqs. (8.13)-(8.16), we introduce additional labels to distinguish different functions transforming with the same irrep.

In order to identify allowed and forbidden transitions (selection rules), it is most convenient to apply the Wigner-Eckart Theorem (see Sec. 2.4) for point groups. To this end it is necessary to know the C_{3v} irreps associated with the momentum matrix operators \widehat{P}_d and then with the Kane matrices. Since dipolar operator transforms like a vector, we obtain [3] that P_x and (P_y, P_z) form two sets of irreducible tensorial operators (ITO) which are associated with the irreps A_1 and E respectively. For the Kane matrices (4.12), represented by a 2×4 matrix, we can directly verify this properties using the transformation law

$$\vartheta_{g^{-1}} P_i = (W^{J=1/2})^{-1} P_i W^{J=3/2} \quad (9.10)$$

Within the irrep E various choices of ITO's are possible: $P_\pm = \frac{1}{\sqrt{2}}(P_y \pm iP_z)$ is also an interesting set corresponding to circularly polarized optical fields and related to a matrix representation of E in which σ_{v1} is antidiagonal and for $g = \sigma_{v1}$ we obtain: $P'_+ = +iP_-$, $P'_- = -iP_+$. The *generalized* WET (gWET) [25] would provide further selection rules (with respect to WET), when certain Clebsch-Gordan coefficients vanish and these selection rules will be different for the two sets of ITO's just mentioned and depend upon the basis used.

For C_{3v} , the basis presented in Fig. 9.1 automatically reduce the 3D rotation representation and the linear polarization is the best choice respecting the symmetry of the problem. In Ch. 10, some others groups are studied with the MSR formalism. The sub-group C_n , $n = 4$ of the pure rotation group $SO(3)$ is present and we showed that reduction to a diagonal form of the

3D representation is computed by introducing circular polarization with the basis $\{\hat{e}_x, \hat{e}_{\sigma_+}, \hat{e}_{\sigma_-}\}$ where $\hat{e}_{\sigma_{\pm}} = \frac{1}{\sqrt{2}}(\hat{e}_y \pm i\hat{e}_z)$.

Conduction band $j = 1/2$ spinors

Up to now the classification of conduction states has been made without taking into account spin (i.e. without the double group irreps). Since the electron spin factors out in a trivial manner every energy bands is twice degenerate and it might seem trivial to build the corresponding double-group spinors on the basis of the single group envelope functions. The Bloch basis related to $j = 1/2$ transform like the irrep $E_{1/2}$ (Wigner operators $W^{j=1/2}$). For every single group irrep Γ_s , we obtain the corresponding double group irreps Γ_d by considering the representation product $\Gamma_d = \Gamma_s \otimes E_{1/2}$. The C_{3v} direct product table 2.4 predicts that $A_i \otimes E_{1/2} \approx E_{1/2}$ for $i = 1, 2$ and $E \otimes E_{1/2} \approx E_{1/2} \oplus {}^1E_{3/2} \oplus {}^2E_{3/2}$. In opposition to the valence band, corresponding to $j = 3/2$, in the electronic $j = 1/2$ conduction band, the Wigner representation is equivalent to the irrep $E_{1/2}$. As discussed in Sec. 3.2, Wigner operators for conduction and valence band have different parity with respect to the roto-inversion (inversion is factorized out). In principle Wigner representation still correspond to the OBB for $j = 1/2$ (the representation is irreducible and no reduction is needed for the conduction band), but, in the same way as in Eq. (8.8), we nevertheless choose the equivalent representation given by $W^{j=1/2}(g) = D^E(g)\chi^{2E_{3/2}}(g)$ corresponding to the central 2×2 block of the reduced matrix $W^{j=3/2}(g)$ (see Eq. (8.7)).

The advantage is that conduction band decomposition simply correspond to the two central components of the valence band eigenstates presented in Eq. (8.13)-(8.16). To associate single group irreps to double group irreps, we consider as zero the functions corresponding to the other irreps.

For the 1D irreps A_1 and A_2 we obtain

$$\underline{\psi}_1^{E_{1/2}(A_1)}(\mathbf{r}) = \begin{pmatrix} \psi^{A_1}(\mathbf{r}) \\ 0 \end{pmatrix}, \quad \underline{\psi}_2^{E_{1/2}(A_1)}(\mathbf{r}) = \begin{pmatrix} 0 \\ \psi^{A_1}(\mathbf{r}) \end{pmatrix} \quad (9.11)$$

$$\underline{\psi}_1^{E_{1/2}(A_2)}(\mathbf{r}) = \begin{pmatrix} 0 \\ \psi^{A_2}(\mathbf{r}) \end{pmatrix}, \quad \underline{\psi}_2^{E_{1/2}(A_2)}(\mathbf{r}) = \begin{pmatrix} -\psi^{A_2}(\mathbf{r}) \\ 0 \end{pmatrix} \quad (9.12)$$

To the two-dimensional irrep E we must now associate four degenerate spinors in accordance with the direct product table. The first two are asso-

ciated to the 2D $E_{1/2}$ and the last two to the 1D ${}^iE_{3/2}$

$$\begin{aligned}\underline{\psi}_1^{E_{1/2}(E)}(\mathbf{r}) &= \frac{1}{\sqrt{2}} \begin{pmatrix} \psi_1^E(\mathbf{r}) \\ -\psi_2^E(\mathbf{r}) \end{pmatrix} \\ \underline{\psi}_2^{E_{1/2}(E)}(\mathbf{r}) &= \frac{1}{\sqrt{2}} \begin{pmatrix} -\psi_2^E(\mathbf{r}) \\ -\psi_1^E(\mathbf{r}) \end{pmatrix}\end{aligned}\quad (9.13)$$

$$\begin{aligned}\underline{\psi}^{1E_{3/2}(E)}(\mathbf{r}) &= \frac{1}{\sqrt{2}} \begin{pmatrix} -\psi_2^E(\mathbf{r}) \\ \psi_1^E(\mathbf{r}) \end{pmatrix} \\ \underline{\psi}^{2E_{3/2}(E)}(\mathbf{r}) &= \frac{1}{\sqrt{2}} \begin{pmatrix} \psi_1^E(\mathbf{r}) \\ \psi_2^E(\mathbf{r}) \end{pmatrix}\end{aligned}\quad (9.14)$$

and immediately appear that these four spinor are linearly independent.

WET selection rules

We are now in a position to formulate a complete list of selection rules. First using the double group irreps for the electrons, and the WET, we find that in the x -direction only $\Gamma - \Gamma$ transitions are allowed (P_x is a A_1 operator). In other words the ${}^iE_{3/2} - {}^jE_{3/2}$, $i \neq j$ and $E_{1/2} - {}^iE_{3/2}$ transitions are forbidden for $i = 1, 2$. On the same way, WET applied to a E operator gives that ${}^iE_{3/2} - {}^jE_{3/2} \forall i, j = 1, 2$ are selection rules for a perpendicular direction (in the plane). It is however often interesting to remain with the single group representations for the electrons (A_1 , A_2 and E), because of the absence of spin-orbit coupling. The transposition of the previous selection rule predicted by the WET gives that

- $A_i - {}^jE_{3/2}$, $i, j = 1, 2$ are forbidden transitions in the parallel x polarization
- there are no simple WET selection rules for the $E - \Gamma$ transitions ($\forall \Gamma$)

Application of MSR formalism

With our decomposition into single group irreps of the spinorial components, every WET and gWET selection rules can be directly obtained computing the square of the modulus of dipolar matrix elements (9.8).

The Kane matrices corresponding to our $j = 1/2$ and $j = 3/2$ OBBs are

given by

$$\begin{aligned}
P_x &= P_0 \begin{pmatrix} 0 & \sqrt{2/3} & 0 & 0 \\ 0 & 0 & \sqrt{2/3} & 0 \end{pmatrix} \\
P_y &= P_0 \begin{pmatrix} 0 & -i/\sqrt{6} & 0 & 1/\sqrt{2} \\ 1/\sqrt{2} & 0 & i/\sqrt{6} & 0 \end{pmatrix} \\
P_z &= P_0 \begin{pmatrix} -1/\sqrt{2} & 0 & i/\sqrt{6} & 0 \\ 0 & i/\sqrt{6} & 0 & 1/\sqrt{2} \end{pmatrix}
\end{aligned} \tag{9.15}$$

where

$$P_0 = \langle S | \hat{P}_x | X \rangle = \langle S | \hat{P}_y | Y \rangle = \langle S | \hat{P}_z | Z \rangle \tag{9.16}$$

is the Kane matrix element.

For every irrep, we obtain the dipolar matrix elements $M_d^{\Gamma_c, \Gamma_v}$ with corresponding selection rules, where i and $l = 1, 2$

$$M_x^{A_i, lE_{3/2}} = 0 \quad , \quad M_x^{A_i, E_{1/2}} = \frac{2}{3} |\langle \psi_c^{A_i} | \psi_v^{A_i} \rangle|^2 \quad , \quad M_x^{E, \Gamma_v} = \frac{4}{3} |\langle \psi_c^E | \psi_v^E \rangle|^2 \tag{9.17}$$

$$\begin{aligned}
M_y^{A_i, lE_{3/2}} &= M_z^{A_i, lE_{3/2}} = \frac{1}{2} |\langle \psi_c^{A_i} | \psi_v^{A_i} \rangle|^2 \\
M_y^{A_i, E_{1/2}} &= M_z^{A_i, E_{1/2}} = \frac{1}{6} |\langle \psi_c^{A_i} | \psi_v^{A_i} \rangle|^2 \\
M_y^{E, lE_{3/2}} &= M_z^{E, lE_{3/2}} = \frac{1}{3} |\langle \psi_c^E | \psi_v^E \rangle|^2 \\
M_y^{E, E_{1/2}} &= M_z^{E, E_{1/2}} = |\langle \psi_c^E | \phi_v^E \rangle|^2 + |\langle \psi_c^E | \varphi_v^E \rangle|^2 + \frac{1}{3} |\langle \psi_c^E | \psi_v^E \rangle|^2
\end{aligned} \tag{9.18}$$

Moreover, we simply noted $\langle \psi_c^E | \psi_v^E \rangle = \langle \psi_{c,1}^E | \psi_{v,1}^E \rangle = \langle \psi_{c,2}^E | \psi_{v,2}^E \rangle$ and is understood that in $M_\alpha^{\Gamma_c, \Gamma_v}$ the valence band envelope functions $\psi_v^{\Gamma_c}$ are related to the Γ_v spinor!

With the particular form of P_y and P_z given in Eq. (9.15), in the perpendicular plane we obtain $M_z^{\Gamma_1, \Gamma_2} = M_y^{\Gamma_1, \Gamma_2}$ for every couple of irreps Γ_1, Γ_2 corresponding to a perfect isotropy of polarization in the plane.

The $M_x^{A_i, lE_{3/2}} = 0$ correspond to the selection rule still obtained with the WET theorem.

Finally, we note that in this picture remarkable analytical ratios appear between parallel/orthogonal directions and these predictions are a specific feature of the full symmetrization of the envelope functions allowing to replace the scalar product between envelope functions with scalar product between function with the same symmetry.

Dipolar matrix element spectra

Spectra of squared interband dipolar transition matrix elements at ZC are known to usually give a very good understanding of the general shape of experimental PLE absorption spectra [19]. Figs. 9.6 (a) and 9.6 (b) show such calculated spectra for the parallel x direction (along the C_{3v} -QWR axis) and for the y direction in the perpendicular plane respectively where, to discuss the symmetry properties of transitions, only the lowest electronic and hole eigenstates are taken into account and only the most important $e_{n_c} - h_{n_v}$ transitions are labelled. In Fig. 9.7, we present, without labelling,

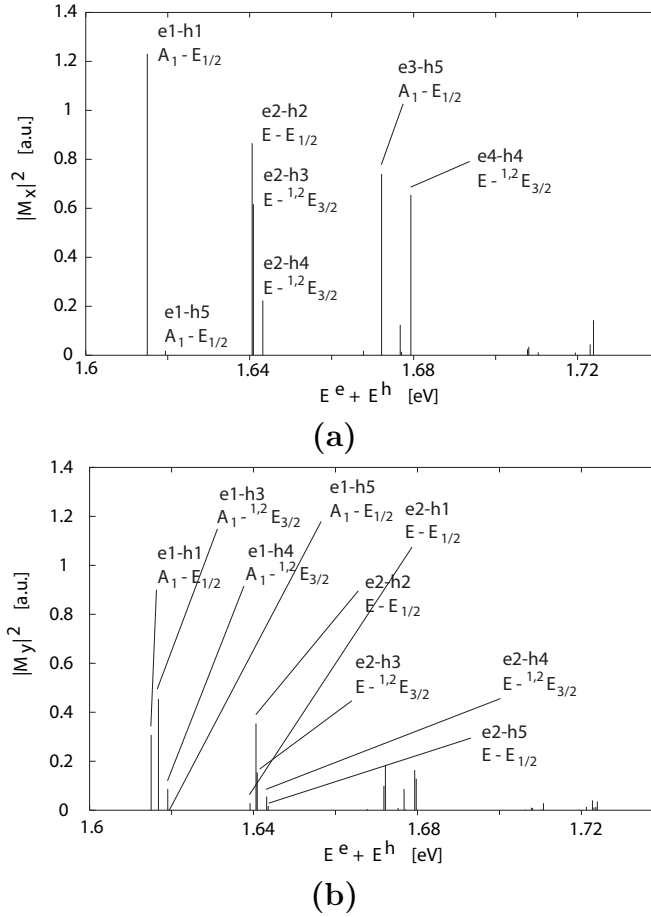


Figure 9.6: Square of the optical matrix elements for $n_c = 1, \dots, 7$ and $n_v = 1, \dots, 5$ (a) x -polarization (\parallel direction, along the wire) (b) y -polarization (\perp direction, in the plane)

the full spectra including all confined states (3 A_1 , 1 A_2 , 3 E and 8 ${}^1E_{3/2}$,

$8 {}^2E_{3/2}$, $16 E_{1/2}$). A first remarkable feature is a strong optical anisotropy of the ground transition between parallel and perpendicular linear polarization directions. This result is sound and was anticipated on the basis of the fact that the C_{3v} -QWR has a lateral aspect ratio close to one, resulting, for the ground subband, in equally strong confinement effects in the two orthogonal lateral directions, and therefore equally strong band mixing and polarization anisotropy. We also see that the ground subband absorption is stronger for a parallel polarization, as expected.

Polarization anisotropy

Concerning the polarization anisotropy, Eqs. (9.17) and (9.18) allow to obtain some simple analytical conclusions: due to the ratio aspect close to one, P_y and P_z play the same role in the spectra and we obtain a perfect polarization isotropy in the plane. In Fig 9.8, we present the polarization anisotropy between a parallel and orthogonal direction, given by

$$A_{x-y}(n_c, n_v) = \frac{[M_x(k=0)]_{n_c, n_v} - [M_y(k=0)]_{n_c, n_v}}{[M_x(k=0)]_{n_c, n_v} + [M_y(k=0)]_{n_c, n_v}} \quad (9.19)$$

Every selection rule in the x direction give rise a -1 in the anisotropy spectra, but we remark a lot of transitions corresponding to 0.6 . Comparing the simple expressions (9.17) and (9.18) for parallel and orthogonal directions, we can analytically justify the 0.6 polarization anisotropy: this correspond to transitions $A_i - E_{1/2}$ and $E - {}^lE_{3/2}$ four times stronger in x direction as predicted by our new MSR theory. The only non constant anisotropy transitions, are the $E - E_{1/2}$ (separately presented in Fig. 9.9).

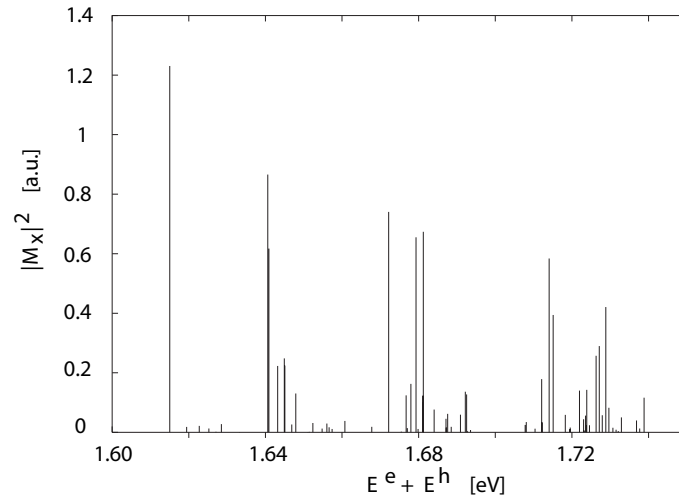
It should be pointed out that in V-groove QWRs the polarization anisotropy (for the lowest transitions) is very different [19], since only one perpendicular polarization is very anisotropic. This is due to the fact that the V-groove geometric structure is reminiscent of an anisotropic quantum well with a weak lateral confinement.

9.2.4 Additional symmetries and symmetry breaking

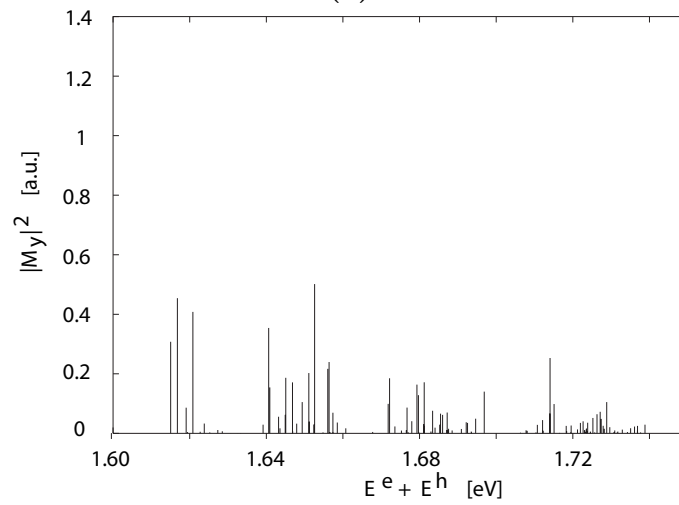
Missing transitions in dipolar spectra

The only real selection rules in the optical matrix spectra are those obtained in Eq. (9.17), namely $A_i - {}^lE_{3/2}$ transitions for $i, l = 1, 2$ in the x polarization (i.e. $e_1 - h_3, e_1 - h_4, \dots$).

The absence of the forbidden transitions is clear in Fig. 9.10 (a) and (b) or (c), where we present the spectra (x -direction) for the first A_1 , A_2 and E electronic states, where the $E - \Gamma$ and $A_2 - \Gamma$ are shifted to match with

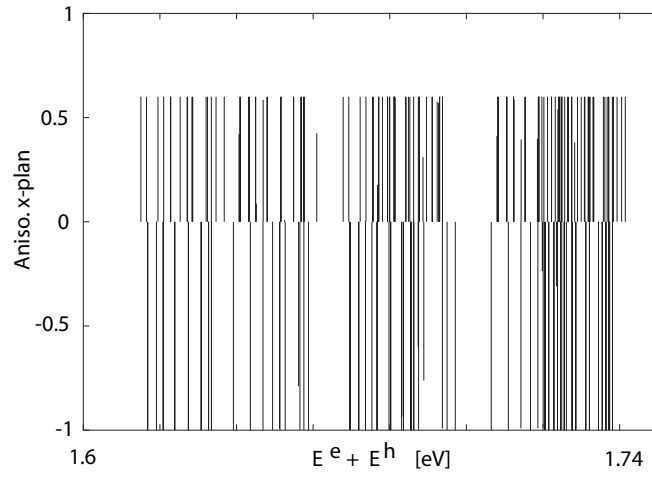
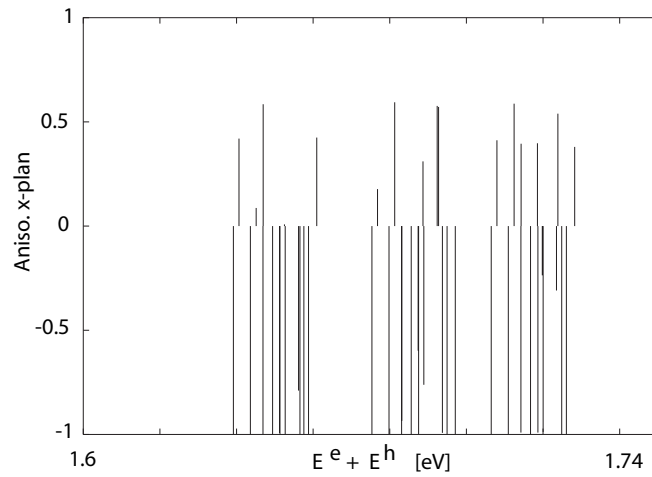


(a)



(b)

Figure 9.7: Square of the optical matrix elements (full spectrum) (a) x -polarization (\parallel direction, along the wire) (b) y -polarization (\perp direction, in the plane)

Figure 9.8: Polarization anisotropy for $\parallel - \perp$ directionFigure 9.9: Polarization anisotropy for $\parallel - \perp$ direction, only transitions with $\Gamma_c = E$ and $\Gamma_v = E_{1/2}$

the $e_1 - h_1$ transition. We see however in Fig. 9.6 that there seems to be remaining some “forbidden transitions”, for example $e_1 - h_2$ ($A_1 - E_{1/2}$ transition) in both x and y direction, or $e_2 - h_1$ ($E - E_{1/2}$ transition) in x direction.

Approximated ZC-symmetry

We now intend to explain the “missing” lines seen in dipolar transitions. We remark that the valence band Hamiltonian is not invariant with respect to a perpendicular σ_h symmetry plane since the microscopic structure of diamond did not present such a symmetry, then the quantum structure do not display the so-called Zone-Center (ZC) symmetry group at the center of Brillouin zone.

However one of the first idea that may come to mind is to test whether we may still have an approximate ZC symmetry, so that a symmetrized Hamiltonian with respect to σ_h

$$\begin{aligned} H^{sym}(\mathbf{k}, \mathbf{r}) &= \frac{1}{2} \left(H(\mathbf{k}, \mathbf{r}) + \vartheta_{\sigma_h^{-1}} H(\mathbf{k}, \mathbf{r}) \vartheta_{\sigma_h^{-1}}^{-1} \right) \\ &= \frac{1}{2} \left(H_L(\mathbf{k}, \mathbf{r}) + \vartheta_{\sigma_h^{-1}} H_L(\mathbf{k}, \mathbf{r}) \vartheta_{\sigma_h^{-1}}^{-1} \right) + V(\mathbf{r}) \end{aligned} \quad (9.20)$$

would describe well the missing lines. Let us now investigate step by step the symmetry of $H^{sym}(\mathbf{k}, \mathbf{r})$. First it is possible to prove that all previous symmetry operations *are kept* since the second term of Eq.(9.20) is invariant *because σ_h commutes with all symmetry operations of C_{3v}* . Second the additional symmetry of $H^{sym}(\mathbf{k}, \mathbf{r})$ can be written as

$$H^{sym}(\mathbf{k}_\perp, k, \mathbf{r}) = W^{-1}(\sigma_h) H^{sym}(\mathbf{k}_\perp, -k, \mathbf{r}) W(\sigma_h) \quad (9.21)$$

which is typical of ZC-symmetry, restored by this procedure. Eq.(9.21) holds because in the second line of Eq.(9.20) we have used the fact that the confinement potential $V_v(\mathbf{r}_\perp)$ is invariant with respect to σ_h , and because in the Luttinger part the spatially-dependent Luttinger parameters $\gamma_l(\mathbf{r}_\perp)$, $l = 1, 2, 3$ are also strictly invariant, therefore on this term only the spinorial part of $\vartheta_{\sigma_h^{-1}}$ and the inversion of k are relevant.

We can view the symmetric second term of Eq.(9.20), $\vartheta_{\sigma_h^{-1}} H(\mathbf{k}, \mathbf{r}) \vartheta_{\sigma_h^{-1}}^{-1}$, as the Hamiltonian of the same problem expressed in σ_h -symmetric coordinates, therefore we can deduce that it has the same energy spectrum. However it should be pointed out that the role of k and $-k$ (and the corresponding eigenfunctions) is exchanged. The respective eigenfunctions, although linked by

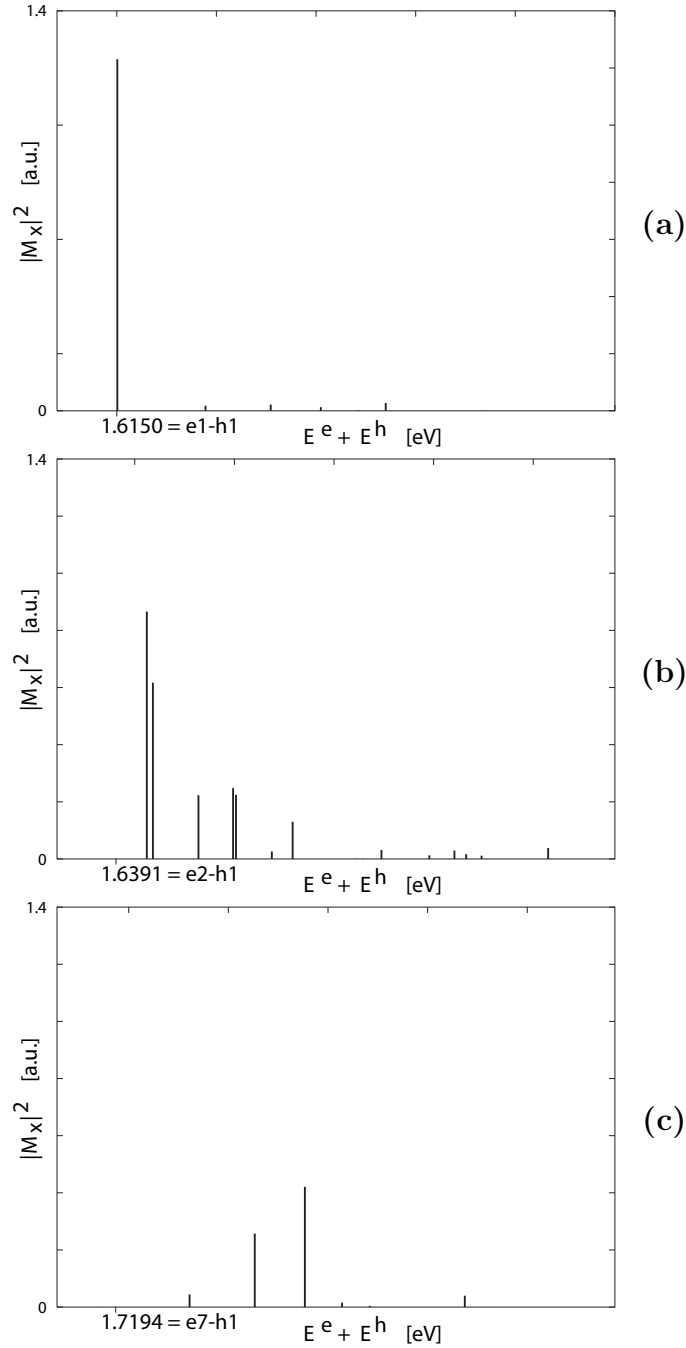


Figure 9.10: Square of the optical matrix elements **(a)** x -polarization, for $n_c = 1$ (A_1) and every hole state **(b)** x -polarization, with $n_c = 2$ (E) and every hole state, with the whole spectrum shifted such that the first optical transition is aligned to the ground transition $e_1 - h_1$ **(c)** x -polarization, with $n_c = 7$ (A_2) and every hole state, with the whole spectrum shifted such that the first optical transition is aligned to the ground transition $e_1 - h_1$

time reversal, are slightly different. However it is important to notice that *the new symmetric Hamiltonian has a slightly different spectrum, with different eigenfunctions, although we sum two Hamiltonians with same spectrum!*

The new p, q, r, s parameters for the symmetrized Hamiltonian are easily obtained and exactly correspond to the original parameters presented in (9.3) where a and b parameter are simply replaced by $a^{sym} = Re(a)$ and $b^{sym} = i Im(b)$, with Re and Im respectively the real and imaginary part.

In Fig. 9.11 we present the band structure of the symmetrized Hamiltonian compared with the band dispersion of the normal Hamiltonian. At $k = 0$ the energy difference for the first subband is extremely small ($0.017 meV$) and at $k = 0.5 nm^{-1}$ still very small ($0.365 meV$). For the higher subband dispersions the discrepancy is increased, as can be seen in Fig.(9.11), but the results at $k = 0$ still stay quite accurate and we conclude that the lack of σ_h symmetry has only a small influence on the results. Let us now investigate whether the restoration of a symmetry by the symmetrization (9.20) provides enough selection rules to explain the “missing” transitions in the spectra.

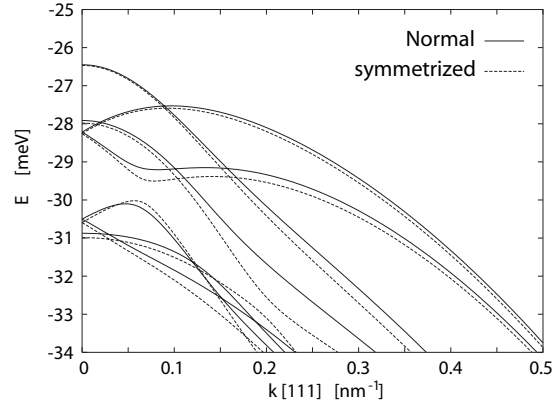


Figure 9.11: Comparison of band structures for the normal and symmetrized problem

The symmetry group of the symmetrized Hamiltonian H^{sym} is the tensorial product $D_{3h} = C_{3v} \otimes C_s$. It should be remarked that our construction makes D_{3h} a symmetry group of $H^{sym}(k)$ only for $k = 0$, i.e. a ZC-symmetry group (and the ensuing selection rules hold only at $k = 0$). D_{3h} is however a symmetry of the total Hamiltonian (when one considers all the k values simultaneously, because σ_h operation connect $+k$ and $-k$ sub-blocks).

The irreps of the single group D_{3h} are two sets of representations (A'_1, A'_2, E') and (A''_1, A''_2, E'') analogous to the C_{3v} representations but respectively even

and odd under σ_h . For the double group the situation is significantly different since all representations are two-dimensional and bear different names ($E_{1/2}, E_{3/2}, E_{5/2}$) [3].

Let us now study the selection rules associated with optical interband transitions on the basis of the classification of every eigenstate of $H^{sym}(k)$ by the irreps of D_{3h} . To this end, it is first useful to obtain the double group representations of conduction band states, which, with spin, transform like $A'_i \otimes E_{1/2} \approx E_{1/2}$ for $i = 1, 2$ and $E' \otimes E_{1/2} \approx E_{3/2} \oplus E_{5/2}$. The scalar electronic functions, transform like the even (with respect to σ_h) irreps. In fact, at the particular point $k = 0$, σ_h act on the wave functions in a trivial way. For valence-band states, subduction tables give the descent of symmetry for $D_{3h} \rightarrow C_{3v}$, $E_{3/2} \rightarrow {}^1E_{3/2} \oplus {}^2E_{3/2}$, $E_{1/2} \rightarrow E_{1/2}$ and $E_{5/2} \rightarrow E_{1/2}$. The P_x operator transform like A''_2 (even with respect to σ_{v1} , odd with respect to σ_h) and (P_y, P_z) like E' (even with respect to σ_h), then in the same way as for C_{3v} group, using WET we obtain that the only permitted transition in x direction are $E_{1/2} - E_{5/2}$, $E_{5/2} - E_{1/2}$, $E_{3/2} - E_{3/2}$. In y direction, permitted transitions are $\Gamma_i - \Gamma_j$ where $i \neq j = 1, 3, 5$. Every irreps of D_{3h} is self-conjugate (real irreps), then if $\Gamma_i - \Gamma_j$ transition are permitted, $\Gamma_j - \Gamma_i$ are permitted too. With the single group irreps label, we obtain the following selection rules for D_{3h} :

- for a polarization along the x -axis $A'_i - E_{3/2}$ (corresponding to the WET selection rule for C_{3v} group obtained in precedence), $A'_i - E_{1/2}$, $E' - E_{5/2}$ with $i = 1, 2$ are forbidden
- for a polarization in the perpendicular plane $A'_i - E_{1/2}$ with $i = 1, 2$ are forbidden

Therefore there are many more selection rules that the $A'_i - {}^lE_{3/2}$, $i, l = 1, 2$ transitions obtained before applying WET to C_{3v} symmetry. The other absent peaks in the spectra presented in Fig. 9.7, are real selection rules only if we neglect the lack of horizontal symmetry plane.

Every $E_{1/2}$ irreps of C_{3v} group split into $E_{1/2}$ or $E_{5/2}$ in D_{3h} but, how may we distinguish them? This is what we intend to understand with MSR formalism.

MSR and description of the approximate ZC symmetry

With the new MSR formalism, in the same way as for C_{3v} one can decompose into single group functions every spinorial component. The OBB for D_{3h} allow to reduce Wigner representation to $E_{5/2} \oplus E_{3/2}$ and OBB is labelled

$\{|E_{5/2}, 1\rangle, |E_{5/2}, 2\rangle, |E_{3/2}, 1\rangle, |E_{3/2}, 2\rangle\}$. With respect to this new basis, the Luttinger Hamiltonian take a different block-diagonal form

$$H_L = -\frac{\hbar^2}{m_0} \begin{pmatrix} (p-q)I_2 & A \\ A^+ & (p+q)I_2 \end{pmatrix} ; A = \begin{pmatrix} -s^+ & r \\ r^+ & s \end{pmatrix} \quad (9.22)$$

To construct the $E_{i/2}$ irreps, we first directly obtain the matrices corresponding to $g \in C_{3v}$, then, for the additional σ_h operation, we reduce the Wigner operator allowing to obtain

$$D^{E_{1/2}}(\sigma_h) = \begin{pmatrix} 0 & 1 \\ -1 & 0 \end{pmatrix} = -D^{E_{5/2}}(\sigma_h) = -D^{E_{3/2}}(\sigma_h) \quad (9.23)$$

and then construct the $\sigma_h g$ matrices.

The decomposition into single group irreps (where we consider zero every function related to the odd A_1', A_2', E'' and expressed with respect to the same basis as for C_{3v} in such a way that eigenstates can then immediately be compared with those given in Eqs. (8.13)-(8.16)) reads

$$\underline{\psi}_1^{E_{3/2}}(\mathbf{r}) = \begin{pmatrix} \psi^{A_1'}(\mathbf{r}) \\ -\psi_2^{E'}(\mathbf{r}) \\ -\psi_1^{E'}(\mathbf{r}) \\ \psi^{A_2'}(\mathbf{r}) \end{pmatrix}, \quad \underline{\psi}_2^{E_{3/2}}(\mathbf{r}) = \begin{pmatrix} -\psi^{A_2'}(\mathbf{r}) \\ \psi_1^{E'}(\mathbf{r}) \\ -\psi_2^{E'}(\mathbf{r}) \\ \psi^{A_1'}(\mathbf{r}) \end{pmatrix} \quad (9.24)$$

$$\underline{\psi}_1^{E_{1/2}}(\mathbf{r}) = \begin{pmatrix} -\psi_2^{E'}(\mathbf{r}) \\ \psi_1^{E'}(\mathbf{r}) \\ -\psi_2^{E'}(\mathbf{r}) \\ \psi_1^{E'}(\mathbf{r}) \end{pmatrix}, \quad \underline{\psi}_2^{E_{1/2}}(\mathbf{r}) = \begin{pmatrix} \psi_1^{E'}(\mathbf{r}) \\ -\psi_2^{E'}(\mathbf{r}) \\ -\psi_1^{E'}(\mathbf{r}) \\ \psi_2^{E'}(\mathbf{r}) \end{pmatrix} \quad (9.25)$$

$$\underline{\psi}_1^{E_{5/2}}(\mathbf{r}) = \begin{pmatrix} \psi_2^{E'}(\mathbf{r}) \\ \psi^{A_1'}(\mathbf{r}) \\ \psi^{A_2'}(\mathbf{r}) \\ -\psi_1^{E'}(\mathbf{r}) \end{pmatrix}, \quad \underline{\psi}_2^{E_{5/2}}(\mathbf{r}) = - \begin{pmatrix} \psi_1^{E'}(\mathbf{r}) \\ -\psi^{A_2'}(\mathbf{r}) \\ \psi^{A_1'}(\mathbf{r}) \\ \psi_2^{E'}(\mathbf{r}) \end{pmatrix} \quad (9.26)$$

We note that when we break the σ_h symmetry:

- the $E_{3/2}$ functions became independent (${}^1E_{3/2}(C_{3v})$ and ${}^2E_{3/2}(C_{3v})$)
- comparing $E_{1/2}$ and $E_{5/2}$ to $E_{1/2}(C_{3v})$ (8.16), we remark that the central part $\frac{1}{\sqrt{2}}(\psi^{A_i} + \psi_i^E)$ are split in D_{3h} into ψ^{A_i} (see 9.26) and ψ_i^E (see 9.25)!

In C_{3v} the lack of σ_h symmetry has only a small effect, then every eigenstate will have very small A_i part or very small E part. We note that ground state correspond to a $E_{5/2}(D_{3h})$ and display a character 96% A_1 ! The first excited

state is a $E_{1/2}(D_{3h})$ with a very small $\%A_1$.

In a more rigorous way, every $E_{1/2}$ state can be identified using the transformation law with respect to the S_3^+ and S_3^- symmetry operations (different character with respect to $E_{1/2}(D_{3h})$ and $E_{5/2}(D_{3h})$) and every “missing” transitions in the spectra Fig. 9.7 can be explained: every (D_{3h}) selection rule correspond to a very small (“missing”) transition in the C_{3v} group when the lack of σ_h has only a small effect on the energy and wave functions!

Finally we obtain the new “selection rules”

$$A'_l - E_{1/2} \Rightarrow (e_1 - h_2, e_3 - h_2, \dots) \quad (9.27)$$

for all directions and

$$E' - E_{5/2} \Rightarrow (e_2 - h_1, e_4 - h_1, \dots) \quad (9.28)$$

for the x direction.

Then, every $E_{1/2}(D_{3h})$ state correspond to a “missing transition” related to a A'_i - or E - transition.

This simple analysis of this approximate ZC symmetry group D_{3h} , shows that with the help of the MSR formalism one can understand in a qualitative and quantitative way the effects of an approximate symmetry at the envelope function level!

Absorption spectra and ZC-like lines

A further word of caution is in order concerning these “missing transitions” in the spectra of matrix elements. Although the C_{3v} -QWR absorption spectrum is dominated by $k = 0$ matrix elements thanks to singularity of the 1D density of states, it does also involve contributions from $k \neq 0$ tails. On Fig. 9.12 we see the tail of the matrix element in the x -polarization, for transitions $e_1 - h_1$ and $e_1 - h_2$, as a function of k . Outside zone-center the matrix element of the “missing” transitions increases to a value that is comparable to another transition. It is interesting to see also that our symmetrized Hamiltonian (9.20) mimics also well the dependence of this matrix element as a function of k (it becomes non-zero since D_{3h} is not anymore a symmetry group outside ZC). In Fig. 9.13 we compare the $e_1 - h_1$ and $e_1 - h_2$ matrix elements for the C_{3v} and symmetrized D_{3h} Hamiltonians. As a result of this analysis we can predict that in a C_{3v} -QWR absorption spectrum there should be in principle shallow observable absorption lines, that we call ZC-like lines, corresponding the “missing” transitions in dipolar matrix element spectra at $k = 0$. Moreover, such transitions, in spectra computed without the electron-hole Coulomb interaction, will not display the typical features of a singular

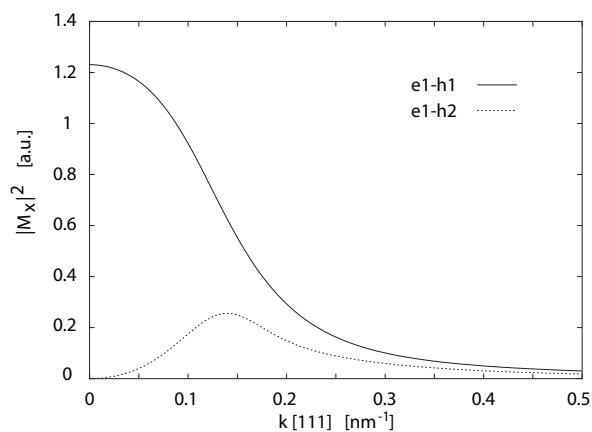


Figure 9.12: Matrix element in the x -polarization, for transitions $e_1 - h_1$ and $e_2 - h_2$ as a function of k

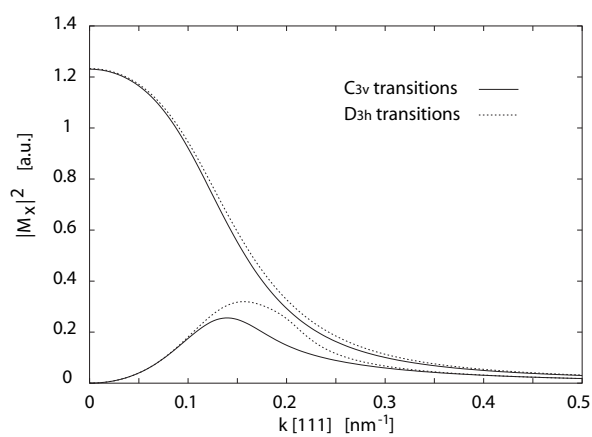


Figure 9.13: Comparison of matrix element in the x -polarization, for transitions $e_1 - h_1$ and $e_1 - h_2$ as a function of k . C_{3v} and D_{3h} Hamiltonians

1D density of states (DOS), but will have an *asymmetric bell shape*. To confirm this prediction we display on Figs. 9.14(a) and (b) the absorption spectra in the x and y polarization, computed using the golden-rule formula

$$P_{if} = \frac{2\pi}{\hbar} \left(\frac{e E_0}{2m_0\omega} \right)^2 \sum_{i,f} |M_{\epsilon,i,f}|^2 \delta(E_f - E_i - \hbar\omega) \quad (9.29)$$

therefore absorption coefficient as function of the photon energy reads

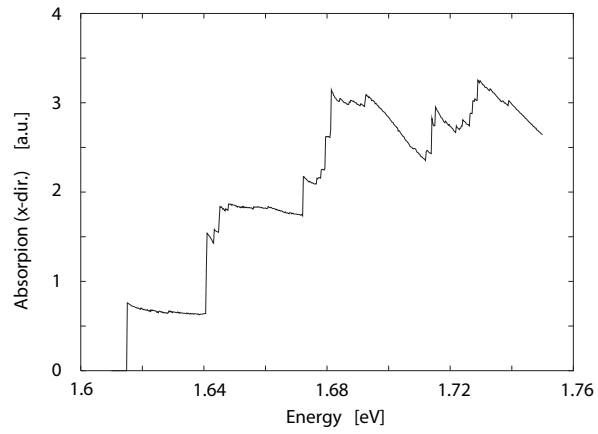
$$\alpha(E_\gamma) \sim \sum_{i,f} \int d\mathbf{k} \frac{|M_{\epsilon,i,f}|^2}{E_\gamma} \delta(E_f - E_i - \hbar\omega) \quad (9.30)$$

In Fig. 9.15, we present a typical contribution of the shallow optical bands linked with ZC-like lines and compare with standard transition displaying the singularity due to the 1D DOS. The question whether ZC lines appear in QWRs with different lateral symmetry than C_{3v} is relevant. We would like to point out that similar lines should appear also in all QWRs with higher lateral symmetry than C_s presenting a ZC (or an approximate) symmetry group giving additional selections rules at $k = 0$. For example, already in C_{2v} QWR's, a related effect was found in [17] where the authors discuss the $e_1 - h_2$ transition in C_s versus C_{2v} QWRs.

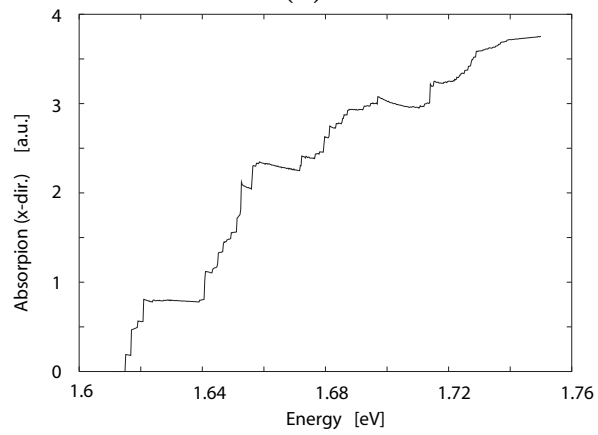
C_{3v} symmetry breaking down to C_s symmetry

In the C_{3v} single group, we have two 1D irreps A_i and a 2D irrep E . A_1 is even with respect to the vertical mirror σ_{v1} and A_2 is odd. From Eq. (2.20) applied to the σ_{v1} operation, we obtain symmetry properties with respect to $z \rightarrow -z$: $\psi^{A_1}(y, -z) = \psi^{A_1}(y, z)$ and $\psi^{A_2}(y, -z) = -\psi^{A_2}(y, z)$. For the 2D irrep E , we can choose the two partner functions respectively even and odd with respect to σ_1 as presented in Eq. (2.40). In the same way, valence band states are (even,odd,even,odd) or (odd,even,odd,even) with respect to σ_{v1} (see Eqs. (8.13)-(8.16)). Obtaining parity conditions with respect to a symmetry plane is not amazing considering that C_s is a subgroup of C_{3v} .

Let us shortly discuss the effect of breaking the C_{3v} symmetry of the problem by removing the QW wing oriented along the y -direction (see Fig. 9.1). The resulting structure keeps only the symmetry subgroup $C_s \subset C_{3v}$, like the T-shape and V-shape QWRs already discussed in the literature [17]. Every irrep of C_s is 1D and every single and double band split into two different bands. In the Fig. 9.16 conduction band of the C_s symmetry is presented. Comparing to C_{3v} results (Fig. 9.2), splitting of the E subbands into two distinguished bands is clearly shown. In the same way, in the valence band, the degenerate $E_{1/2}$ subbands become split.



(a)



(b)

Figure 9.14: Optical absorption. The dotted line correspond to the symmetrized Hamiltonian. (a) x -polarization (b) y -polarization

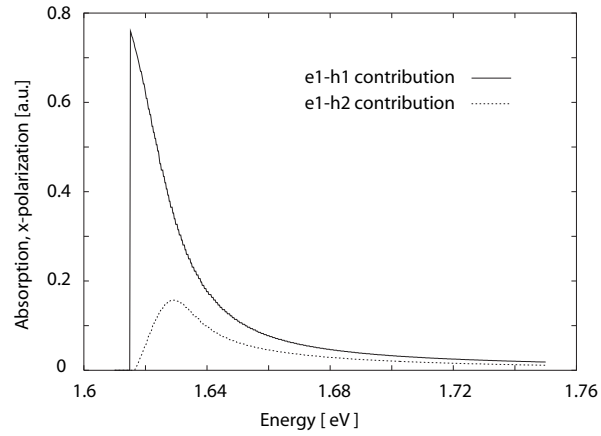


Figure 9.15: Comparison of contributions to the absorption spectra in the x -polarization, for normal transitions ($e_1 - h_1$) and ZC-like transitions ($e_1 - h_2$) as a function of The energy

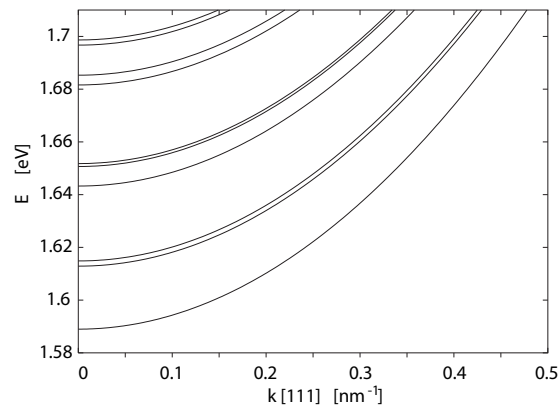


Figure 9.16: Conduction band for the C_s structure

Two other effects should by now be obvious: the “ZC-like lines” turn into normal transitions with a singular density of states, and the polarization anisotropy evolve a bit toward the different polarization anisotropy of V-shape QWRs.

9.2.5 Additional study

The oppositely oriented C_{3v} structure and C_{6v} group

The preceding discussion on ZC symmetry has critically showed the importance of the rotation C_2 , the component of $\sigma_h = iC_2$ that breaks the invariance under the horizontal symmetry plane in Luttinger Hamiltonian. A natural question arises then whether the oppositely oriented C_{3v} structure, presented in Fig. 9.17, is significantly different from the original one presented in Fig. 9.1. In such a structure the bulk crystal and the C_{3v} heterostructure are oppositely oriented with respect to each other, but still retain overall a C_{3v} symmetry. Let us write the new total Hamiltonian as

$$H^{C_2}(\mathbf{k}, \mathbf{r}) = H_L(\mathbf{k}, \mathbf{r}) + V(\Re(C_2)\mathbf{r}_\perp) \quad (9.31)$$

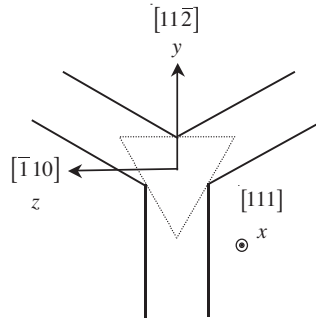


Figure 9.17: Model of the opposite oriented structure

We recall that potential only depend on \mathbf{r}_\perp then is invariant with respect to σ_h . Using $i = \sigma_h C_2$ we rewrite the new Hamiltonian as $H^{C_2}(\mathbf{k}, \mathbf{r}) = H_L(\mathbf{k}, \mathbf{r}) + V(\Re(i)\mathbf{r}_\perp)$. To progress at this point let us make one essential additional assumption: we consider that the Luttinger parameters are not anymore spatially-dependent $\gamma_l(\mathbf{r}_\perp) \equiv \gamma_l, l = 1, 2, 3$. At the end of this subsection, we discuss the effects of spatially dependence of Luttinger parameters by a numerical calculation and show that this effect is negligible in our C_{3v} structure (strong confinement due to the heterostructure potential). Finally,

using the invariance of the Luttinger part with respect to the inversion, we obtain

$$H^{C_2}(\mathbf{k}, \mathbf{r}) = \vartheta_{i-1} H(\mathbf{k}, \mathbf{r}) \vartheta_{i-1}^{-1} \quad (9.32)$$

and the new Hamiltonian for the oppositely oriented structure is obtained by application of the inversion to the original Hamiltonian then has the same spectrum as the original structure. Therefore, we have analytically proven that if the Luttinger parameters are not spatially-dependent the oppositely oriented C_{3v} structure has exactly the same band structure. The respective eigenfunctions can also be obtained without further calculations by symmetry.

Another way to understand the invariance of the energy values is to rewrite the new Hamiltonian as

$$\begin{aligned} H^{C_2}(\mathbf{k}, \mathbf{r}) &= H_L(\mathbf{k}, \mathbf{r}) + \vartheta_{C_2^{-1}}^{3D} V(\mathbf{r}_\perp) \vartheta_{C_2^{-1}}^{3D-1} \\ &= \vartheta_{C_2^{-1}}^{3D} (\vartheta_{C_2}^{3D} H_L(\mathbf{k}, \mathbf{r}) \vartheta_{C_2}^{3D-1} + V(\mathbf{r}_\perp)) \vartheta_{C_2^{-1}}^{3D-1} \end{aligned} \quad (9.33)$$

where ϑ^{3D} correspond to the spatial part of the operator (see Ch. 2). Always in the assumption of Luttinger parameters spatially-independent, application of $\vartheta_{C_2}^{3D}$ to Luttinger part simply correspond to replace a by $-a$ in the Luttinger operators r, s defined in (9.3) and we obtain $\vartheta_{C_2}^{3D} H_L(k, \mathbf{k}_\perp, \mathbf{r}) \vartheta_{C_2}^{3D-1} = H_L(-k, \mathbf{k}_\perp, \mathbf{r})$. The band structure is symmetric with respect to $k \rightarrow -k$ and obtain same energy levels.

In our case we computed the calculation with constant Luttinger parameter ($x = 0.06$ corresponding to the Al% of the VQWR). comparison between constant and variable parameters is presented in Fig. 9.18. For example, a numerically estimation of the energy difference due to the spatial dependence of the Luttinger parameters gives, for the first subband, at $k = 0$ $0.024 meV$ (around 0.07% error) and at $k = 0.5$ $0.081 meV$ ($\sim 0.22\%$). This negligible difference also justifies our choice to ignore the Foreman contributions (interface terms). In the same way, for the conduction band we obtain very small difference considering the effective mass as a constant. At $k = 0$ and $k = 0.5$ we obtain respectively $0.623 meV$, 0.04% and $1.24 meV$, 0.07%.

To conclude, what occurs when we consider a new potential, symmetrized with respect to C_2 , $\frac{1}{2}(V(\mathbf{r}_\perp) + V(\mathfrak{R}(C_2)\mathbf{r}_\perp))$?

This potential correspond to a heterostructure presenting a C_{6v} symmetry group. The elements of this group can be constructed from C_{3v} by $\{g, gC_2\}$ where $g \in C_{3v}$. For the single group, to every irrep of C_{3v} correspond two irreps of C_{6v} (same dimension, respectively even/odd with respect to C_2). For the double group, we have three irreps $E_{1/2}, E_{3/2}, E_{5/2}$. In the same way

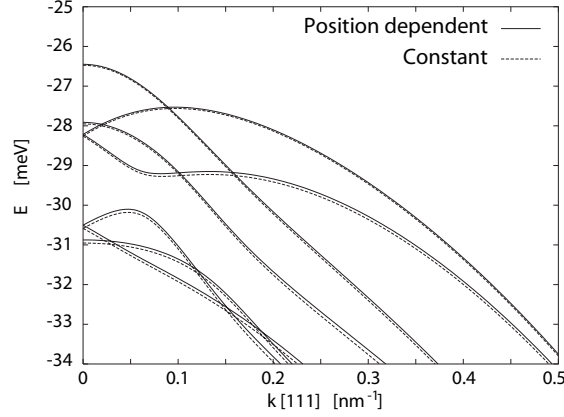


Figure 9.18: Valence band (only first energy levels) for the AlGaAs VQWR with constant and position dependent parameters

as D_{3h} , subduction table given by Altmann [3] gives $E_{1/2}(C_{6v}) \rightarrow E_{1/2}(C_{3v})$, $E_{5/2}(C_{6v}) \rightarrow E_{1/2}(C_{3v})$ and $E_{3/2}(C_{6v}) \rightarrow {}^1E_{3/2}(C_{3v}) \oplus {}^2E_{3/2}(C_{3v})$.

The MSR formalism can of course be applied to the C_{6v} group and allow to obtain the reduced states and Hamiltonian for both the single and double group irrep on the minimal domain corresponding to $1/12$. In Sec. 10.1 more details about the C_{6v} group are given.

Parametric Study and comparison with experience

Some parameters of the structure shown in Fig. 9.1 are in reality not very well known, and one needs indirectly fit them. To this end we present in Fig. 9.19 the dependence of the $e_1 - h_1$ energy and amplitude of transition as a function of the Al concentration of the VQWR, keeping the other parameters of Section 9.1 constant. The dependence as a function of the width L of the lateral QWs is also presented in Fig. 9.19. Clearly, increasing the concentration or decreasing the width have identical effects. Although the transition energy increases, the behavior of the oscillator strength indicates an overall decrease of quantum confinement, due to the spreading of the wavefunction in the nearby barriers. The width-dependence of the quantum confinement is due to the non-trivial geometry of the potential landscape.

We recently compare our theoretical and numerical results with experimental photoluminescence (PL) spectra obtained in our laboratory at EPFL (laboratory of physics of nanostructures). As presented in [83], taking into account a rigid shift (theoretical model do not include excitonic effects), the transitions obtained theoretically in the dipolar approximation are in excellent

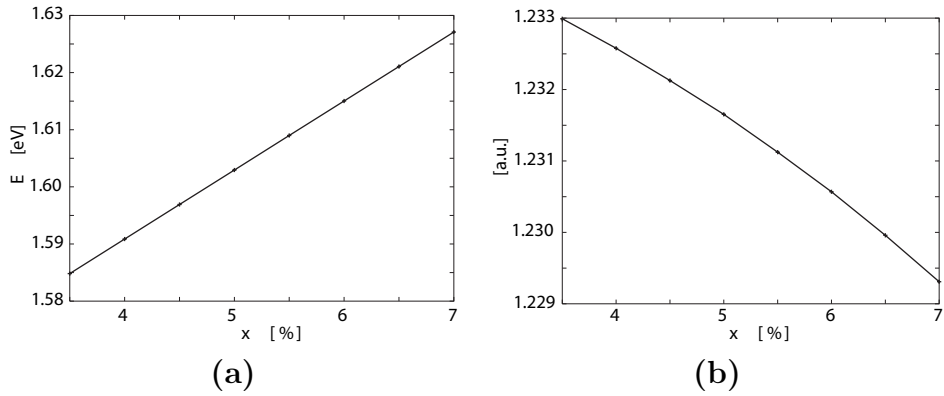


Figure 9.19: Dependence of $e_1 - h_1$ transition energy **(a)** and amplitude of transition (x polarization) **(b)**, as a function of Al VQWR concentration

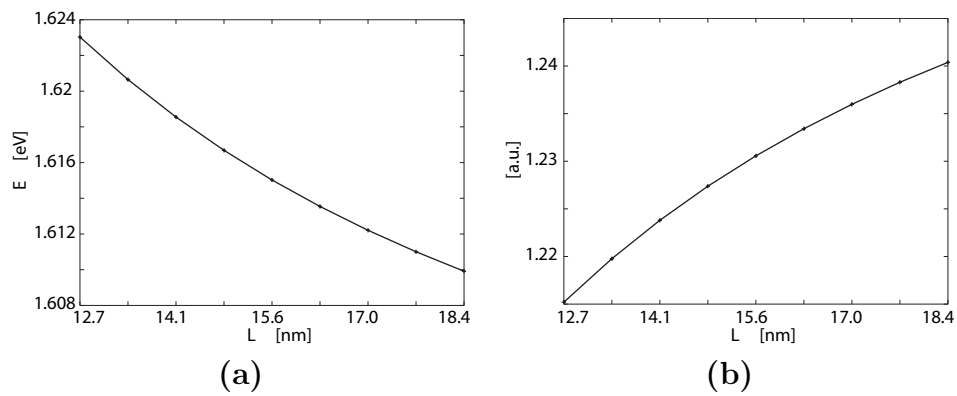


Figure 9.20: Dependence in QW width of $e_1 - h_1$ energy **(a)** and amplitude of transition (x polarization) **(b)**

agreement with the PL spectra.

Chapter 10

Application of MSR formalism to some other group

In this chapter we discuss the application of MSR formalism to some other group: C_{6v} is an higher symmetry group as C_{3v} with hexagonal symmetry quickly introduced in 9.2.5, D_{3h} correspond to the center of zone group for C_{3v} and C_n are the pure rotational sub-groups (without roto-inversions). The last example presented is the C_s group, where we explicitly show that our MSR formalism reduce to the old techniques for low symmetry groups.

We do not carry out the reduced Hamiltonians but discuss the symmetry of envelope functions by taking into account optimal choice of Bloch function basis and 3D spatial basis.

10.1 C_{6v} group

C_{6v} is an higher symmetry group with respect to C_{3v} presenting a 6 fold axis and some real structure like the wurtzite-based GaN/AlN QDs [24, 84] display hexagonal symmetry (see Fig. 6.8 for a schematic of an hexagonal QD).

We can explicitly construct C_{6v} from C_{3v} by adding the π -rotation C_2 : $\mathcal{G} = \{g, gC_2\} \quad \forall g \in C_{3v}$. We have four 1D and two 2D irreps (A_i, B_i and E_i , $i = 1, 2$) for the single group, half of these are even, and the other half is odd with respect to the new operation C_2 . For the double group, we have three 2D irreps ($E_{i/2}$, $i = 1, 3, 5$).

As presented in Sec. 3.4, for the valence band Luttinger Hamiltonian every p, q, r, s operators is considered as a second order polynomial in \mathbf{k} . We note P, Q, R, S the corresponding 3×3 “matrices” of coefficients in such a way that $p = \mathbf{k}^t P \mathbf{k}$, ... , $s = \mathbf{k}^t S \mathbf{k}$. In C_{3v} , (r, s) form an ITO transforming with

the E irrep and the corresponding matrix representation of the ITO can be written, from Eq. (9.3) as

$$R^{C_{3v}} = \begin{pmatrix} 0 & a & 0 \\ a & b & 0 \\ 0 & 0 & -b \end{pmatrix} \quad S^{C_{3v}} = \begin{pmatrix} 0 & 0 & a \\ 0 & 0 & -b \\ a & -b & 0 \end{pmatrix} \quad (10.1)$$

where $a = a(\mathbf{r})$ and $b = b(\mathbf{r})$ are some spatially dependent constant, depending on the Luttinger parameters given in (9.4) and describing the heterostructure, therefore invariant respect to the C_{6v} symmetry operations.

In C_{6v} , we write $r = r_1 + r_2$ and $s = s_1 + s_2$, where (r_i, s_i) are ITOs transforming like E_i irreps and we obtain

$$R_1^{C_{6v}} = \begin{pmatrix} 0 & \tilde{a} & 0 \\ \tilde{a} & 0 & 0 \\ 0 & 0 & 0 \end{pmatrix} \quad R_2^{C_{6v}} = \begin{pmatrix} 0 & 0 & 0 \\ 0 & \tilde{b} & 0 \\ 0 & 0 & -\tilde{b} \end{pmatrix} \quad (10.2)$$

$$S_1^{C_{6v}} = \begin{pmatrix} 0 & 0 & \tilde{a} \\ 0 & 0 & 0 \\ \tilde{a} & 0 & 0 \end{pmatrix} \quad S_2^{C_{6v}} = \begin{pmatrix} 0 & 0 & 0 \\ 0 & 0 & -\tilde{b} \\ 0 & -\tilde{b} & 0 \end{pmatrix} \quad (10.3)$$

where the $\tilde{a} = Re(a)$ and $\tilde{b} = iIm(b)$ are related to the E_1 and, respectively, E_2 ITO.

The effects of the increasing of symmetry $C_{3v} \rightarrow C_{6v}$ appear clearly: first the parameters a and b are simplified, second every parameter is related to a different irrep E_i .

Another way to explicitly obtain the C_{6v} Luttinger Hamiltonian from the C_{3v} Hamiltonian, is to symmetrize the Hamiltonian with respect to the C_2 operation, considering spatial dependent Luttinger parameters invariant with respect to the C_{6v} symmetry operations, as

$$H^{C_{6v}}(\mathbf{r}, \mathbf{k}) = \frac{1}{2} \left(H^{C_{3v}}(\mathbf{r}, \mathbf{k}) + \vartheta_{C_2^{-1}} H^{C_{3v}}(\mathbf{r}, \mathbf{k}) \vartheta_{C_2^{-1}}^{-1} \right) \quad (10.4)$$

For C_{6v} the Wigner representation reduce to $E_{1/2} \oplus E_{3/2}$ and the Luttinger Hamiltonian expressed in the $1/2, -1/2, 3/2, -3/2$, basis becomes as

$$H_L = -\frac{\hbar^2}{m_0} \begin{pmatrix} (P-Q)I_2 & A \\ A^+ & (P+Q)I_2 \end{pmatrix} \quad ; \quad A = \begin{pmatrix} -s^+ & r \\ r^+ & s \end{pmatrix} \quad (10.5)$$

The decomposition of the valence band states (still re-expressed with respect to the $+3/2, +1/2, -1/2, -3/2$ basis allowing to immediately compare the result with the C_{3v} decompositions given in (8.13)-(8.16)) into single group irreps is given by

$$\underline{\psi}_1^{E_{1/2}} = \frac{1}{\sqrt{2}} \begin{pmatrix} -\psi_2^{E_1} - \psi_2^{E_2} \\ \psi_1^{A_1} + \phi_1^{E_1} \\ \psi_1^{A_2} - \phi_2^{E_1} \\ \psi_1^{E_1} + \psi_1^{E_2} \end{pmatrix}, \quad \underline{\psi}_2^{E_{1/2}} = \frac{1}{\sqrt{2}} \begin{pmatrix} \psi_1^{E_1} - \psi_1^{E_2} \\ -\psi_1^{A_2} - \phi_2^{E_1} \\ \psi_1^{A_1} - \phi_1^{E_1} \\ \psi_2^{E_1} - \psi_2^{E_2} \end{pmatrix}$$

$$\begin{aligned} \underline{\psi}_1^{E_{3/2}} &= \frac{1}{\sqrt{2}} \begin{pmatrix} -\psi^{A_1} - \psi^{B_1} \\ -\psi_2^{E_1} - \psi_2^{E_2} \\ \psi_1^{E_1} - \psi_1^{E_2} \\ \psi^{A_2} + \psi^{B_2} \end{pmatrix}, & \underline{\psi}_2^{E_{3/2}} &= \frac{1}{\sqrt{2}} \begin{pmatrix} -\psi^{A_2} + \psi^{B_2} \\ \psi_1^{E_1} + \psi_1^{E_2} \\ \psi_2^{E_1} - \psi_2^{E_2} \\ -\psi^{A_1} + \psi^{B_1} \end{pmatrix} \\ \underline{\psi}_1^{E_{5/2}} &= \frac{1}{\sqrt{2}} \begin{pmatrix} \psi_2^{E_1} + \psi_2^{E_2} \\ \psi^{B_1} + \phi_1^{E_2} \\ \psi^{B_2} - \phi_2^{E_2} \\ -\psi_1^{E_1} - \psi_1^{E_2} \end{pmatrix}, & \underline{\psi}_2^{E_{5/2}} &= \frac{1}{\sqrt{2}} \begin{pmatrix} \psi_1^{E_1} - \psi_1^{E_2} \\ -\psi^{B_2} - \phi_2^{E_2} \\ \psi^{B_1} - \phi_1^{E_2} \\ \psi_2^{E_1} - \psi_2^{E_2} \end{pmatrix} \end{aligned} \quad (10.6)$$

where the argument \mathbf{r} of functions is omitted from now.

The different components indicate, according to the subduction table $C_{6v} \rightarrow C_{3v}$ [3], that $E_{1/2}$ and $E_{5/2}$ are related to $E_{1/2}(C_{3v})$ and $E_{3/2}$ to ${}^1E_{3/2} \oplus {}^2E_{3/2}$. The reduced Hamiltonians can be calculated using the reduction formalism presented above.

10.2 D_{3h} group and study of approximated symmetries

In the last chapter, a C_{3v} -symmetry Quantum Wire was studied with the help of the new MSR formalism. At the mesoscopic point of view, due to the translation invariance with respect to the x -direction (see Fig. 9.1), the heterostructure display a $D_{3h} = C_{3v} \otimes C_s = \{g, g\sigma_h\} \forall g \in C_{3v}$ symmetry group, where σ_h is the horizontal symmetry plane, but the microscopic atomic structure of AlGaAs is not invariant with respect to σ_h . The minimal common symmetry is C_{3v} and the Hamiltonian do never display the so called zone center (ZC) symmetry D_{3h} at $k = 0$. Studying a well symmetrized Hamiltonian with respect to σ_h (restoring the ZC symmetry) we showed that the lack of symmetry has only a small influence on the energy and eigenstates. In 9.2.4, we have presented how effects of an approximate symmetry can be understood in a qualitative and quantitative point of view using the new formalism and that the study of an approximate symmetry group can be a useful tool to better understand and interpret the physical and numerical results.

10.3 The C_n groups: subgroups of the rotations group

The subgroups of the pure rotation group $SO(3)$ C_n , $n \in \mathbb{N}$ are important groups corresponding to the symmetry of Hamiltonians with any symmetry plane (roto-inversion). A typical example of C_n Hamiltonians, are C_{nv} structures in presence of magnetic field. In fact, C_n groups are cyclic and commutative (abelian) groups, then every simple and double group irreps are non degenerate (according to the splitting of degeneracy due to magnetic field). In this case, the reduction of 3D and Wigner representation is equivalent to a diagonalization of the representations. In [72,75], the author study C_{4v} and C_{6v} QDs with and without magnetic field even using C_n models (no spatial-spin separation is computed and diagonalization of representation are computed for block-diagonalize the full Hamiltonian just before the numerical result). Even in this simple C_n case, using fully symmetrized basis and spatial reduction allow to obtain some analytical and numerical simplifications.

We present as example the C_4 symmetry group, a typical QD section is presented in Fig. 6.9 (b), which has four single group irreps $A, B, {}^iE$ and four double group irreps ${}^iE_{1/2}, {}^iE_{3/2}$, $i = 1, 2$. The ${}^iE, {}^iE_{1/2}, {}^iE_{3/2}$ are self conjugated irreps and even for the spinless problem we have an additional degeneracy at the center of zone $k = 0$ due to time reversal symmetry. In the OBB, the Wigner operators are of course diagonals. The 3D rotation representation constructed with Eq. (2.22) has the block diagonal form $A \oplus ({}^1E \otimes {}^2E)$. The 2×2 block can be reduced to ${}^2E \oplus {}^1E$ with the optimal 3D basis given by $\left\{ \hat{e}_x, \hat{e}_{\sigma+} = \frac{1}{\sqrt{2}}(\hat{e}_y + i\hat{e}_z), \hat{e}_{\sigma-} = \frac{1}{\sqrt{2}}(\hat{e}_y - i\hat{e}_z) \right\}$ and corresponding to a circular polarization in the plane.

In the fully symmetrized 3D and Bloch basis, we obtain very simply decomposition of spinorial eigenstates and selection rules.

For $j = 3/2$, we reduce the Wigner representation to ${}^1E_{3/2} \oplus {}^1E_{1/2} \oplus {}^2E_{1/2} \oplus {}^2E_{3/2}$ and obtain the spinorial decomposition for the ${}^iE_{1/2}$

$$\underline{\psi}^{1E_{1/2}} = \begin{pmatrix} \psi^B \\ \psi^A \\ \psi^{2E} \\ \psi^{1E} \end{pmatrix} \quad \underline{\psi}^{2E_{1/2}} = \begin{pmatrix} \psi^{2E} \\ \psi^{1E} \\ \psi^A \\ \psi^B \end{pmatrix} \quad (10.7)$$

and ${}^iE_{3/2}$ components

$$\underline{\psi}^{1E_{3/2}} = \begin{pmatrix} \psi^A \\ \psi^B \\ \psi^{1E} \\ \psi^{2E} \end{pmatrix} \quad \underline{\psi}^{2E_{3/2}} = \begin{pmatrix} \psi^{1E} \\ \psi^{2E} \\ \psi^B \\ \psi^A \end{pmatrix} \quad (10.8)$$

For $j = 1/2$, we reduce the Wigner representation to ${}^1E_{1/2} \oplus {}^2E_{1/2}$ and, in the same way as for C_{3v} , for every irreps the spinors decomposition correspond to the central part of the corresponding $j = 3/2$ decomposition. With respect to the 3D and spinorial symmetrized basis, the Kane matrices are given by

$$\begin{aligned} P_x^A &= P_0 \begin{pmatrix} 0 & \sqrt{2/3} & 0 & 0 \\ 0 & 0 & \sqrt{2/3} & 0 \end{pmatrix} \\ P_{\sigma+} &= P_0 \begin{pmatrix} 0 & 0 & 1/\sqrt{3} & 0 \\ 1 & 0 & 0 & 0 \end{pmatrix} \\ P_{\sigma-} &= P_0 \begin{pmatrix} 0 & 0 & 0 & 1 \\ 0 & -1/\sqrt{3} & 0 & 0 \end{pmatrix} \end{aligned} \quad (10.9)$$

We obtain that the only permitted transition between a conduction and a valence band state are ${}^jE_m - {}^iE_n$ and ${}^iE_m - {}^jE_m$ transitions, where $i = 1, 2$ for, respectively, σ_-, σ_+ polarization, $j \neq i$ and $m \neq n = 1/2, 3/2$. Of course only $\Gamma - \Gamma$ transitions are permitted in x direction.

10.4 Return to the C_s group

We developed the new formalism for study HSH. For a C_s low symmetry heterostructure like T or V-shaped QWRs, the novel formalism reduce to the old resolution technique: choose an “optimal quantization axis” perpendicular to the symmetry plane σ . This particular choice allow to diagonalize the Wigner operator related to the vertical symmetry plan $W(\sigma)$ and obtain even/odd envelope functions (single group irreps A', A'' are 1D). However $C_s = \{E, \sigma\}$ and the basis diagonalizing σ correspond to the OBB in which Wigner representation is completely reduced to ${}^1E_{1/2} \oplus {}^2E_{1/2} \oplus {}^1E_{1/2} \oplus {}^2E_{1/2}$ (double group irreps ${}^iE_{1/2}$, $i = 1, 2$ are 1D). In this particular case, the diagonalization of the Wigner representation can be computed with a rotation matrix parametrized by the three Euler angles (α, β, γ) an corresponding to a “3D rotation” $\mathfrak{R}(\alpha, \beta, \gamma)$ of the quantization axis direction. Considering the 3D basis presented in Fig. 9.1, for a vertical plane normal to the \hat{e}_z direction, the 3D representation is reduced to $A' \oplus A' \oplus A''$. The $j = 3/2$ states are

decomposed as

$$\underline{\psi}^{1E_{1/2}} = \begin{pmatrix} \psi^{A'} \\ \psi^{A''} \\ \phi^{A'} \\ \phi^{A''} \end{pmatrix} \quad \underline{\psi}^{2E_{1/2}} = \begin{pmatrix} \psi^{A''} \\ \psi^{A'} \\ \phi^{A''} \\ \phi^{A'} \end{pmatrix} \quad (10.10)$$

where, for every $iE_{1/2}$, ψ^Γ and ϕ^Γ are different function with the same symmetry and, as usual, the $j = 1/2$ states decomposition correspond to the central part of $j = 3/2$ functions. The dipolar transition operators P_x and P_y in the symmetry plane are even with respect to σ (A') and the operator P_x perpendicular to the axis is odd (A''). The odd A'' operator P_x only couple mutually conjugated bands ($M_x^{\Gamma,\Gamma} = M_y^{\Gamma,\Gamma} = 0$ then $\Gamma - \Gamma$ are selection rules) and the even A' operators P_x, P_y only allow $\Gamma - \Gamma$ transitions.

Chapter 11

Conclusion and outlook

11.1 Conclusion

We developed a novel Maximal Symmetrization and Reduction (MSR) formalism for wavefunctions in solid-state nanostructures (Chs. 7-8) and explicitly exploited this new tool to study the electronic and optical properties of a C_{3v} Vertical Quantum Wire (VQWR).

The heart of the new theoretical formalism consists in bringing the analysis of the effects of heterostructure symmetry *at the envelope function level*. The method is very general, well adapted to solve High Symmetry Heterostructure (HSH) scalar or spinorial-like problems and independent of the dimensionality of the heterostructure.

For scalar problems, we developed first a systematic Spatial Domain Reduction (SDR) technique: it allows, for every different symmetry of the problem (irrep), to find the independent sub-domains (independent variables) and to obtain a reduced Hamiltonian involving only the independent sub-domains (minimal reduced domain). From the theoretical point of view, this allows to highlight the symmetry properties of eigenstates and the coupling between a minimum set of independent variables in the Hamiltonians. In addition we were able to obtain explicitly the non-trivial boundary conditions on the reduced domain. From the numerical point of view, it is possible to solve smaller optimized problems for every irreps: the size of the matrices are minimized, whilst the band structure can be conserved. As a result, the computation time (CPU time) can be considerably reduced (by a factor $108/5 \cong 22$ for C_{3v}) as well as the memory requirements.

For spinorial-like problems, we first explicitly separate the spatial and spinorial part of the operators and we choose optimal basis in both spaces according to the symmetry of the problem (symmetry group of the Hamiltonian).

With respect to the optimal spinorial basis, the coupling between components is minimized and allows to introduce in the simplest way single group decompositions of the scalar envelope functions (spinorial components) and of the operators like the Hamiltonian. In the last step we compute the SDR for every scalar function appearing in the decomposition of the components. The advantages of a full symmetrization of the basis are manifold. First, the Hamiltonians display the simplest form and the introduction of single group labels for every component allows to explicitly highlight the effects of coupling between different components. Second, the amplitudes of the matrix elements of any operator with a given symmetry take a very simple form due to the additional single group selection rules which can be used.

Symmetry breaking or eventual approximated symmetries can be understood at the envelope function level in a qualitative and quantitative way. The study of more complicated subsequent problems, like the excitonic or polaronic problems, involving envelope functions and other operators, can be considerably simplified.

It is also essential to note that it is not necessary to use a symmetrized code. The projectors allow to symmetrize the eigenstates after numerical resolution and the method can be used as post processing.

11.2 Outlook

The MSR formalism was developed with the aim of studying a C_{3v} VQWR but the method is so general that it can be adapted to study many other problems. Beside trivial generalizations to other dimensionality (e.g. quantum dots) or different symmetry groups, other interesting problems related to nanostructures with high symmetry properties can be studied with MSR formalism. To give an example, the resolution of Maxwell equations in a photonic band-gap: the Bloch function basis related to a half integer j for the electronic band structure of a heterostructure is replaced by $j = 1$ (3D basis!) in a photonic band-gap. The “spinorial” basis functions transform in this instance with the single group irreps (optimal basis can be used, allowing to decompose the scalar components with respect to the symmetry before apply SDR). The method can also be applied to tensorial strain equations, and even to an arbitrary set of non-linear partial differential equations having a given global symmetry.

Finally, the formalism is independent of the technique used for the numerical resolution (e.g. finite elements, finite differences or decomposition into plane waves). Additional numerical optimization can be reached, for example, using adaptive or irregular meshing in the reduced domain.

Bibliography

- [1] Y. Ducommun, A. Hartmann, D. Oberli, and E. Kapon. *phys. stat. sol. (b)*, **224**:431, 2001.
- [2] F. Michelini, M.-A. Dupertuis, and E. Kapon. *Appl. Phys. Lett.*, **84**(No. 20):4086, 2004.
- [3] S. L. Altmann and P. Herzig. *Point-Group Theory Tables*. Clarendon Press, Oxford, 1994.
- [4] D. S. Citrin and Y. C. Chang. *J. Appl. Phys.*, **68**(No. 1):161, 1990.
- [5] P. C. Sercel and K. J. Vahala. *Phys. Rev. B*, **44**(No. 11):5681, 1991.
- [6] M. Ogawa, T. Kunisama, T. Ito, and T. Miyoshi. *J. Appl. Phys.*, **84**(No. 6):3242, 1998.
- [7] M. Ogawa, M. Itoh, and T. Miyoshi. *Physica B*, **27**:65, 1996.
- [8] B. Lassen, V. C. L. Y. Voon, M. Willatzen, and R. Melnik. *Solid State Comm.*, **132**:141, 2004.
- [9] C. Girard. *Rep. Prog. Phys.*, **68**:1883, 2005.
- [10] A. D. Yoffe. *Advances in Physics*, **51**(No. 2):799, 2002.
- [11] K. Sakoda. *Optical properties of photonic crystals*. Springer, Berlin, 2005.
- [12] R. M. Stevenson, R. J. Young, P. Atkinson, K. Cooper, D. A. Ritchie, and A. J. Shields. *Nature*, **439**:179, 2006.
- [13] S. Kako, K. Hoshino, S. Iwamoto, S. Ishida, and Y. Arakawa. *Appl. Phys. Lett.*, **85**:64, 2004.
- [14] A. D. Andreev and E. P. O'Reilly. *Phys. Rev. B*, **62**:15851, 2000.

-
- [15] H. Akiyama. *J. Phys.: Condens. Matter*, **10**:3095–3139, 1998.
- [16] E. Runge. *Solid State Phys.: Advances in Research and Appl.*, **57**:149–305, 2002.
- [17] M.-A. Dupertuis, E. Martinet, D. Y. Oberli, and E. Kapon. *Europhys. Lett.*, **52**:420, 2000.
- [18] M.-A. Dupertuis. *Phys. stat. sol. (b)*, **221**:323, 2000.
- [19] F. Vouilloz, D. Y. Oberli, M.-A. Dupertuis, A. Gustafsson, F. Reinhardt, and E. Kapon. *Phys. Rev. B*, **57**:12378, 1997.
- [20] P. C. Sercel and K. J. Vahala. *Appl. Phys. Lett.*, **57**:545, 1990.
- [21] U. Bockelmann and G. Bastard. *Europhys. Lett.*, **15**:215, 1991.
- [22] D. S. Citrin and Y. C. Chang. *Phys. Rev. B*, **43**:11703, 1990.
- [23] A. Hartmann, Y. Ducommun, K. Leifer, and E. Kapon. *J. Phys.: Condens. Matter*, **11**:5901, 1999.
- [24] P. Tronc, V. P. Smirnov, and K. S. Zhuravlev. *phys. stat. sol. (b)*, **241**(No. 13):2938, 2004.
- [25] J. F. Cornwell. *Group Theory In Physics, Vol I*. Academic Press, London, 1984.
- [26] J. Shertzer and L. R. Ram-Mohan. *Phys. Rev.*, **41**(No. 14):9994, 1990.
- [27] G. Bastard. *Wave Mechanics Applied to Semiconductor Heterostructures*. Les Editions de Physique, Paris, 1988.
- [28] P. C. Sercel and K. J. Vahala. *Phys. Rev. B*, **42**(No. 6):3690, 1990.
- [29] F. Bassani and G. Pastori Parravicini. *Electronic states and optical transitions in solids*. Pergamon Press, Oxford, 1975.
- [30] A. Messiah. *Mécanique quantique*. Dunod, Paris, 1969.
- [31] M. Nakahara. *Geometry, topology and physics*. Institute of physics publishing, Bristol, 2002.
- [32] G. F. Koster, J. O. Dimmock, G. Wheeler, and R. G. Statz. *Properties of the thirty-two point groups*. MIT Press, Cambridge, USA, 1963.

-
- [33] T. Inui, Y. Tanabe, and Y. Onodera. *Group theory and its application in physics*. Springer-Verlag, Berlin, 1990.
- [34] M. Lax. *Symmetry Principles in Solid State and Molecular Physics*. John Wiley and Sons, New York, 1974.
- [35] G. L. Bir and G. E. Pikus. *Symmetry and Strain-induced Effects in Semiconductors*. John Wiley and Sons, New-York, 1974.
- [36] V. Heine. *Group theory in quantum mechanics*. Pergamon Press, Exeter, 1960.
- [37] E. P. Wigner. *Group theory and its application to the quantum mechanics of atomic spectra*. Academic Press, New York, 1971.
- [38] A. Messiah. *Quantum mechanics*. Wiley, New York, 1958.
- [39] G. Fishman. *Energie et fonction d'onde des semi-conducteurs*. Les éditions de la physique, Les Ulis, 1988.
- [40] J. H. Davies. *The physics of low-dimensional semiconductors : an introduction*. Cambridge University Press, Cambridge, 1998.
- [41] J. M. Luttinger and W. Kohn. *Phys. Rev.*, **97**:869, 1955.
- [42] E. Rosencher and B. Vinter. *Optoelectronics*. Cambridge University press, Cambridge, 2002.
- [43] E. Rosencher and B. Vinter. *Optoélectronique*. DUNOD, Paris, 2002.
- [44] F. Michelini. *Modélisation de structures semi-conductrices en théorie $k \cdot p$ multibandes*. PhD thesis, INSAT, 2000.
- [45] M. E. Rose. *Relativistic electron theory*. Wiley, New York, 1961.
- [46] G. Dresselhaus. *Phys. Rev.*, **100**:580, 1955.
- [47] J. M. Luttinger. *Phys. Rev.*, **102**:1030, 1956.
- [48] D. L. Boiko, P. Féron, and P. Besnard. *Phys. Rev. B*, **73**:35204, 2006.
- [49] N. Holonyak, R. Kolbas, R. Dupuis, and P. Dapkus. *IEEE J. Quantum Electron.*, **16**(No. 2):170, 1980.
- [50] E. Kapon. *Proc. IEEE*, **80**(No. 3):398, 1982.

-
- [51] Y. Ducommun. *Semiconductor quantum dots grown in inverted pyramids*. PhD thesis, EPFL, 2001.
- [52] F. Vouilloz. *Optical spectroscopy study of carriers recombination in quantum wires*. PhD thesis, EPFL, 1998.
- [53] G. Fishman. *Phys. Rev. B*, **52**(No. 15):11132, 1995.
- [54] M. G. Burt. *J. of Phys.: Cond. Mat.*, **4**:6651, 1992.
- [55] B. A. Foreman. *Phys. Rev. B*, **48**:4964, 1993.
- [56] L. R. Ram-Mohan and K. H. Yoo. *J. Phys.: Condens. Matter*, **18**:R901, 2006.
- [57] C. Kittel. *Introduction to solid state physics*. John Wiley & Sons, USA, 2005.
- [58] C. Kittel. *Physique de l'état solide*. DUNOD, Paris, 1983.
- [59] N. W. Ashcroft and N. D. Mermin. *Solid state physics*. Holt, Rinehart and Winston, USA, 1976.
- [60] P. Harrison. *Quantum Wells, Wires and Dots*. Wiley, Chichester, 2005.
- [61] F. T. Vasko and A. V. Kuznetsov. *Electronic states and optical transitions in semiconductor heterostructures*. Springer, New York, 1999.
- [62] H. Haugh and S. Koch. *Quantum theory of the optical and electronic properties of semiconductors*. World scientific, Singapore, 1990.
- [63] S. Glutsch. *Excitons in low-dimensional semiconductors*. Springer, Berlin, 2004.
- [64] J. Comte. *Calcul d'éléments de matrice de Coulomb pour un fil quantique de symétrie C_{3v}* . Master's thesis, EPFL, 2007.
- [65] E. B. Becker, G. F. Carey, and J. T. Oden. *The Texas Finite Elements Series*. Prentice-Hall International, London, 1981.
- [66] L. R. Ram-Mohan. *Finite element and boundary element applications in quantum mechanics*. Oxford university press, Oxford, 2002.
- [67] R. B. Lehouck, D. C. Sorensen, and C. Yang. *Arpack Users Guide: Solution of Large Scale Eigenvalue Problems by implicitly restarted Arnoldi Methods*. SIAM Publications, Philadelphia, USA, 1997.

-
- [68] J. Rappaz and M. Picasso. *Introduction à l'analyse numérique*. PPUR, Lausanne, 2000.
- [69] M.-A. Dupertuis, D. Marti, and F. Michelini. *phys. stat. sol. (b)*, **234**(No. 1):329, 2002.
- [70] D. H. Marti, M.-A. Dupertuis, and B. Deveaud. *Phys. Rev. B*, **72**(No. 7):075357, 2005.
- [71] D. H. Marti, M.-A. Dupertuis, and B. Deveaud. *IEEE J. Quant. Electron*, **41**(No. 6):848, 2005.
- [72] N. Vukmirović, D. Indjin, V. Jovanović, Z. Ikonić, and P. Harrison. *Phys. Rev. B*, **72**:75356, 2005.
- [73] S. Wolfram. *The mathematica book*. Wolfram media, Campaign, USA, 1996.
- [74] M. G. Burt. *J. of Phys.: Cond. Mat.*, **11**:R53, 1999.
- [75] N. Vukmirović, Z. Ikonić, D. Indjin, and P. Harrison. *J. Phys.: Condens. Matter*, **18**:6249, 2006.
- [76] D. Obreschkow, F. Michelini, S. Dalessi, E. Kapon, and M.-A. Dupertuis. *Phys. Rev. B*, **76**:35329, 2007.
- [77] G. Tarel, S. Dalessi, F. Michelini, and M.-A. Dupertuis. *Phys. Rev. B*. To be submitted.
- [78] G. Tarel. *Calcul de systèmes fil-boîte couplé*. Master's thesis, EPFL, 2007.
- [79] M. A. Herman, D. Bimberg, and J. Christen. *J. Appl. Phys.*, **70**(No. 2):R1, 1991.
- [80] A. Gustafsson, M.-E. Pistol, L. Montelius, and L. Samuelson. *J. Appl. Phys.*, **84**(No. 4):1715, 1998.
- [81] M. H. Baier. *Correlated photon emission from pyramidal quantum dot heterostructures*. PhD thesis, EPFL, 2005.
- [82] C. Delannoy. *Programmer en fortran 90*. Eyrolles, Paris, 1993.
- [83] Q. Zhu, E. Pelucchi, S. Dalessi, K. Leifer, M.-A. Dupertuis, and E. Kapon. *Nano Letters*, **6**(No. 5):1036, 2006.

- [84] D. Simeonov, E. Feltin, J.-F. Carlin, R. Butté, M. Ilegems, and N. Grandjean. *J. Appl. Phys.*, **99**:83509, 2006.
- [85] S. Dalessi, F. Michelini, and M.-A. Dupertuis. *Phys. Rev. B*. To be submitted.
- [86] S. Dalessi and M.-A. Dupertuis. *Phys. Rev. B*. To be submitted.

Publications and conferences

Main publications

The more important part of this PhD work was devoted to develop the new MSR formalism and apply the novel tools to study a triangular C_{3v} VQWR. Two big papers summarizing MSR formalism and application (corresponding to Chapters 6-10) are currently in the final phase before submission to Phys. Rev. B :

- S. Dalessi and M.-A. Dupertuis, **A formalism for maximal symmetrization and reduction of wavefunctions in solid state nanostructures and photonic band-gaps** [85]
- S. Dalessi, F. Michelini and M.-A. Dupertuis, **Electronic and optical properties of C_{3v} vertical quantum wires self-formed in inverted tetrahedral pyramids** [86]

Other publications

- Q. Zhu and E. Pelucchi and S. Dalessi and K. Leifer and M.-A. Dupertuis and E. Kapon, **Alloy Segregation, Quantum Confinement, and Carrier Capture in Self-Ordered Pyramidal Quantum Wires** [83]
- D. Obreschkow and F. Michelini and S. Dalessi and E. Kapon and M.-A. Dupertuis, **Non-orthogonal theory of polarons and application to pyramidal quantum dots** [76]
- G. Tarel, S. Dalessi, F. Michelini and M.-A. Dupertuis, **Coupling heterostructures of different dimensionality**, to be submitted [77]

International conferences

- Optics of Excitons in Confined Systems (OECS) 9, Southampton (United Kingdom), Sept 5 - 11 2005, S. Dalessi, F. Michelini and M.-A. Dupertuis, **Electronic and optical properties of C_{3v} Vertical Quantum Wires (VQWRs) self-formed in inverted tetrahedral pyramids**, Poster session
- International Conference on Superlattices, Nano-structures and Nano-devices (ICSNN) 2006, Istanbul (Turkey), July 30 - August 4 2006, S.

Dalessi, F. Michelini and M.-A. Dupertuis, **A novel method for heterostructures with high symmetry: spatial domain reduction and fully symmetrized Bloch function basis**, Poster session

Summer School

- Monte Verità summer school on semiconductor quantum dots : physics and devices, Ascona (Switzerland), september 5 - 10 2004, S. Dalessi, F. Michelini and M.-A. Dupertuis, **Electronic states in vertical quantum wires Formed in pyramidal quantum dot heterostructures**, Poster session

Curriculum vitæ

DALESSI Sascha

sascha.dalessi@a3.epfl.ch

Nationality : Swiss
Date of birth : May 11, 1976
Place of birth : CH-6600 Locarno (Ticino, Switzerland)
Place of origin : CH-6690 Caviglioglio (Ticino, Switzerland)

Education

- 2003-2007 PhD student and teaching assistant:
Laboratory of Physics of Nanostructures,
Institute of Quantum Electronics and Photonics,
Physics Section,
Ecole Polytechnique Fédérale de Lausanne (EPFL)
- 2003 EPF Physics engineer degree (Master in Physics):
Diploma thesis at the Institute of Theoretical Physics,
Ecole Polytechnique Fédérale de lausanne (EPFL)
- 1997 Maturità Federale scientifica (tipo C):
Liceo Cantonale Locarno (Ticino, Switzerland)